Ecology and Development Series No. 40, 2006

Editor-in-Chief:
Paul L.G.Vlek

Editors:
Manfred Denich
Christopher Martius
Charles Rodgers

Fafré Bagayoko

Impact of land-use intensity on evaporation and surface runoff: Processes and parameters for eastern Burkina Faso, West Africa

Cuvillier Verlag Göttingen

To my twins Rachid and Rachidatou

ABSTRACT

Land-use is one of the main factors affecting the hydrological cycle in the Volta river basin, where two major projects (GLOWA-Volta and VinVal) are dealing with the elaboration of a land-use planning and decision support system for sustainable agricultural production and water resource management. Both projects, especially GLOWA-Volta need information about the seasonal dynamics of the actual evaporation and surface runoff. Therefore, the inter-annual dynamics of the actual evaporation, effect of land-use on the evaporation and on land surface models were analyzed via surface flux measurements during the first long-term eddy covariance measurement over the savanna vegetation in West Africa. The investigation took place in eastern Burkina Faso; the analysis covers almost two years, including one relatively wet (2003) and one relatively dry (2004) year. Surface runoff and scale effect were also investigated in three adjacent watersheds with different land-use intensity during the 2004 rainy season.

The collected surface fluxes were reliable and representative according to the energy balance closure and footprint analysis. The energy balance closure was affected by rain during the rainy season, and by sampling problems during the transition periods (April-May and October-November). The relevance of the dominant wind direction in the representation of the measurements was also discussed. With respect to the inter-annual partitioning of the available energy between the latent heat (actual evaporation) and sensible heat flux, a conservative relationship between the decrease of the annual rainfall (33 %) and the cumulative of the increase of sensible heat flux (20 %) and decrease of latent heat flux (10 %) was somehow observed. The latent heat flux was the main consumer of the available energy during the rainy season (71 %), while sensible heat flux was dominant during the dry season (77 %). In term of water balance, 1229 mm of rainfall was observed in 2003 against 351 mm evaporated, while 825 mm of rainfall was observed in 2004 against 268 mm. During the dry season, the latent heat flux was strongly coupled to the atmosphere, where the decoupling coefficient (Ω) ranged from 0.18 to 0.4, but was greatly reduced due to the poor soil moisture availability and high vapor pressure deficit ($VPD > 4$ kPa). During the rainy season, the latent heat flux was decoupled from the atmosphere ($0.6 \leq \Omega < 0.9$). Following this pattern of coupling and decoupling, a new formulation of actual evaporation and surface conductance was proposed.

The effect of the land-use on the land surface models was investigated by the sensitivity of the National Centers for Environmental Prediction (NCEP), the Oregon State University, the Air Force and the Hydrologic Research Lab land surface model (NOAH LSM) via the seasonal dynamics of the aerodynamic property of vegetations (roughness length for momentum). This sensitivity was tested by comparing the simulated surface fluxes using a fixed value of the roughness length for momentum as mentioned in the standard form of the model and the roughness length for momentum having the true seasonal values. The results show that the NOAH LSM was not sensitive to the change of the aerodynamic property of vegetation on a seasonal basis nor on a daily basis, which was found to be abnormal. The formulation of the coefficient (B_c) coupling the canopy transpiration to the atmosphere was found to be the main cause for this. A new formulation for B_c was proposed to remedy the insensitivity and to improve the performance of the model. Recommendations are also given to enhance the overall performance of the model in the savanna environment.

The surface albedo was also investigated, as it is an important parameter in many models such as crop growth models, the eco-hydrological models, and the General Circulation Models (GCM). There was a clear seasonal dynamics of the surface albedo, which had a negative impact on the actual evaporation. This effect was found to be insignificant on a daily basis. The models calibrated to simulate the seasonal dynamics of surface albedo of *Vitellaria paradoxa* (sheanut tree) and *Sorghum vulgare* (sorghum) gave a satisfactory estimation, but they were very sensitive to leaf area index (LAI).

Finally, the surface runoff was measured with a set of runoff plots in three small watersheds (Tanyele, Bounou and Sambouali) each with different agricultural land-use intensity. Tanyele had high land-use intensity; Bounou had medium land-use intensity, while Sambouali was not under agriculture but was covered with natural vegetation. Each set consisted of one short plot of 0.80 m x 1.25 m and one long plot of 2 m x 5 m. The scale effect was measured by dividing the runoff coefficient of the long plot (C_{10}) by the runoff coefficient of the short plot (C_1) and then compared to the ratio of the surface (S_1 / S_{10}). Total runoff on a watershed scale was estimated and compared with the total discharge at the outlet. A clear reduction of the surface runoff with increasing slope length and with decreasing land-use intensity was observed. A difference in the interception and the frictional resistance of the vegetation was found to be important in the process of the scale effect and decrease of the surface runoff with decreasing land-use intensity.

Although it was not possible to directly measure the ground heat flux and the net radiation, the results of this study can be relevant inputs of the eco-hydrological models in the semi-arid region of West Africa.

TABLE OF CONTENTS

ACKNOWLEDGEMENTS

LIST OF ABBREVIATIONS AND ACRONYMS

ABL	Atmospheric Boundary Layer
ALTEDDY	Software for the processing of eddy fluxes
DOY	Day of year
CIEH	Comité Inter-africain d'Etude Hydraulique
EC	Eddy covariance
GCM	General Circulation Model
HAPEX-Sahel	Hydrological and Atmospheric Pilot Experiment-Sahel
HEATREG	Software for the processing of daily soil heat storage
MATLAB	Software for mathematics
NOAH LSM	National Center for Environmental Prediction (NCEP), Oregon State University, Air Force and Hydrologic Research Lab land surface model
ORSTOM	Office de la Recherche Scientifique et Technique Outre-Mer
RMSE	Root mean square error
MBE	Mean bias error
SEBEX	Sahelian energy balance experiment
SONABEL	SOciété Nationale Burkinabè de l'ELectricité
SVAT	Soil-Vegetation-Atmosphere transfer schemes

LIST OF SYMBOLS

Symbol	Meaning	Unit
E	Actual evaporation	[mm h^{-1}]
E_{imp}	Imposed evaporation	[mm h^{-1}]
E_{eq}	Equilibrium evaporation	[mm h^{-1}]
E_b	Bare soil evaporation	[mm h^{-1}]
E_c	Dry canopy transpiration	[mm h^{-1}]
E_t	Total evaporation	[mm h^{-1}]
E_p	Potential evaporation	[mm h^{-1}]
K_{sat}	Saturated hydraulic conductivity	[mm h^{-1}]
S_o	Sorptivity	[mm $s^{-0.5}$]
W_c	Intercept canopy water content	[mm]
S	Maximum canopy water content	[mm]
P	Rainfall depth	[mm]
d	Displacement height	[m]
x	Upwind distance	[m]
X_m	Maximum distance upwind	[m]
L	Monin-Obukhov length	[m]
z	Measurement height (eddy covariance)	[m]
z_s	Soil depth	[m]
z_{0m}	Roughness length for momentum	[m]
z_{0h}	Roughness length for heat	[m]
A	Altitude of the station	[m]
H_f	Forest height	[m]
h_c	Crop height	[m]
L_s	Slope length	[m]
R_{hy}	Hydraulic radius	[m]
S_c	Wetted section	[m^2]
R_r	Correction coefficient	[W m^2 mbar^{-1}]
R_n	Net radiation	[W m^{-2}]
λE	Latent heat flux	[W m^{-2}]
H	Sensible heat flux	[W m^{-2}]
G	Ground heat flux	[W m^{-2}]
R_s	Shortwave radiation	[W m^{-2}]
R_{su}	Upward shortwave radiation	[W m^{-2}]
R_{Ld}	Downward longwave radiation	[W m^{-2}]
R_{Lu}	Upward longwave radiation	[W m^{-2}]
R_a	Clear sky radiation	[W m^{-2}]
I	Extraterrestrial radiation	[W m^{-2}]

R_g	Global radiation	[W m^{-2}]
σ	Stephan Bolzman constant	[W m^{-2} K^{-4}]
Y_l	Mean live span of leaf	[cm^2]
S_l	Leaf size	[cm^2]
d_c	Calendar days	[DOY]
d_0	Starting date of stress-calendar	[DOY]
c	Cloud cover	[%]
T_s	Surface temperature	[K]
T_a	Air temperature	[C]
T	Soil temperature	[K]
T_{ref}	Reference air temperature	[C]
R_h	Relative humidity	[%]
VPD	Vapor pressure deficit	[kPa] or [mbar]
Θ_1	Soil water content	[m^3 kg^{-1}]
Θ_{wp}	Soil water content at wilting point	[m^3 kg^{-1}]
Θ_{fc}	Soil water content at field capacity	[m^3 kg^{-1}]
R_m	Root density	[m m^{-3}]
ρ_v	Density of water vapor	[kg m^{-3}]
ρ_a	Density of moist air	[kg m^{-3}]
q	Specific humidity	[kg m^{-3}]
q'	Standard deviation of the q from the mean	[kg m^{-3}]
F_m	Specific mass flux	[kg m^{-2} s^{-1}]
ρ_w	Density of water	[kg m^{-3}]
t	Time	[s]
R	Gas constant	[J kg^{-1} K^{-1}]
λ	Latent heat of vaporization	[kJ kg^{-1}]
c_p	Specific heat of moist air	[J kg^{-1} K^{-1}]
k_v	Molecular diffusity	[m s^{-1}]
V	Air velocity	[m s^{-1}]
u	Air velocity following x axis	[m s^{-1}]
u^*	Friction velocity	[m s^{-1}]
u'	Standard deviation of u from the mean	[m s^{-1}]
v	Air velocity following y axis	[m s^{-1}]
v'	Standard deviation of v from the mean	[m s^{-1}]
w	Air velocity following z axis	[m s^{-1}]
w'	Standard deviation of the z from the mean	[m s^{-1}]
g_c	Surface conductance	[m s^{-1}]
g_a	Aerodynamic conductance	[m s^{-1}]
B_c	Canopy coefficient	[m s^{-1}]
θ	Potential temperature	[C]

θ'	Standard deviation of θ from the mean	[C]
P_a	Atmospheric pressure	[mbar]
P_b	Recorded pressure at the stream bed	[mbar]
P_s	Surface pressure	[mbar]
e_s	Saturated air pressure	[mbar]
e_a	Actual air pressure	[mbar]
γ	Psychometric constant	[mbar K^{-1}]
Δ	Slope of the vapor pressure curve	[mbar K^{-1}]
g	Gravitational acceleration	[m^2 s^{-1}]
α_T	Thermal diffusity	[m^2 s^{-1}]
h	Sun declination	[°]
Z	Sun zenith angle	[°]
Dir	Wind direction	[°]
$Long$	Longitude	[UTM]
Lat	Latitude	[UTM]
C_V	Volumetric heat capacity	[J K^{-1} m^{-3}]
$R_{c\min}$	Minimum surface resistance	[s m^{-1}]
$R_{c\max}$	Maximum surface resistance	[s m^{-1}]
R_c	Surface resistance	[s m^{-1}]
R_e	Roughness Reynolds number	[m^2 s^{-1}]
I	Slope of the stream channel	[ ]
ε_a	Clear sky emissity	[ ]
ε_s	Surface emissity	[ ]
C_{10}	Runoff coefficient for the long plot	[ ]
C_1	Runoff coefficient for the short plot	[ ]
km	Surface roughness	[ ]
β_b	Soil moisture factor	[ ]
α_f	Green vegetation fraction	[ ]
β	Bowen ratio	[ ]
EF	Evaporative fraction	[ ]
LAI	Leaf Area Index	[ ]
ω	Scattering coefficient	[ ]
α_v	Canopy surface albedo	[ ]
α_{v0}	Base albedo	[ ]
α	Surface albedo	[ ]
α_{ca}	Crop surface albedo	[ ]
α_c	Albedo fully developed crop canopy	[ ]
α_u	Albedo of the underlying soil surface	[ ]
α_{uw}	Effect of soil wetness	[ ]
α_l	Single leaf albedo	[ ]

α_{cS}	Albedo of a semi-infinite canopy	[ ]
k_e	Extinction coefficient	[ ]
f_c	Weighting factor for canopy	[ ]
f_l	Weighting factor for leaves	[ ]
Ω	Decoupling coefficient	[ ]
C_h	Surface exchange coefficient for heat and moisture	[ ]
B	Zilitinkevich coefficient	[ ]
ν	Kinematic molecular viscosity	[ ]
a_T	Thermal coefficient	[ ]
I_{p0}	Factor severe drought	[ ]
m_a	Daytime mean optical air mass at sea level	[ ]
P	Relative station atmospheric pressure	[ ]
a_l	Relative age of leaves	[ ]
d_r	Relative stress-calendar	[ ]
W	Relative stem cover	[ ]
F_l	Canopy leaf cover	[ ]
f_{HF}	Function of vegetation height	[ ]
f_a	Function of relative leaf age	[ ]
f_{ss}	Function of the seasonal biological stress	[ ]
f_p	Function of the climatic factor	[ ]
f_{mp}	Function of the optical air mass factor	[ ]

1   GENERAL INTRODUCTION

1.1   Introduction

According to de Sherbinin (2002), land-use is the term that describes human uses of the land, or immediate actions modifying or converting land cover. It includes human settlements, protected areas and agriculture. In this study, the term land-use refers to agricultural activities (extension of cropland), transhumance (livestock extension), wood extraction and the subsequent attributes (clearing of the vegetation, overgrazing and bush fire). Land-use intensity is used for comparison purposes, and it is the degree of exploitation that characterizes a particular site in the same agro-ecosystem.

Land-use is the major cause of the widespread decline of the vegetation cover in West Africa, especially in the Volta Basin, resulting from the slash-and-burn practice or shifting cultivation (Duadze, 2004). It is also the main factor affecting the hydrological cycle in the Volta Basin (Andreini et al., 2000). In West Africa, especially in Burkina Faso, economic motivations and government policies stimulate people to cultivate the land in order to increase agricultural production. This has been achieved by an expansion of the cultivated area as well as by higher productivity per hectare. The need for new agricultural land was a strong argument for the extensive clearing of natural vegetation (Ungaro et al., 2004). The situation in the White Volta River (sub-basin of Black Volta) illustrates this widespread environmental problem. According to Mahe et al. (2005), the natural vegetation in the White Volta basin declined from 43 % to 13 % of the total basin area between 1965 and 1995, the cultivated areas being increased from 53 % to 76 %, and the area of bare soil nearly tripled from 4 % to 11 %.

However, it has been widely recognized that the vegetation plays an important role in the modulation of the earth's climate and hydrological system (Dale, 1997). The changes in the vegetation cover have potential effects on the local and global environment with regard to the increase in the concentration of atmospheric carbon dioxide, changes in temperature and precipitation, loss of biodiversity, increased runoff and flooding, soil erosion, watershed process and to the biogeochemical cycles (Helmer et al., 2000). Similarly, the morphology of the vegetation influences the amount of absorbed incoming shortwave radiation as well as the aerodynamic resistance affecting the turbulence exchanges of momentum, heat, and moisture. Also, changes in the

vegetative cover are associated with changes in the vegetation physiology, which could alter the surface fluxes in the absence of other forcing factors and consequently the climate both at regional and global scales (Dale, 1997; Bounoua et al., 2002). To prevent an exhaustive utilization of natural resources and agricultural land in the Volta basin, a project was initiated entitled: *Impact of changing land cover on the production and ecological functions of vegetation in inland valleys in West Africa (VinVal).* The overall objective of this project was to develop a tool for integrated land-use planning at a watershed scale to improve the sustainable agricultural production systems. This tool should take into account the balance between production and protection objectives and should assist in making informed decisions on allocation of land-use activities of smallholder farmers across the watershed on both agricultural and natural land. Such decisions are based on knowledge of the productive value of these land-use activities and their impact on ecological functions. With this purpose, an accurate knowledge of the seasonal dynamics of surface fluxes introduced by agricultural activities is necessary. Therefore, the first focus of this research was*:* How does the land-cover change coupled to seasonal farming activities affect actual evaporation (E)? The relevance of this question finds its response in the fact that E is an important component of the ecosystem water balance and strongly related to the gross ecosystem production in terrestrial vegetation (Law et al., 2001). According to Oguntunde (2004), E is responsible for 70 % of the lateral global energy transport and plays an important role in the redistribution of water on the earth's surface (Mauser and Schädlich, 1998). Consequently, its quantification is critical for water resources management, and its accurate estimation is a basic tool for computing the water balance (Pereira et al., 1999). E is also needed in the evaluation of energy partitioning, which is an important part in the understanding of the link between the surface energy balance and climate in a given environment. However, despite the importance of E, understanding of its process in tropical zones is less advanced than in temperate regions. In general, the models available for the estimation of E are calibrated for the temperate regions, where the feedback mechanisms in the boundary layer are related to the soil wetness. For the tropical zones, especially for the savanna regions, these feedbacks are more related to the way the vegetation releases water into the atmosphere (Schüttemeyer, 2005). Similarly, the effect of land-use on E is obvious, but there is no real assessment

available on that issue in West Africa, where competition for water resources is very high.

Understanding the process of the actual evaporation is also an integral part of the objective of the GLOWA-Volta project, which aims to *analyze the physical and socio-economic determinants of the hydrological cycle and to develop a scientifically sound decision support for the assessment, sustainable use and development of water resources in the Volta Basin* (van de Giesen et al., 2002). This objective involves the understanding of the biosphere-atmosphere interactions considering the effect of the climate on the ecosystem functions and the potential feedbacks of the land surface to the physical climate (Oguntunde, 2004). The eco-hydrological models, which require a spatial and a temporal quantification of the surface fluxes, are relevant for this purpose.

Land-use impacts also surface runoff and its process. Removal of the vegetation from the watershed can result in a significant increase in the surface runoff because of the decrease in the interception of rainfall by the tree canopy as well as greater surface sealing. The phenomenon is obvious in West Africa where, in spite of the decline in the annual rainfall, increasing surface runoff is observed at the outlet of the major gauged basin (Mahe et al., 2005). However, as in all research fields, hydrological research in West Africa is less advanced than the other regions of the world, and the studies on the surface runoff are limited to the empirical formulas that relate the watershed characteristics to one characteristic of the flow at the watershed outlet (e.g. van de Giesen et al., 2000). The most important of these studies are those on the average yearly outflow or the 10-year peak flow (Rodier and Auvray, 1965; Rodier, 1976; Puech and Chabi-Goni, 1984). The empirical formulas are more oriented on the engineering purposes and are not relevant for water resources management. Recently, some physically based approaches have been applied in Côte d'Ivoire, Burkina Faso, Ghana (van de Giesen et al., 2000; Ajayi, 2004) related to the scale effect on surface runoff and more oriented towards water resources management at field level. These studies showed that not all the water that can be observed on the surface during a rainstorm reaches the bottom of the slope. This scale effect is found to be related to the spatial variability of soil physical properties (Julien and Moglen, 1990) and the temporal dynamic of rainfall intensity (van de Giesen et al., 2000). Actually, there is an increasing interest of researchers to understand this effect, because the water

redistribution across the watershed is particularly important for agricultural water management. If the scale effect is pronounced, only some part of the watersheds needs to be protected, i.e, mainly the lower part. In contrast, if the scale effect is negligible, all parts of the watershed contribute to the surface runoff and the whole watershed needs to be managed (van de Giesen et al., 2004). The handling of the scale effect on surface runoff in land-use planning can contribute substantially to both reducing the cost of watershed management and to maintaining the soil quality. Therefore, the second focus of this research contributes to the study of the scale effect. The findings can be regarded as a contribution to a better understanding of the role of the vegetation cover in pronouncing the scale effect. It could also be a good argument for decision-makers for preventing an extensive clearing of vegetation.

In this research, we use the measurement of surface fluxes and automatic weather data (from May 2003 to November 2004), a field based measurement of the surface runoff at the plot and on the watershed scale, and other complementary measurements to achieve the objectives. When compared to Sahelian Energy Balance EXperiment (SEBEX) (Sellers et al., 1996) and Hydrological and Atmospheric Pilot Experiment-Sahel (HAPEX-Sahel) (Goutorbe et al. 1997), this study is the first long-term eddy covariance measurement ever reported in the savanna zones of West Africa The study will help to understand the energy partitioning in the savanna, and the results can be easily extrapolated to other areas of the region, since they all share similar agro-ecosystem.

The specific objectives are:

1. To investigate the energy balance closure over *Vitellaria paradoxa* (sheanut tree), over the *Sorghum vulgare* (sorghum) and maize;

2. To investigate the surface fluxes and to develop new alternative models for the estimation of the actual evaporation on a monthly time step;

3. To quantify the roughness length for momentum and the effect on the land surface models on a seasonal basis and on a daily basis;

4. To measure *in situ* and model surface albedo for sheanut trees and sorghum;

5. To investigate the scale effect on surface runoff in the savanna zone under a monomodal rainfall pattern and to show the influence of vegetation cover on this process.

1.2   Research justification

This research finds its justification in the scarcity of micrometeorological and hydrological studies in the savanna zones of West Africa as compared to the temperate regions. With respect to the micrometeorological studies, the only available documentations and serious research are the SEBEX project and the HAPEX-Sahel project. These studies are limited in time and space and give a partial insight into the dynamics of the surface fluxes in the savanna vegetation. According to Oguntunde (2004), recent research on improving the representation of the land-surface-atmosphere interactions within General Circulation Models (GCMs) led to the investigation of a wide variety of the different Soil-Vegetation-Atmosphere Transfer (SVAT) schemes. Forty-four different SVAT models were identified with the majority of them are calibrated to temperate zones. Similarly, most of the SVAT models failed to simulate the dynamics of the surface fluxes in the savanna zone, because the feedback mechanisms in the boundary layer in temperate zones to which the models were run are completely different to those in savanna zones (Schüttemeyer, 2005). Therefore, pertinent to the objective of the VinVal and GLOWA-Volta projects, there was a need for a long-term investigation of the savanna surface fluxes to improve the limited knowledge of the effect of land-use on surface fluxes, especially on actual evaporation. Beyond local application, the research will also improve our understanding of the role of savanna vegetation in the regional and the global climate circulation.

Similar to micrometeorological studies, hydrological studies, especially of surface runoff, are less advanced in tropical zones than in temperate zones (van de Giesen et al., 2000). In the particular case of West Africa, rough empirical formulas based on the research of ORSTOM and CIEH (Valentin, 1981; Albergel, 1987) are appear in the literature with respect to surface runoff. These empirical formulations were designed for large-scale estimation of the surface runoff in time and space and for engineering purposes. These empirical formulations do not have explicit representation of scale effect on surface runoff or are not an integrant part of the process of the surface runoff. Therefore, there was a need to show the relevance of scale effect on surface runoff in the savanna zone. This will be useful for an accurate representation of the scale on surface runoff effect in model of the savanna zone of West Africa.

1.3 Thesis outline

This report is divided into eight chapters. Chapter 2 focuses on the general descriptions of the study area, energy fluxes and actual evaporation as well as surface runoff. The first specific objective is investigated in Chapters 3 to 6, while the second objective is investigated in Chapter 7. Chapter 3 shows the quality and the representativeness of the data by the energy balance closure and the footprint analysis. Chapter 4 describes the inter-annual energy partitioning and the implication on the estimation of the actual evaporation and surface conductance. Chapter 5 is an extension of Chapter 4 and discusses the effect of the seasonal dynamics of vegetation cover on land surface models, while Chapter 6 focuses on surface albedo measurements and modeling for sheanut nut trees and sorghum canopies. Chapter 7 focuses on the study of the scale effect on surface runoff under different land-use conditions. The Final conclusion summarizes and discusses the main results of the study. Chapters 3 to 7 are each presented as articles and include the respective methodology and results.

2   GENERAL DESCRIPTION OF METHODS AND MATERIALS

2.1   Description of the study area

According to the selection criteria required to meet the overall objective of the VinVal project, three small watersheds were selected in the province of Kompienga (10°55&11°55 N-01°25&01°23 E). These watersheds were in the same agro-ecosystem and showed a gradient of agricultural land-use intensity from high (Tanyele), medium (Bounou) to no agricultural land-use with natural vegetation (Sambouali). All watersheds covered an area of about 10 km^2 (Kabore et al., 2003). Figure 2.1 shows the location of the watersheds.

These two major land-use types were practiced in these watersheds: Agriculture activities were carried out by the local communities (Gourmantche and Mossi) during the rainy season, especially in Tanyele and Bounou, and in all watersheds transhumance was practiced by shepherds (Fulani). The crops were rain-fed crops such as sorghum, millet, maize, sesame and cotton. The population living in the watersheds was about 765, 706 and 330 in Tanyele, Bounou and Sambouali, respectively (Diallo et al., 2002).

2.1.1   Climate and vegetation

According to the phytogeographical classification of White (1983), the south-east region of Burkina Faso belongs to the Sudan climate zone. For the study area, the annual precipitation lies between 900 and 1000 mm (Kabore et al., 2003). A rainfall peak was observed between May and October with another pronounced peak in August or September. Temperatures are very high with a peak of about 40 °C in March-April. Lower temperatures were observed in August and between December and January (22 °C on average). The region is characterized by the *Vitellaria paradoxa* tree, which dominates the vegetation cover. Other important trees are *Parkiia biglobosa*, *Andansonia digitata*, and *Anea microcarpa*. The fallow land are dominated is *Combretum micrantum* and the herbaceous stratum by *Androogon gayanus*, and *Penninsetum pedicelatum*.
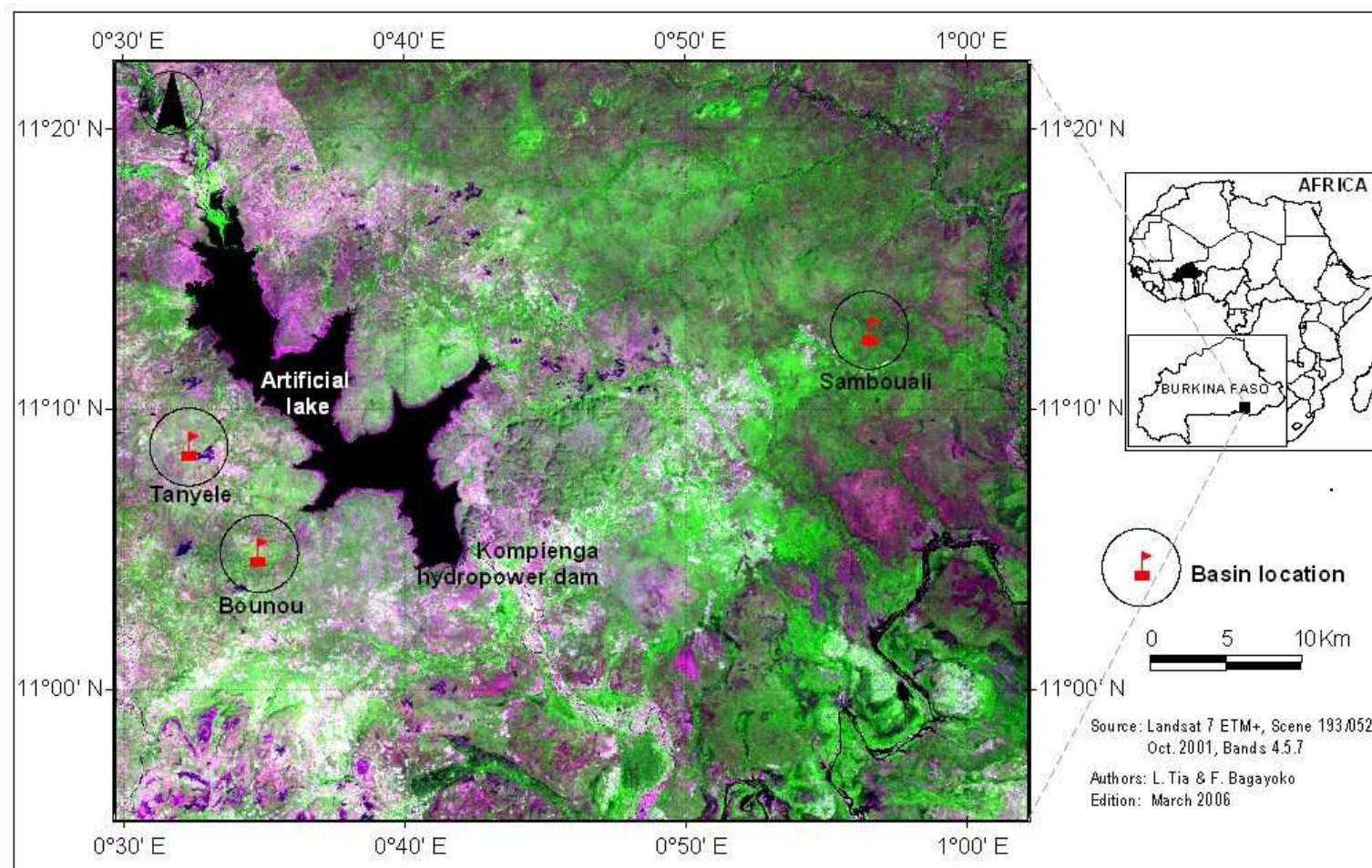
Figure 2.1: Location of the experimental sites: Tanyele (high land-use intensity); Bounou (medium land-use intensity); Sambouali (without agricultural land-use and covered with natural vegetation)

2.1.2 Geology, soil and land cover

In all the watersheds, the up-land and the low-land are characterized by breastplate mounds and some emergent granite rock formations, which mark their crests. The terrains are flat (slope ≤ 3 ‰) and the main type of soil is Lexisoil (> 60 %) as is true in most of West Africa (Braimoh, 2004). With respect to the soil texture, in Tanyele, the soil consists of sandy loam (71 % sand, 24 % silt and 5 % clay), in Bounou of loam (34 % sand, 48 % silt and 16 % clay) and in Sambouali of clay loam (25 % sand, 47 % silt and 28 % clay). Tables 2.1 and 2.2 show the major types of soil and land cover in each watershed.

Table 2.1:   Soil types and the relative percentage in each watershed

Soil type	Tanyele (%)	Bounou (%)	Sambouali (%)
Lexisoil	63	46	63
Gleysoil	31	0	6
Cambisoil	0	45	23
Marginal soil	6	9	6

Source: Kabore et al. (2003)

Table 2.2:   Land cover types and their relative percentage in each watershed

Landcover type	Tanyele (%)	Bounou (%)	Sambouali (%)
Farm land	20	18	0
Shrub land and old fallow	76	72	41.5
Woody savanna	3.5	9.8	58
Herbaceous savanna	0.5	0.2	0.5

Source: Kabore et al. (2003)

2.2   Energy fluxes and actual evaporation

The main energy fluxes used in hydrological modeling are shortwave and longwave radiation, sensible heat, latent heat and ground heat flux. Solar radiation is the main source of shortwave radiation, while longwave radiations are from the reflection process at earth's surface, cloud and fine particles in the atmospheres. Sensible heat (H) and ground heat flux (G) are related to the heat transfer resulting from the temperature gradient between two surfaces (Clark et al., 1989). Sensible heat transfer occurs between an evaporating surface (free water surface, soil surface and vegetation) and the atmospheric overhead, while the ground heat flux is the result of a difference in temperature between two regions in the soil. If the evaporating surface is warmer than

the ambient environment, then the sensible heat flux will be from that surface to the environment and vice-versa. Similarly, the latent heat flux (λE) represents the energy removed from the evaporating surface in the liquid-to-vapor phase change of evaporated water and is the product of the heat of vaporization (λ) and the evaporation rate (E).

2.2.1   Definition of the different form of evaporation

Evapotranspiration is the combined process of direct evaporation from the soil surface or the free water surface and the transpiration from the plant leaves and intercepted water to satisfy an atmospheric demand. When the water supply is limited, the resulting evapotranspiration is called *actual evapotranspiration*, while the term potential evaporation (Penman,1948) is used to describe the maximum or the potential level of evaporation resulting from a non-limiting water condition and the satisfaction of the energy budget (Clark, 1989). The reference crop evaporation (Burman et al., 1980; Doorenbos and Pruitt, 1977) is commonly used and refers to the evaporation from a specified uniform green grass surface, which is actively growing, of uniform height of 12 cm, a fixed canopy resistance of 70 s m^{-1} and an albedo of 0.23, completely shading the ground, and under well-watered conditions.

2.2.2   Factors influencing energy fluxes and actual evaporation

a. Abiotic factors

Energy fluxes are mainly influenced by solar radiation (shortwave radiation: 0.3 to 4 micrometers) constituting the primary input of energy. A part of this shortwave radiation is reflected as long-wave radiation (4 to 80 micrometers, Campbell, 1977) or absorbed by clouds, fine particles in the atmosphere and the earth surface. The reflectivity of a surface to the shortwave solar radiation is known as the surface albedo. The higher the reflectivity of the surface, the higher the surface albedo. The budget of the reflecting and the absorbed part of solar radiation is known as net radiation (R_n). Therefore, sensible heat, latent heat and ground heat flux depend on the net radiation. The percentage of net radiation allocated to each of these components depends on the availability of moisture. When moisture being abundant, the latent heat flux (λE) will be the main consumer of the net radiation, while the sensible (H) and ground heat flux (G) will be the main consumer in dryer areas. Energy fluxes and actual evaporation

depend on the ambient air temperature (T_a) as well as on the relative humidity (R_h). Both parameters determine the vapor pressure deficit (VPD) and strongly impact the actual evaporation rate of the vegetation canopy (Jarvis and McNaughton, 1986).

Air movement also plays a major role in the transport of energy fluxes. Both sensible heat and latent heat fluxes are transported actively by turbulent eddies in the air as well as the water vapor transpired from the plant (Clark, 1989). Wind can also help to maintain a significant vapor pressure deficit around the plant canopy.

b. Biotic factors

Energy fluxes are affected by the physiological properties of the vegetation canopy, i.e, by their albedo, type, variety and development stage. For instance, young crops have a higher surface albedo than mature crops (Oguntunde, 2004).

2.2.3   Measurement techniques

Several techniques and methods for measuring energy fluxes and actual evaporation are available in the literature. Recently, efforts have been made to determine energy fluxes, spatial distribution and temporal variability of actual evaporation by modeling approaches that are facilitated by both remote sensing and GIS-based techniques. In the 1930s, different methods such as weighing lysimeters, large-tree porometers, ventilated chambers, profile micro-meteorological measurement, and injection of indicator substances were developed to estimated actual evaporation. Large-aperture scintillometers also provide a good estimation of the actual evaporation (Schüttemeyer, 2005) as well as sap flow techniques (Granier, 1985 and 1987). In the past decade, the use of the eddy covariance (EC) technique in the surface layer investigations has increased (Martano, 1999). It provides a tool that allows a direct measurement of energy fluxes at a canopy scale. The theoretical basis of this technique is straightforward (Brutsaert, 1982; Sumner, 1996). It provides a direct flux measurement through the combination of wind speed, air humidity and temperature data, without any crude assumption on turbulent diffusivities, shape of the wind profile or influence of the turbulent forces. Nevertheless, the requirements on the instrumentation are quite restrictive. According to Brutsaert (1982), the inherent difficulties are: 1) the sensor must have a sufficiently fast response time, i.e., between 10 to 50 Hz; 2) the average

period must be sufficiently long (at least 30 min), while the average time should be as short as possible to guarantee stationary time series without the effect of any trend, but should also be long enough to cover even the slowest fluctuations of the turbulent spectrum; 3) the orientation and placement of the velocity sensors should be precise. In addition to these constraints, the sensors have to cleaned regularly (once a week) with distilled water. The system consists of two major sensors (Figure 2.2): the sonic anemometer (e.g. Gill Instruments Ltd., UK) measuring wind velocity, air temperature; the Krypton hygrometer (e.g. model KH2O, Campbell Scientific, UK) for the measurement of air humidity.
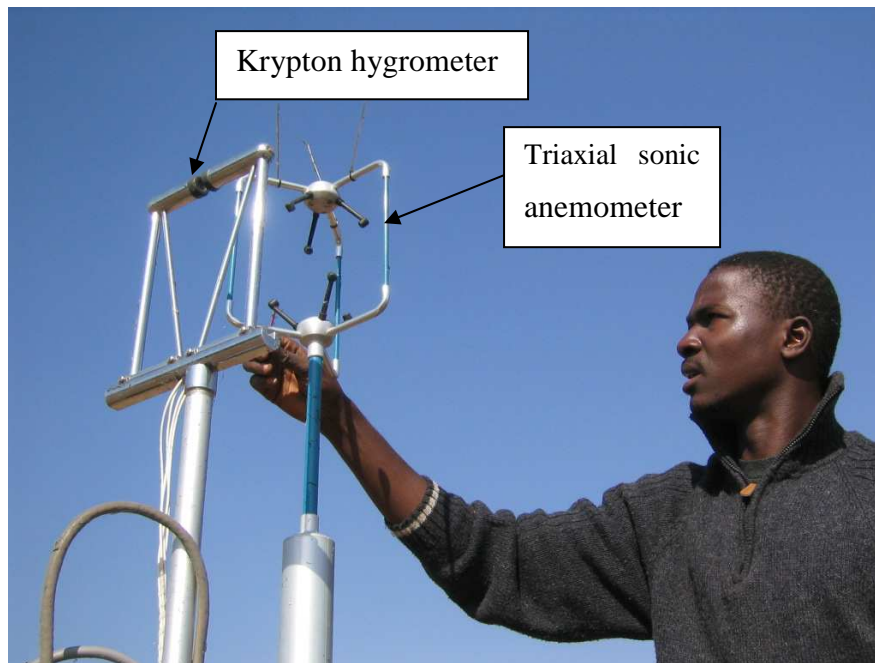

Figure 2.2:   Eddy covariance devices

a. Theoretical framework of the eddy covariance method

The eddy covariance system determines the turbulent fluxes of water vapor, momentum, sensible heat flux or and any other admixture from covariance (Brutsaert, 1982). The method is based on the following three laws:

1. Conservation of water vapor;
2. Conservation of momentum for an incompressible fluid with constant viscosity;
3. Conservation of energy for an incompressible fluid.

These laws applied in an Atmospheric Boundary Layer (ABL) allow establishing the equations of latent heat and sensible heat flux.

What is atmospheric boundary layer (ABL)?

In the atmosphere, the largest changes in wind, temperature and humidity usually take place vertically and very close to the surface (Brutsaert, 1982). For this reason, the air near the surface may be regarded as a boundary layer. Therefore, the atmospheric boundary layer can be defined as the lower part of the atmosphere where the nature and properties of the surface affect the turbulence directly. Under normal atmospheric conditions, there are numerous factors that affect the major mass, momentum, and energy transport phenomena in the boundary layer. However, if the ABL is considered under the simplest conditions, satisfactory results of the energy fluxes can be obtained. These conditions may be specified as a steady motion, parallel to the uniform plane surface, intermediary between the cyclonic and the anti-cyclonic flow driven by parallel equidistant straight isobars.

Determination of latent and sensible heat flux

As previously mentioned, the eddy covariance method determines the latent heat flux by the law "Conservation of water vapor". In the absence of the phase of transition water vapor in the air is a conservative scalar admixture. Any conservative substance admixed in a moving fluid is transferred relative to the fixed coordinate system, first by convection with the fluid, and next by molecular motion superimposed on the convective motion of fluid (Brutsaert, 1982). The total specific mass flux is:

$$F = \rho_v V + F_m \tag{2.1}$$

where $V = iu + jv + kw$ (u, v and w are the components of the velocity following the x, y and z axes and i, j, k are vectors) is the velocity of the air, F_m is the specific mass flux due to molecular diffusion, and ρ_v is the mass of water vapor.

F_m may be taken to be proportional to the local gradient of the water vapor density, in accordance with Ficks's law:

$$F_m = -k_v \nabla \cdot \rho_v \qquad (2.2)$$

where k_v is the molecular diffusivity of water vapor in the air.

The equation of continuity of the water vapor in the absence of sinks is:

$$-\nabla \cdot F = \frac{\partial \rho_v}{\partial t} . \qquad (2.3)$$

Similarly, the equation of continuity of the moist air is:

$$-\nabla (\rho_v) = \frac{\partial \rho}{\partial t} \qquad (2.4)$$

Upon combining Eq. (2.1), (2.3) and (2.4) we have:

$$-(v \cdot \nabla) q - \rho_a^{-1} \nabla \cdot F_m = \frac{\partial q}{\partial t} . \qquad (2.5)$$

If ρ and k_v are assumed to be spatially constant, substitution of Eq. (2.2) in Eq. (2.5) yields:

$$\frac{\partial q}{\partial t} + (v \cdot \nabla) q = k_v \nabla^2 q . \qquad (2.6)$$

where $q = \dfrac{\rho_v}{\rho_a}$ is the specific air humidity, ρ_v is the density of water vapor and ρ_a is the density of moist air.

Eq. (2.6) is the basic equation of conservation of the water vapor, but is not directly applicable, because the atmosphere is almost always turbulent. To simplify this equation, Reynolds (1894) decomposed the dependent variables into means and turbulent fluctuation, namely:

$$u = \bar{u} + u' \ , \ v = \bar{v} + v' \ , w = \bar{w} + w' \ \text{and} \ q = \bar{q} + q'$$

After applying the customary time average over a suitable time period and using the equation of continuity ($\nabla \cdot \bar{V} = 0$) we have:

$$\frac{\partial \bar{q}}{\partial t} + \bar{u}\frac{\partial \bar{q}}{\partial x} + \bar{v}\frac{\partial \bar{q}}{\partial z} + \bar{w}\frac{\partial \bar{q}}{\partial z} = -\left[\frac{\partial\left(\overline{u'q'}\right)}{\partial x} + \frac{\partial\left(\overline{v'q'}\right)}{\partial y} + \frac{\partial\left(\overline{w'q'}\right)}{\partial z}\right] + k_v \nabla^2 \cdot \bar{q} \quad (2.7)$$

In the ABL, because of the condition that the horizontal gradients and vertical velocities are negligible as compared to the vertical gradients and horizontal velocities, Eq. (2.7) becomes:

$$k_v \frac{\partial^2 \bar{q}}{\partial z^2} - \frac{\partial\left(\overline{w'q'}\right)}{\partial z} = 0. \quad (2.8)$$

In the sub-layer of ABL where the vertical turbulent fluxes do not change appreciably from their value at the surface, Eq. (2.8) is similar to:

$$E = \rho_a \overline{w'q'} \quad (2.9)$$

This quantity multiplied by the latent heat of vaporization (λ) gives the latent heat flux. When a similar procedure is applied to the law of the conservation of energy for an incompressible fluid, sensible heat flux can be determined and is expressed as follows:

$$H = \rho_a c_p \overline{w'\theta'} \quad (2.10)$$

where c_p is the heat capacity of the air, and θ' is the fluctuation of the potential temperature from the mean.

2.3　Surface runoff

Surface runoff is the water running over land resulting from the infiltration excess during a rainfall (or snow water melt) event. Horton (1933) was the first to study this process, and proposed an infiltration-capacity-based model now referred to as the Hortonian overland flow. Later, Dunne (1970, 1978) proposed a saturation-based (saturation excess) runoff generation process and outlined the importance of a rising water table in initiating and sustaining surface runoff (Ajayi, 2004). There are several well-documented studies in the literature on surface runoff, but most of them were carried out in temperate regions. Likewise, because of agricultural interests and management purposes, many studies were related to the understanding of soil erosion processes and nutrient dynamics (Littleboy et al., 1996; Ajayi, 2004) by model- or statistics-based runoff plot measurements or a catchment observation. Plot-based measurement and the measurement of rainfall intensity with appropriate rain gauges are the basis for better insight into the process of surface runoff and understanding of the factors influencing that process at a small scale.

2.3.1　Factors influencing surface runoff

The combined effect of rainfall intensity and the physical properties of the soil surface are the main factors influencing the surface runoff generation process. These factors interact simultaneously and the magnitude of each of them depends on the circumstances, the study area and the method.

a. Temporal dynamics of rainfall intensity

Rainfall is the primary input in the runoff generation process, because it provides water the system, and when this supply surpasses a certain level, surface runoff occurs depending on the surface physical properties. In West Africa, some of the available empirical models use the annual rainfall to evaluate the yearly outflow or the 10-year flow. However, in surface runoff processes rainfall intensity better description, which is not constant over time. It can be of higher or lower intensity which determines the time in which the infiltration capacity is surpassed, after which point all subsequent rainfall will generate surface runoff. The repartition, velocity and discharge level depend on the surface properties and their spatial variability.

b. Spatial variability of soil physical properties

The spatial variability of soil physical properties is related to hydraulic conductivity, sorptivity, microtopography, slope and the vegetation cover (surface roughness). From one point to another or one area to another, these parameters can change significantly resulting in different responses in surface runoff. These parameters are also related to the land-use pattern. The importance of microtopography is sometimes associated with the effect of the tillage practice controlling the magnitude and the distribution of the surface runoff (Ajayi, 2004). Changing land-use results in changes in the canopy cover and the degradation of the vegetation cover (leaf area index), and increases the soil disturbance. This affects soil roughness and thus surface runoff, and soil erosion increases (Navar and Synott, 2000; Kincaid et al., 1966; Lane et al., 1997). Different land-use may also increase or diminish soil infiltration, ultimately affecting surface runoff. Fieldler et al. (2002) show the effect of overgrazing on the overland flow in semi-arid grassland with its effect on the point-scale infiltration conductivity resulting in an increase in surface runoff. Bush fires and a short-term change in vegetation based on cropping pattern can also change surface runoff processes (Ajayi, 2004).

c. Scale effect on surface runoff

The understanding of the scale effect on surface runoff has gained increased interest in the past two decades. It depends on both temporal dynamics of rainfall intensity (van de Giesen et al., 2000) and spatial variability of soil physical proprieties (Yair and Lavee, 1985; Lal, 1997; van de Giesen et al., 2000; Masiyandima et al., 2003; Joel et al., 1985; Esteves and Lapetite, 2003). All these studies have provided evidence that not all the surface runoff that can be seen on the surface during a rainstorm may reach the bottom of the slope. The longer the slope, the higher the reduction of surface runoff. However, Sharman et al. (1983), and Lal (1997) concluded that an increasing slope length induces a corresponding increase in runoff volume from a plot. Their results show that the scale effect might be dependent on the local situation even if they are some of the few authors to come tot this conclusion.

2.3.2 Measurement techniques

Surface runoff is commonly measured using runoff plots or by a discharge measurement structures at the outlet of the catchment.

a. Plot based measurement

In the plot-based measurement technique, runoff plot are installed on the trial site. The plot can be square or rectangular with a variable area. The plot is oriented downhill and is connected by a gutter to a runoff collector (in general buried oil drums). If the size of plot is larger, two or more collectors can be used to receive all surface runoff from the plot. External runoff is prevented from running into the plot by a metal sheet with a height of about 20 cm deeply buried in the soil (Figure 2.3). Rain is prevented from entering the collectors through screw-tops or appropriate lids. The total runoff from the plot is measured by emptying the oil drum using a measuring cylinder or by direct reading if a graduated bucket is inserted in the oil drum. The main difficulty of this method is that cumulative runoff from several rainfall events could be attributed one rainfall event. For instance, several rainfall events can take place in the night after which only one reading is made.

Figure 2.3:   Runoff plots installed in Tanyele. Left: short runoff plot (1 m²); right size: long runoff plot (10 m²)

b. Measurement at the outlet of the watershed

For the whole watershed, discharge measurement structures are used at the outlet. Because of their simplicity, H-flumes are generally used. However, the structure can also be built of concrete (Figure 2.4) and the estimation of the discharge is done by frequent reading of the level meter measuring water level passing over the structure.

The water level value is then used in to the discharge equation corresponding to the respective structure to estimate the total discharge. Recently, the use of data-logging pressure transducers has increased. Here, in defined time steps, the pressure exercised by the layer of water passing over the measurement structure is recorded. The difference between the pressure recorded (P_b) and ambient atmospheric pressure (P_a), gives the depth of the layer of water passing over the measurement structure. The method is more accurate than the traditional way of reading on water level-meter and allows an accurate monitoring of peak flows.

Figure 2.4:   Construction of weir for discharge measurement at watershed scale in Tanyele

3 ENERGY BALANCE CLOSURE AND FOOTPRINT ANALYSIS[1]

3.1 Introduction

The energy balance of the earth's surface is a fundamental component of all models of land-surface/atmosphere interaction (Culf et al., 1997). The energy balance stipulates that the available energy at the surface (difference between net radiation and ground heat flux) is equal to the sum of sensible heat and latent heat flux. When the components of the energy balance are measured separately, a perfect balance is seldom obtained but can be approached reasonably if the measurements have been well conducted. Therefore, micrometeorological researchers always use the energy balance closure to test for the reliability and quality of their measurements. A dataset with an energy balance closure within 10 % is often considered reliable (Culf et al.,1997).

The review of the literature reveals that Russian expeditions in the 1970's and the 1980's were the first to report the problem of the energy balance closure. In these studies, the energy balance closure was up to 80 % (Elagina et al., 1978; Elagina et al., 1973; Orlenko and Legotina, 1973; Tsvang et al., 1987). Wilson and Baldocchi (2000) obtained a similar result over temperate deciduous forest. More recently, better results were obtained. For example, Shutteworth et al. (1984) reported 7 % over tropical forest, Jarvis et al. (1997) found 3 % over boreal black forest and Finch and Harding (1998) recorded 5 % over pasture. Similarly, Aubinet et al. (2000) presented some energy balance closures of the EUROFLUX forest site as the plot of $(R_n - G)$ versus $(H + \lambda E)$. Good regression fits were obtained with the slope varying from 0.99 in the best case to 0.77 in the worst. In West Africa, this issue has not received much attention because of the lack of micrometeorological studies. An exception is the energy balance closure over pattern-woodland and fallowed vegetation determined during the HAPEX-Sahel project in Niger (Kabat et al., 1997) and more recently by Shüttemeyer (2005) in central and Northern Ghana. In the light of these studies, it appears that a good energy balance closure depends on the instruments used, climate (wind turbulence), measurement techniques and especially vegetation types.

---

[1] Material in this chapter is accepted for publication in Hydrology and Earth System Sciences (HESS) with N.C. van de Giesen and S. Yonkeu as co-authors.

The representativeness is also an important focus of the reliability and the quality of the micrometeorological measurements. This representativeness is often determined by analysis of the footprint, i.e., the effective fetch and the sensor footprint or source area (Ghash, 1985; Lloyd, 1994; Baldocchi, 1997; Schimid, 2002). However, researchers do not pay much attention to the positioning of the measurement station with respect to the dominant wind direction, which can have a significant effect on the representation of the measurements. In most of the cases, the location of the station is appreciated with the aspect of the environment, the best one being a flat terrain free of tall trees and hills. As the eddy covariance (EC) technique consists of a point measurement of an average flux over a given area (Culf et al., 1997), if the objective of the study is to investigate the surfaces fluxes over a particular vegetation cover, special attention should be paid to covering a higher number of trees, so that the measured fluxes are representative of such vegetation. This becomes more relevant in the savanna regions, especially on farmland, as the vegetation consists of very sparse trees. At the same time, two major wind regimes characterize the savanna region of West Africa such as the Harmattan wind (during the dry season) from the north-east and the monsoonal wind (during the rainy season) from the south. In order to obtain representative surface flux samples over a terrain in such region, the station should be installed such that the fetch area covers the higher number of trees within the dominant wind direction. This aspect is seldom taken into account in the micrometeorological studies. Therefore, the present research conducted within the framework of the GLOWA-Volta (van de Giesen et al.,2002) and VinVal projects, is aimed at contributing to the energy balance closure issue over the savanna vegetation, especially over *Vitellaria paradoxa* (sheanut tree) and *Sorghum vulgare* (sorghum). In addition, the relevance of the dominant wind direction in the representativeness and the quality of the flux measurement is discussed.

The study covers four contrasting periods: the dry season (January to March 2004), the transition period between the dry and the rainy season (April to May 2004), the rainy season (June to September 2004) and the drying up period (mid-September to November 2004). The results can be useful and representative of the savanna zone of West Africa, because sheanut trees dominate the vegetation cover and sorghum is common crop grown widely.

3.2 Methods and materials

All climatic variables used in the analysis, except net radiation (R_n) and ground heat flux (G), were directly measured hourly with an Eddy Covariance (EC) station at 10 m height or processed from the EC raw data. The station was provided with a Krypton Hygrometer (model KH2O, Campbell Scientific, UK) for the measurement of air humidity, while wind speed (u), wind direction (Dir) and air temperature (T_a) were measured with a triaxial sonic anemometer (Gill Instruments Ltd., UK). Sensible heat flux (H) and latent heat flux (λE), friction velocity (u^*), Monin-Obukhov length (L) and necessary corrections were processed from the raw data with ALTEDDY software (Elbers, 2002). The variables u, Dir, and T_a were also measured at 2 m height above the ground surface with an automatic weather station.

3.2.1 Trial site

The site was located in eastern Burkina Faso (11°07' N; 0°33' E). Agricultural production was intensive. The site is characterized by the Sudan climate and vegetation, and the rainfall pattern is monomodal. The main soil type is Lexisoils. The EC station was installed on farm land (average slope of 2 ‰) surrounded (during the dry season) by sheanut trees with an average height of 8 m. The average distance between the trees was 15 m, and density was about 17 trees/ha. During the rainy season, crops and grasses grow and alter the roughness length for momentum over time. Crop density was about 4 plants/m^2. Figure 3.1 shows the location of the study area and gives an impression of the vegetation cover during the rainy and dry seasons.

3.2.2 Energy balance closure

The energy balance closure is usually tested by comparing the sum of sensible heat and latent heat flux ($H + \lambda E$) and the difference between net radiation and ground heat flux ($R_n - G$). R_n and G were estimated with commonly used equations available in the literature.
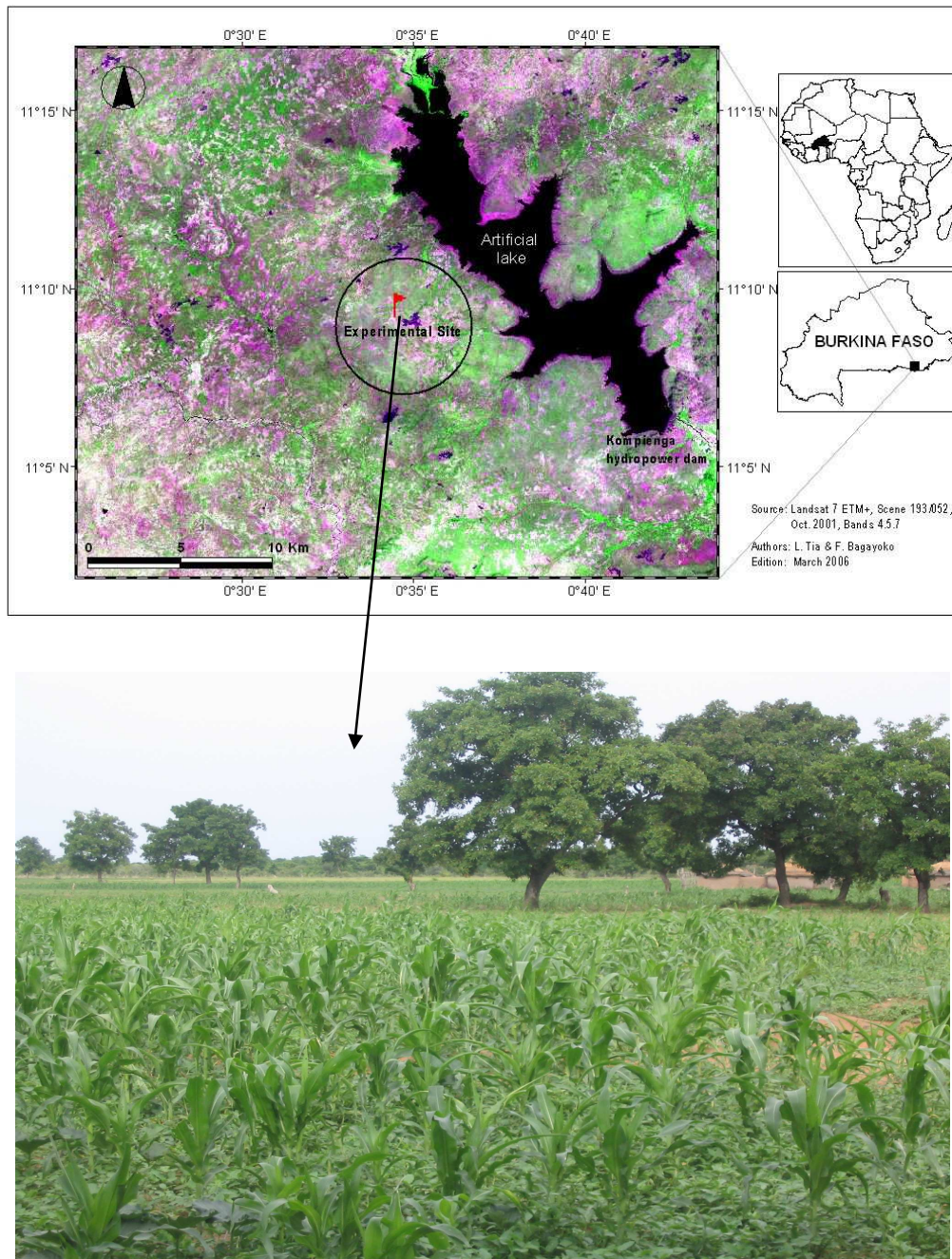
Figure 3.1:   Landsat image showing the location of the experimental site and a picture giving an impression of the field scale uniformity

a. Estimation of net radiation

The energy budget equation was used to estimate R_n and is expressed as follows:

$$R_n = R_s - R_{su} + R_{Ld} - R_{Lu} \tag{3.1}$$

or

$$R_n = (1-\alpha) \times R_s + R_{Ld} - R_{Lu} \tag{3.2}$$

where α is surface albedo [-], R_s is incoming shortwave radiation [W m^{-2}], R_{Ld} is downward long wave radiation and R_{Lu} is upward long wave radiation [W m^{-2}].

The surface albedo was measured every three weeks over bare soil from January to May 2004 and over the sorghum crop from June to September 2004 with a pyranometer (model: SP LITE, Kipp & Zonen, Delft, the Netherlands).

According to Idso and Jackson (1967), R_{Ld} and R_{Lu} are expressed as follow:

$$R_{Ld} = \varepsilon_a (1-c) \sigma T_a^4 + c\sigma T_a^4 + ck \tag{3.3}$$

and

$$R_{Lu} = (1-\varepsilon_s)\left[\varepsilon_a (1-c) \sigma T_a^4 + c\sigma T_a^4 + ck\right] + \varepsilon_s \sigma T_s^4 \tag{3.4}$$

where the first term in Eq. (3.3) represents the radiation from the clear sky as a function of the emission of the clear sky (ε_a), cloud cover (c), air temperature (T_a) in Kelvin and the Stefan-Boltzmann constant ($\sigma = 5.67 \times 10^{-8}$ W m^{-2} K^{-4}). The second term is an estimate of radiation from clouds as a function of the absolute air temperature assuming that the emission is equal to unity. The third term is the product of the fractional cloud cover and an empirical correction factor (k) to adjust for the difference between air temperature and cloud base temperature. In Eq. (3.4), the first term is an estimate of the downward long wave radiation being reflected upward from the surface. The factor ε_s is the emission of the surface for long wave radiation. The second term of Eq. (3.4) is the long wave radiation being emitted upward by the surface at the surface temperature. Combining Eq. (3.3) and Eq. (3.4), the following equation was obtained:

$$R_{Ld} - R_{Lu} = \varepsilon_s \left[\varepsilon_a (1-c) \sigma T_a^4 + c\sigma T_a^4 - \sigma T_s^4\right] + \varepsilon_c ck \tag{3.5}$$

According to Dong et al. (1992), Eq. (3.5) could be simplified by eliminating the term $\varepsilon_s ck$ and good estimation of $R_{Ld} - R_{Lu}$ can be obtained with the following equation:

$$R_{Ld} - R_{Lu} = 0.89\varepsilon_s \left[\varepsilon_a (1-c)\sigma T_a^4 + c\sigma T_a^4 - \sigma T_s^4 \right] \tag{3.6}$$

The coefficient 0.89 is an empirical adjustment factor that eliminates $\varepsilon_c ck$.

According to Llasat and Snyder (1998), Eq. (3.6) holds only for daytime when the solar altitude (h) is greater than 10°. This condition is fulfilled here, since the daytime measurements were used in the analysis.

The clear sky emission (ε_a) was estimated with the equation proposed by Swinbank (1963) as follows:

$$\varepsilon_a = 0.92 \times 10^{-5} T_a^2 \tag{3.7}$$

The cloud fraction (c) was estimated with the equation proposed by Kasten and Czeplak (1980) as follows:

$$\frac{R_s}{R_a} = \left(1 - 0.75 c^{3.4}\right) \tag{3.8}$$

where R_a is the clear sky irradiance [W m^{-2}] and is expressed as follows:

$$R_a = \left(0.79 - \frac{3.75}{h}\right) I \tag{3.9}$$

where I is the extraterrestrial radiation [W m^{-2}] estimated based on Allen (1999). The sun altitude was estimated (Llasat and Snyder, 1998) as:

$$h = \arcsin(I/1367) \tag{3.10}$$

For $h > 10°$ and combining Eq. (3.9) and Eq. (3.10), the following equation was obtained:

$$c = 1.088 \left(1 - \frac{R_s}{R_a} \right)^{0.294} \tag{3.11}$$

b. Estimation of ground heat flux

There are several methods to determine ground heat flux (G). A review of literature reveals that G can be directly measured with heat plates buried at a certain depth in the soil, normally at a few centimeters below the surface (Oke, 1987). Analytical solutions are also available when the surface temperature varies sinusoidally (Carslaw and Jaeger, 1986). These analytical solutions are temperature-gradient and soil-calorimetric methods, which require soil surface temperature (Brutsaert, 1982). Here, the analytical solution based on temperature gradient was used. It describes heat conduction into the soil as follows:

$$\frac{\partial T}{\partial t} = \alpha_T \cdot \frac{\partial^2 T}{\partial z^2} \tag{3.12}$$

and soil heat flux is:

$$Q = -\alpha_T \cdot C \cdot \frac{\partial T}{\partial z_s} \tag{3.13}$$

where T is temperature [C] in the soil at depth z_s [m] and time t [s], α_T is the thermal diffusivity [m^2 s^{-1}] equal to the ratio of the thermal conductivity over the volumetric heat capacity (C) [J K^{-1} m^{-3}].

When the time and depth increment (Δt) and (Δz_s) are sufficiently small, the solution of Eq. (3.12) for $T_{t+\Delta t, z_s}$ is expressed as follows (Anlauf et al., 1987):

$$T_{t+\Delta t, z_s} = \alpha_T \cdot \Delta t / \Delta z_s^2 \cdot \left(T_{t, z_s + \Delta z_s} - 2T_{t, z_s} + T_{t, z_s + \Delta z_s} \right) + T_{t, z_s} \tag{3.14}$$

Eq. (3.13) and (3.14) were programmed in MATLAB based on the similar approach of HEATREG proposed by Anlauf et al. (1987). The initial temperature in the soil layers was set as soil surface temperature, which was calculated by extrapolating the air temperature at 2 m and 10 m above the soil surface. The time and depth increment (Δt) and (Δz_s) were set at 1hr and 10 cm, respectively.

3.2.3 Footprint analysis

The footprint was calculated based on Schuepp et al. (1990) as follows:

$$f(x) = \frac{1}{Q_0}\frac{dQ}{dx} = \frac{2X_m}{x^2}\xi \exp\left[\frac{-2X_m}{x}\xi\right] \qquad (3.15)$$

where the left-hand side represents the flux footprint, x is the distance upwind from the point of measurement [m], X_m is the distance upwind [m] at which the flux footprint is a maximum (effective fetch), and ξ is a momentum stability correction function. Following Dyer (1974), ξ is expressed as:

$$\xi = \left[1 - 16\frac{z}{L}\right]^{-0.25} \qquad (3.16)$$

where z is the measurement height (10 m), and L is the Monin-Obukhov length [m]. Also, according to Dyer (1974), X_m was calculated as follows:

$$X_m = \frac{uz}{u^* 2k} \qquad (3.17)$$

where k is Von Karman coefficient (0.41). X_m was set as the distance of 80 % integration flux and was computed from the raw data with ALTEDDY software (Elbers, 2002), u and u^* are wind speed and friction velocity [m s^{-1}], respectively.

In order to show that the measured fluxes were representative over the investigated terrain, the fetches were roughly represented on the plan, and the major

trees with MATLAB. The coordinates X and Y of the wind source (corresponding to the upwind distance from the station) were calculated as follows:

$$X = X_m \times \cos(Dir) + Lat \qquad (3.18)$$

$$Y = X_m \times \sin(Dir) + Long \qquad (3.19)$$

where Dir is the wind direction [radian]; Lat and $Long$ are the latitude and longitude of the EC station [UTM], respectively. Trees within a 2 km radius around the station were located with a GPS (Etrex summit). The analysis was made for nighttime (unstable condition) and daytime (near-stable condition) measurements.

3.3   Results and discussions`

The energy balance closure was first presented for the whole dataset (from January to November 2004) and the anomalies detected were analyzed by presenting the closure over particular periods such as the dry period (January to March), the dry to wet transition period (April to May), the heavy and permanent rain period (June to September), the wet to dry transition period (mid-September to November). The representativeness of the measurement for these periods is later discussed in the footprint analysis.

3.3.1   Energy balance closure

Figure 3.2 shows the energy balance closure over the whole dataset and showed widely scattered points around the 1:1 line with a determination coefficient of 0.82. The slope and the intercept of the regression fit between ($R_n - G$) and ($H + \lambda E$) were 0.90 and 25 W/m² respectively. At first, a bad estimation of R_n and G was suspected as the reason for the scattering, but the broad distribution of the points around the 1:1 line indicated the inability of the EC station to sometime accurately measure H and λE.
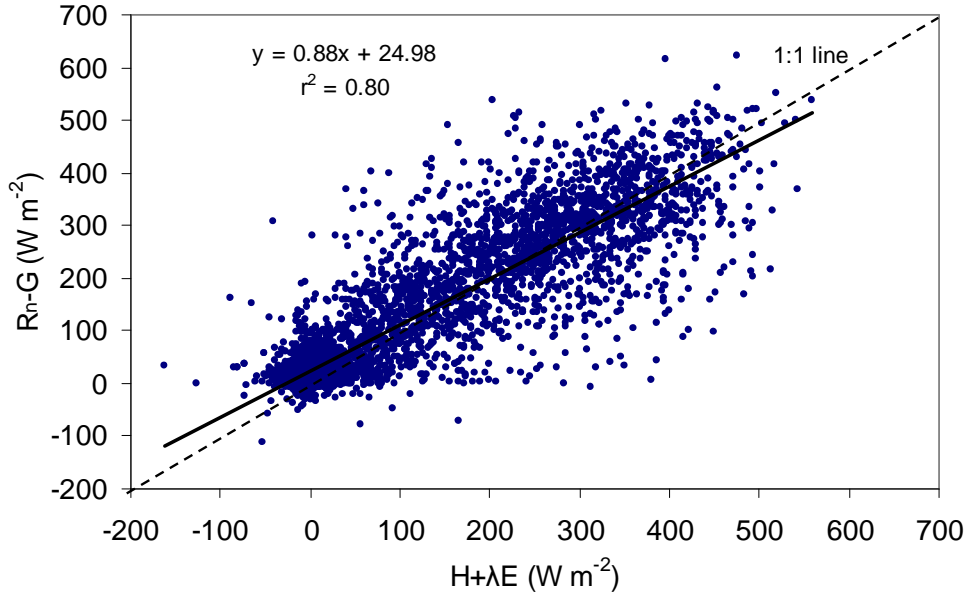
Figure 3.2:   Energy balance closure from January to November 2004

However, the estimation of R_n and G could also account for large part of the observed scattering because the relative bias errors were sometime >50 %, especially during the night, the early morning and days with rain. In fact, when R_n and G are measured with adequate devices, the uncertainties related to their measurement are 5 % and 30 %, respectively (Culf et al., 1997).   When the dataset was analyzed according to the subdivision previously mentioned, one can notice a clear decrease in the goodness of the energy balance closure and the coefficient of determination from the dry to the rainy season, and the trend reverses as soon as the wet to dry period begins (Figure 3.3). The correlation coefficients were 0.91, 0.80, 0.68 and 0.86 according to the analyzed periods, respectively. Therefore, the reason for the scattered pattern of the points observed over the whole data is more likely related to the sensitivity of the measurement device to rain. The high concentration of dust in the air could also be one of the reasons. In fact, a Krypton Hygrometer was used to measure the air humidity, and this is known to be very sensitive to dirty tubing (Leuning and Judd) and to rain droplets obscuring the optical path during rain (Culf et al., 1997; Moors, 1999). The malfunctioning of the Krypton hygrometer during and after the rain can last as long as the lens does not dry. This is confirmed by Figure 3.4, which compare the closure over DOY168 with a total rain of 9.2 mm (Figure 3.4-a) and DOY168 (Figure 3.4-b) without rain. The correlation between ($R_n - G$) and ($H + \lambda E$) during DOY168 (r²=0.53) was poor, whereas it was

better during DOY170 (r²= 0.97). The sensitivity of the Krypton hygrometer to dirty tubing and to rain is one of the big concerns about its use. These concerns can be even more pronounced in the savanna region, where the air is always dusty during the dry season, and during the rainy season the rain is always preceded by violent dusty winds. As proposed by Moors (1997), the sampling tubes have to be changed or cleaned regularly, which was not practically possible during this research because of the location of the station. In fact, the station was maintained only every three weeks and during the rainy season several rain events could take place during this period. The measured available energy ($H + \lambda E$) was also found to underestimate the estimated available energy ($R_n - G$) as mentioned by most of the authors in the literature (Brotzge and Crawford, 2003; Dugas et al., 1991; Goulden et al., 1998; Moore, 1976; Twine et al., 2000). The known causes of the underestimation are the distortion of the flow by the sonic anemometer (Wyngaard, 1988), water vapor fluctuation (Shuttleworth et al., 1988), the experimental design, especially the measurement height that determines the sensor footprint (Culf et al., 1997), the atmospheric condition, and the non-homogeneous of the terrain over which the measurement is carried out (Foken and Wichura, 1996). However, the latter was not of importance in the trial site, because the vegetation was homogenous and the terrain flat with a slope of about 2 ‰. Figure 3.4 (b) also reveals an asymmetry in the daily energy balance closure. The values during the afternoon were smaller and more accurate than those in the early morning. A similar phenomenon was observed during days with rain. This could be related to dew formation (for days without rain) and to rain (for days with rain) on the lens of the Krypton hygrometer. Therefore, before the lens has dried, all measurements of latent flux are overestimated. However, the asymmetry observed over the daytime measurements could also be related to the estimation of ground heat flux, as the asymmetry of the incoming and outgoing radiation was taken into account by the change in the average radiation at the soil surface. Energy balance closure based on the in-situ measurements of all components of the energy balance is necessary for comparison with the above described observations.
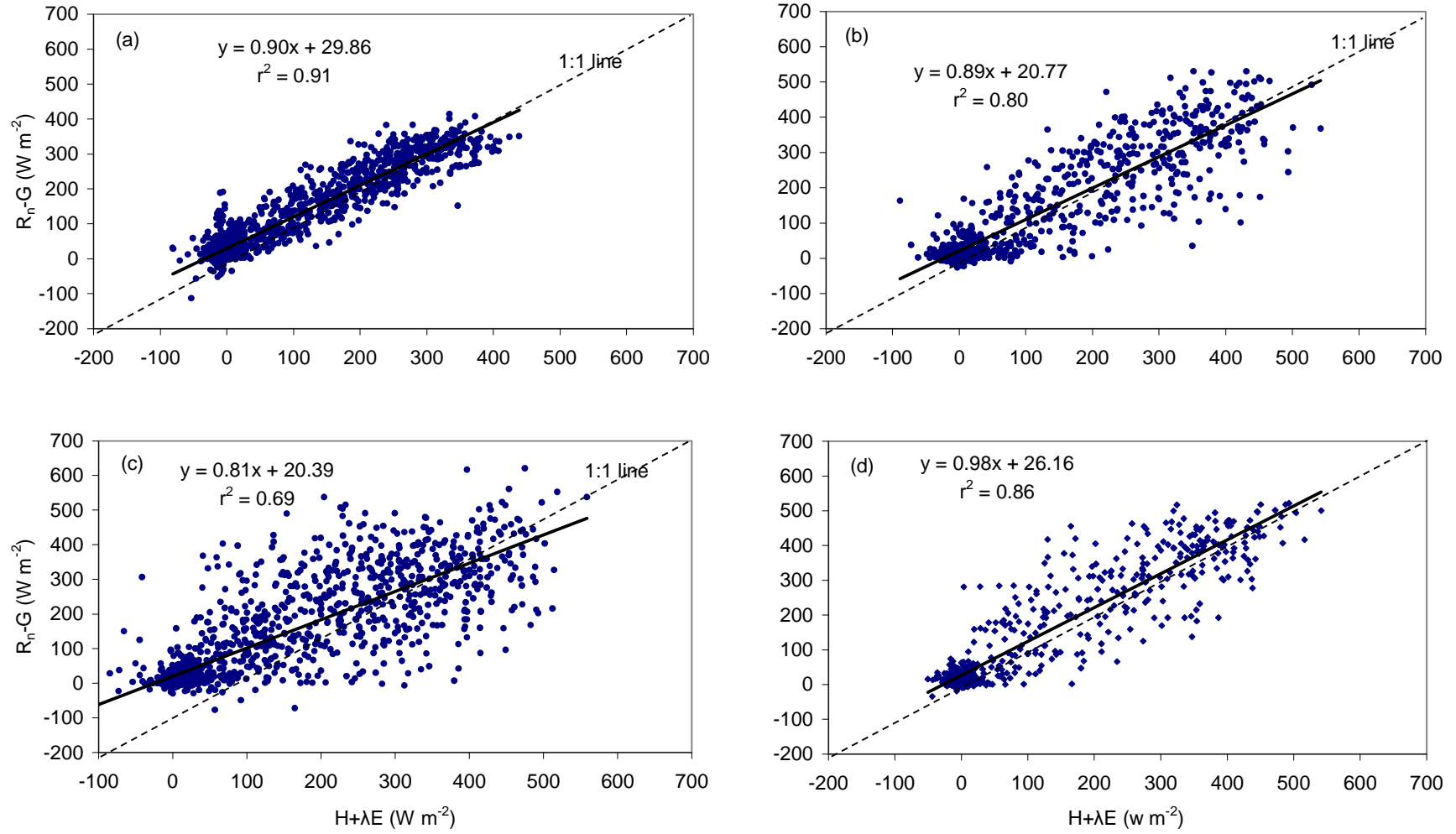
Figure 3.3: Energy balance closure over different periods: (a) dry season (January to April), (b) dry to wet transition period (April to May), (c) rainy season (June to September) and (d) drying period (October to November)
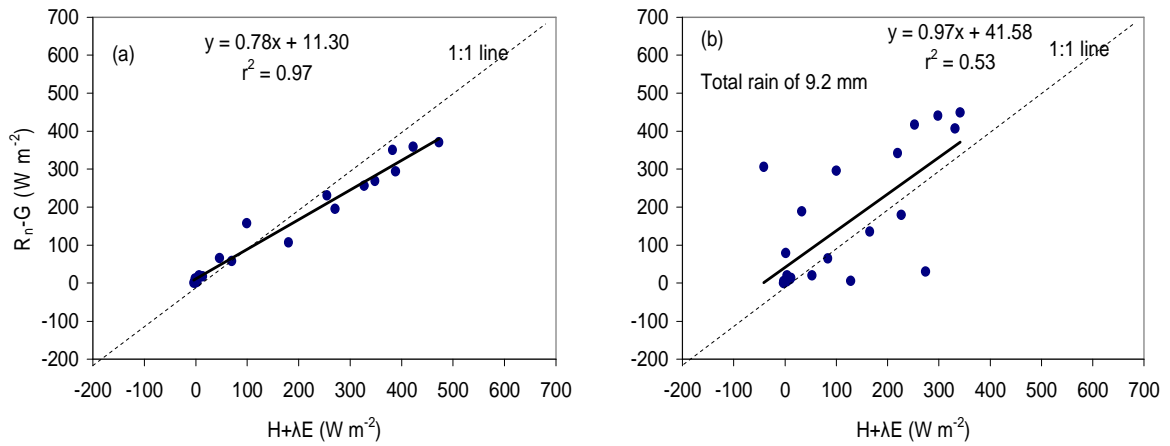
31

Figure 3.4:   Energy balance closure over selected days during the rainy season: (a) DOY170 without rain and (b) DOY168 with 9.2 mm of rain

3.3.2   Footprint analysis

According to Stannard (1993), the source area of an eddy covariance measurement generally extends an upwind distance of about 100 times the sensor height. The analysis of the effective fetch of the station showed that the maximum ranged between 20 and 800 m, which represents 2 to 80 % of the theoretical fetch with a measurement height of 10 m. Generally, the higher values were observed during the night and the early morning, where the atmosphere is very close to stability, while the minimum values were observed around noon, where the atmosphere is unstable. Figure 3.5 illustrates this observation for two contrasting hours selected in DOY31 and in DOY179 and for two contrasting periods (dry season and rainy season). During both periods, the footprint was similar, but with a higher peak during the rainy season. A peaked footprint exists with large contributing areas up to 100 m during the daytime. The results are similar to those obtained by Kabat et al. (1997) in the fallow vegetation and the patterned woodland in Niger during the HAPEX-Sahel project. As the station was located on a farmland, the fetch could be considered as representative during the rainy season, as the scale length of the crops and grasses was a few meters. During that period, all soil, crops and grasses as well as trees contributed to the measured fluxes. However, the representativeness could be problematic during the dry season and the transition periods, as the major contributor to the measured fluxes was the sheanut tree due to the absence of crops, grasses and to the dryness of the soil surface. The scale length of the vegetation-bare soil was higher and ranged between 50 m and 100 m. Therefore,

32

measuring the efficient latent heat fluxes under unstable conditions (daytime) led to sampling problems, as the fetch was not more than 50 m. In such a situation, most of the trees probably do not contribute to the measurement, which could raise the problem of representativeness over the terrain.

The fetch and the trees are roughly represented on the plan on Figure 3.6. It can be seen that only 10 trees at the most were contributing to the measured fluxes over an area of about 1 ha, mainly in the north-west from January to March. The 10 trees are in the high concentration of the fetch around the station corresponding to the daytime measurements (dark part of Figure 3.6-a). In fact, more than 50 % of the winds came from the north-west. During the two transition periods, only 2 (dry to wet transition period) and 5 (drying period) trees were contributing to the measured fluxes, respectively (Figure 3.6-b and 3.6-d). During both periods, winds came from the south-east, and trees were not dense in that direction. Comparing the covered tree density and the average tree density on the terrain (17 tree/ha), it could said that the measured fluxes are representative for the dry season, because a higher number (59 % of trees) were contributing to these fluxes. This could be one of the explanations of the relatively good energy balance closure observed from January to March. In contrast, during the transition periods, only 12 % and 29 % of the trees were contributing to the measured fluxes, which could also partially explain the decrease in the correlation coefficient in those periods in addition to the effect of rain and dust. The results of this study could be used in the positioning and choice of the adequate height of the station to increase the representativeness of the measurements. For instance, before installing the station, the dominant wind direction for the period of intensive measurement could be determined. Secondly, the station should be installed in such a way that a maximum fetch is maintained in the area to be investigated. In the present case, the representativeness of the measured fluxes during the problematic periods could have been increased by installing the station in such a way that a higher number of trees would have contributed from the south-east. This could also have been achieved by increasing the height of the station in order to increase the fetch, especially during the transition periods.

The installation of the station according to the dominant wind direction could imply shifting the station from site to site. However, this could be limited to two times in the savanna zone of West Africa as there are only two dominant wind regimes.
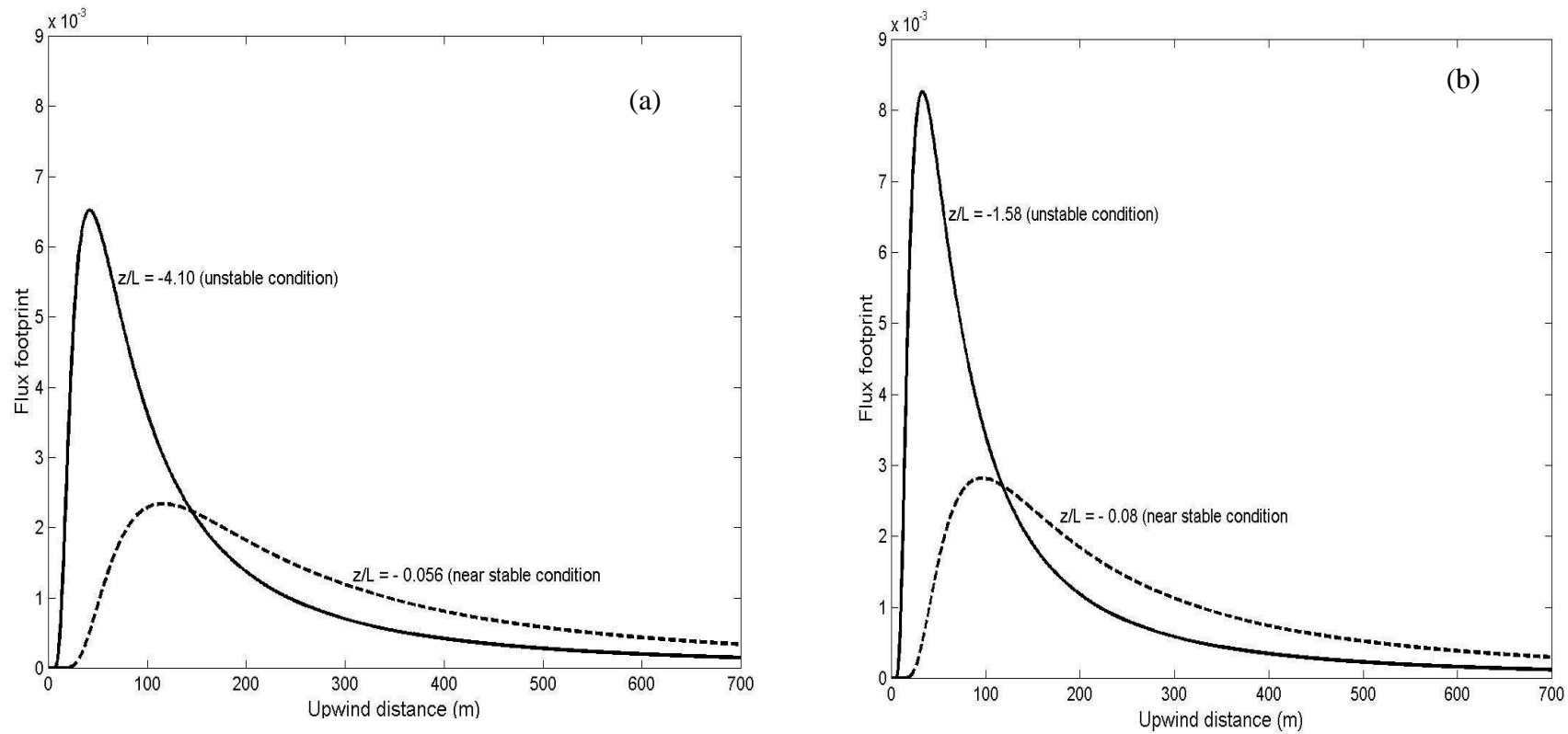
Figure 3.5: Footprint representation for two selected days in the dry season and rainy season: (a) DOY31 (dry season) at 13:00 (unstable condition) and at 8:00 (near stable condition) (b) DOY179 (rainy season) at 12 (unstable condition) and 8:00 (near stable condition). The graph was obtained with Eq. 3.15
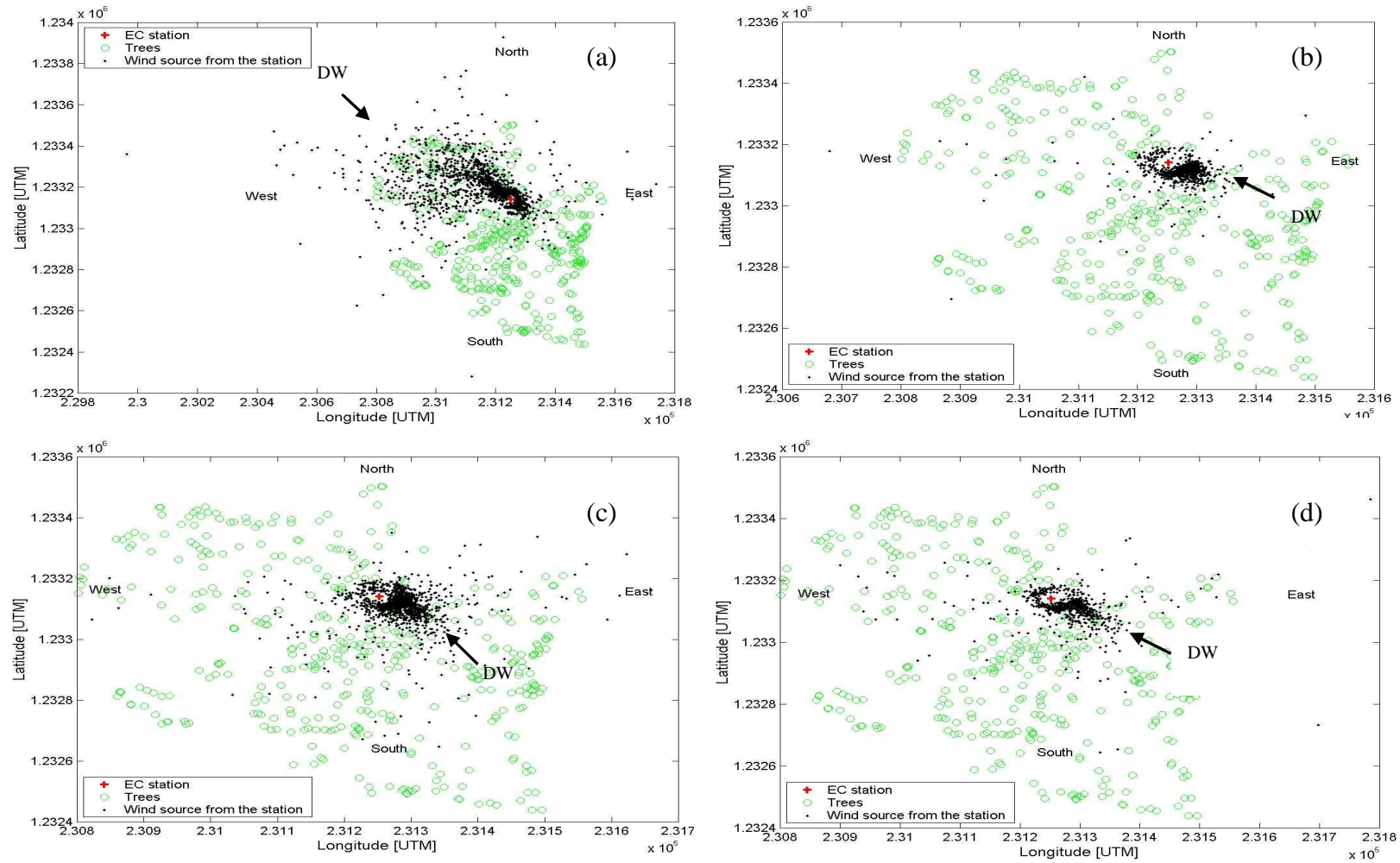
Figure 3.6:   Spatial representation of the fetch overlapped on the major trees around the EC station: DW is the dominant wind direction; (a) dry season; (b) transition period; (c) rainy season; (d) drying period

3.4   Conclusion

The study clearly shows that the EC technique can performed on farm land in the savanna zone, and that the data collected are reliable and representative. However, the sensitivity of the system to rain and dust could have a significant effect on the reliability of the measurements. During the rainy season, the measurements of most of the days with rain were excluded from the analysis, because they did not satisfy the energy balance closure requirement, which may hinder a real evaluation of the dynamics of the surface fluxes during that period. The study also showed an asymmetric effect on the energy balance closure on a daily basis. This seems to reduce the measurement accuracy during the morning. Attention should be given to this issue in future, because the reality of this asymmetry can not be substantiated since the net radiation and the ground heat flux were only estimated.

Finally, the study reveals that the location of the station with regard to the dominant wind direction is very important and can have a significant effect on the representativeness of the measurements. Therefore, this aspect should be added to the traditional criteria of the selection of the best location when installing the eddy covariance system, especially in the savanna vegetation, where the trees are scattered.

4 INTER-ANNUAL ENERGY PARTITIONING OVER THE WEST AFRICAN SAVANNA: EVAPORATION AND SURFACE CONDUCTANCE MEASUREMENTS AND MODELING[2]

4.1 Introduction

Agricultural land-use can have significant effects on energy partitioning as it changes vegetation morphology at large scales. In West Africa, especially in Burkina Faso, economic necessity and government policy stimulate the rural population to cultivate land intensively in order to increase agricultural production. This is being achieved by an expansion of the cultivated area, as well as by higher productivity per hectare. The need for new agricultural land has been a strong argument for the extensive clearing of natural vegetation (Ungaro et al., 2004). According to Mahe et al. (2005), natural vegetation in the White Volta basin declined from 43 % to 13 % of the total area between 1965 and 1995, while the cultivated area increased from 53 % to 76 %, and bare soil nearly tripled from 4 % to 11 %. This widespread change in the vegetation cover coupled to the seasonality of farming activities could influence absorption of incoming shortwave radiation as well as the aerodynamic resistance affecting turbulence exchanges of momentum, heat, and moisture. Similarly, changes in vegetative cover are associated with changes in plant morphology and physiology, which could, in the absence of other forcing factors, alter the surface fluxes and consequently the climate both at local, regional and global scales (Dale, 1997; Bounoua et al., 2002).

Review of the literature reveals that the study of energy partitioning has not received much attention in West African savanna, especially when compared to other regions. The little documentations available on the issue are from the Sahel Energy Balance Experiment (SEBEX) (Seller et al., 1996), the Hydrologic and Atmospheric Pilot Experiment in the Sahel (HAPEX-Sahel) (Goutourbe et al. 1997), and, most recently, Schüttemeyer (2005) in Central and Northern Ghana. Their investigations are limited to short data campaigns of less than one year and give only partial insight into the dynamics of surface fluxes. In this study, the results cover almost two years, including one relatively wet (2003) and one relatively dry (2004) year. The focus lies on

---

[2] Material in this chapter is conditionally accepted for publication in Journal of Hydrology with S. Yonkeu, J. Elbers and N.C. van de Giesen as co-authors.

energy partitioning, which is essential for calculating energy and water budgets in land-surface transfer schemes (LSTs) (Dickinson, 1993; Sellers, 1996) and eco-hydrologic models (see review by Reifsyder, 1988). Energy partitioning is also essential for better water resource management, which has gained much interest in the savanna region of West Africa because of the general water scarcity in the last decade. Therefore, this long-term investigation of energy partitioning was initiated to investigate in detail the dynamics of surface fluxes. The research is a part of the GLOWA-Volta project (van de Giesen et al., 2002) and the VinVal project. On the basis of the long-term surface flux measurements, simple models for the estimation of actual evaporation (E) and surface conductance (g_c) were developed. The study covers the period from May 2003 to November 2003. Two complete rainy seasons (May to October), one dry season (December to April), two dry to wet periods (May to June) and two wet to dry periods (October to November) are covered.

An overview of the measurement techniques and the theories used by the measurement results and finally a section on improved models for the energy partitioning.

4.2 Methods and materials

4.2.1 Trial site

The trial site is located in eastern Burkina Faso (11° 07' N; 0° 31' E). The area is flat with a slope of about 2 ‰ on average. Agriculture is very intensive. The site is characterized by a Sudan climate and vegetation with a monomodal rainfall pattern. The soils are mainly sandy (Lixisoils). Sheanut trees were dominant in the site, had an average height of 8 m, and were separated by an average distance of 15 m. The density of sheanut trees was about 17 trees/ha. During the rainy season, sorghum, millet, maize and groundnut were cultivated between the sheanut trees, and their growth alters the roughness length for momentum over time. This system of trees and crops widely found in the savanna in West Africa. Crop density was about four plants per square meter. The field scale uniformity can be observed on Figure 4.1 showing the location of the station on the Landsat image.
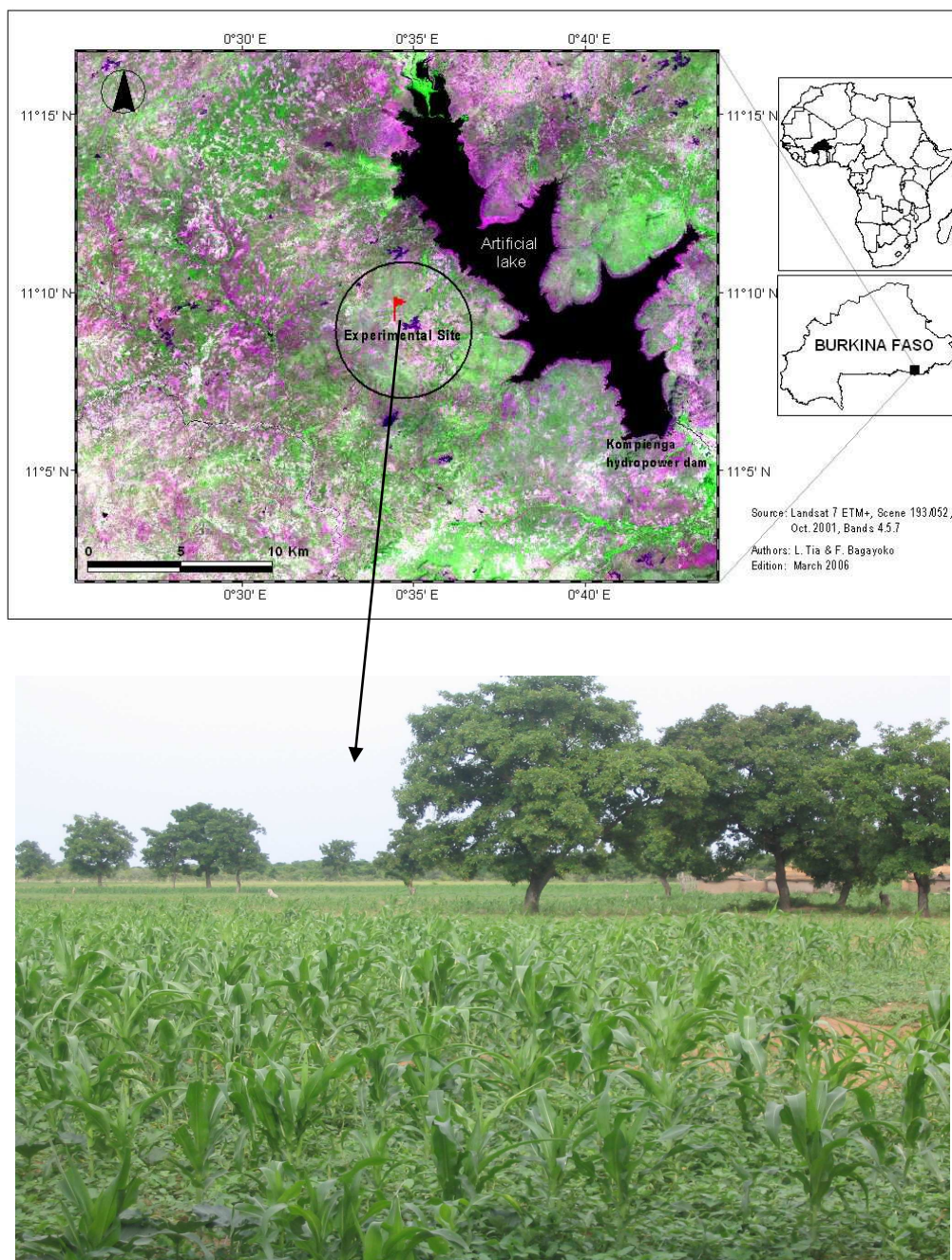
Figure 4.1:   Landsat image showing the location of the experimental site and a picture giving an impression of the field scale uniformity

4.2.2   Collection of micrometeorological data

Eddy covariance measurements were taken continuously from May 2003 to November 2004 at the top of a 10 m tower, about 2 m above the canopy of the sheanut trees and 7 m above the crop canopy. The mean wind speed (u), wind direction (Dir), and air temperature (T_a) were measured with a sonic anemometer (Gill Instruments Ltd., UK).

Air humidity was measured with a Campbell KH2O krypton hygrometer (model KH2O, Campbell Scientific, UK). Measurements were made with a frequency of 10 Hz. Latent heat flux (λE), sensible heat flux (H), friction velocity (u^*), Monin-Obukhov length (L), the flux footprint and the necessary error corrections were processed with ALTEDDY software on hourly basis (Elbers, 2002). A detailed description of the setup and operation of the device is given by Elbers (2002).

A weather station was placed about 5 m from the eddy covariance tower and used to record humidity (R_h), air temperature, wind speed and direction, solar radiation (R_s) and rainfall (P). This station measured at 2 m above the ground surface and a sampling rate was 20 minutes. Net radiation (R_n) and ground heat flux (G) were not directly measured. R_n was estimated using the energy budget equation, while the estimation of G was based on modeling heat conduction into the soil. Both methods are presented in Chapeter 3, section 3.22 (a and b).

Aerodynamic and surface conductances are two important parameters in understanding surface fluxes. According to Granier et al. (2000), aerodynamic conductance (g_a) can be estimated from wind speed using the equation:

$$g_a = \frac{k^2 u(z)}{\left(\ln[(z-d)/z_{0m}]\right)^2} \tag{4.1}$$

where $u(z)\,[\text{m s}^{-1}]$ is the wind speed at the measurement height $z = 10\,\text{m}$, d is the displacement height [m], z_{0m} is roughness length for momentum [m], k is the Von Kármán constant and was set at 0.41. z_{0m} and d express the aerodynamic properties of the vegetation. z_{0m} describes the ability of the stands to absorb momentum from the air moving over it, while d corresponds to the reference displacement height (Eleston and Monteith, 1975). z_{0m} was estimated according to the similarity law of Monin-Obukhov:

$$u(z) = \frac{u^*}{k}\left[\ln\left(\frac{z-d}{z_{0m}}\right) + \psi_m\left(\frac{z_{0m}}{L}\right) - \psi_m\left(\frac{z-d}{L}\right)\right] \tag{4.2}$$

where $u*$ is the frictional velocity [m s^{-1}], L is the Monin-Obukoh length [m] and ψ_m is a function expressing the atmospheric stability.

ψ_m was expressed as follows:

$$\psi_m = \begin{cases} -5\xi & 0 < \xi < 1 \\ 2\ln\left(\dfrac{1+x}{2}\right) + \ln\left(\dfrac{1+x^2}{2}\right) - 2\tan^{-1}(x) + \dfrac{\pi}{2} & -5 < \xi < 0 \end{cases} \qquad (4.3)$$

with

$$\xi = \frac{z}{L} \text{ and } x = (1-16\xi)^{1/4} \qquad (4.4)$$

z_{0m} was found by solving Eq. (4.2) according to Martano (1999) over a monthly dataset of u, u^* and L measured with the EC. The method proposed by Martano (1999) allows a calculation of z_{0m} with a single-level measurement. For extremely sparsely placed roughness elements like the trees at the savanna site and on farmland, the ground surface is the true reference plane and values of d should be close to zero (Bozier, 2002). Here, the displacement height was neglected. This assumption is true for the dry season as trees are very scattered, but should be less accurate for the rainy season because of the growth of crops and grasses.

Surface conductance (g_c) is more complex, and several procedures have been proposed for its derivation (Alves and Pereira, 1999). Here, it was obtained as a residual term from the Penman-Monteith equation (Baldocchi et al., 1998; Paw et al., 2000; Rochette et al., 1991) using the 'top down' approach:

$$\frac{1}{g_c} = \frac{1}{g_a}\left[\frac{\Delta}{\gamma}\left(\frac{R_n - G}{\lambda E_V} - 1\right) - 1\right] + \frac{\rho_a c_p VPD}{\gamma\lambda E_V} \qquad (4.5)$$

where Δ is the slope of the vapor pressure curve [mbar K^{-1}], γ is the psychometric constant [mbar K^{-1}], ρ_a is atmospheric density [kg m^{-3}], c_p is the specific heat of moist

air [J kg^{-1} K^{-1}], λE_V is the contribution of the vegetation to total evaporation [W m^{-2}], λ is the latent heat of vaporization [J kg^{-1}] and VPD is vapor pressure deficit [mbar]. During the rainy season, the vegetation contribution to total evaporation was estimated as follows (see Kabat et al., 1997):

$$\lambda E_V = \frac{\lambda E - \alpha_V \lambda E_S}{1 + \alpha_V} \qquad (4.6)$$

with

$$\lambda E_S = \frac{\Delta}{\Delta + \gamma}(R_n - G) \qquad (4.7)$$

where λE_S is the soil contribution to total evaporation [W m^{-2}], and α_V is the fractional cover of soil. α_V was retrieved from US Geological Survey's (USGS) database and the value are given in Table 4.1. During the dry season, the soil contribution to total evaporation was neglected and $\lambda E_V = \lambda E$.

Table 4.1:   Seasonal value of the vegetation fraction

Month of the year	Vegetation fraction
January	0.04
February	0.02
March	0.05
April	0.08
May	0.24
June	0.4
July	0.47
August	0.56
September	0.61
October	0.51
November	0.3
December	0.12

The Bowen ratio ($H / \lambda E$) was plotted versus g_c to show the influence of vegetation and moisture stress on the energy partitioning. The Priestley-Taylor

coefficient ($\lambda E / \lambda E_{eq}$) was calculated to compare the observed latent heat flux to an expected equilibrium latent heat flux (λE_{eq}). $\lambda E / \lambda E_{eq}$ was also plotted versus g_c to show a global perspective of where our study area lays with respect to other ecosystems. λE_{eq} was calculated as follows:

$$\lambda E_{eq} = a_{PT} \frac{\Delta}{\Delta + \gamma}(R_n - G) \tag{4.8}$$

where a_{PT} is an empirically determined dimensionless correction. a_{PT} was taken as equal to 1.26.

The coupling and decoupling of the transpiration to the atmosphere were analyzed with respect to the decoupling coefficient (Ω). Ω was calculated as follows:

$$\Omega = \frac{\Delta / \gamma + 1}{\Delta / \gamma + 1 + g_a / g_c} \tag{4.9}$$

Ω ranges between 0 and 1. At the limit of $\Omega = 1$, the surface of the canopy would be completely decoupled from overhead conditions, so that E can be directly determined by R_n, and a change in g_c will have no effect on E. In contrast, at the limit $\Omega = 0$, the canopy is completely coupled to the atmosphere and E will essentially depend on VPD and g_c. Thus, a fractional change in g_c will cause an equal fractional change in the transpiration, and the stomata will have complete control of E. At the intermediate levels of Ω, fractional change in g_c will cause decreasing fractional change in E as Ω approaches 1, and physiological control over the evaporation will diminish.

A tipping rain gauge was used to measure the rainfall intensity and was connected to the weather station. Also, three simple rain gauges were distributed about 1 km radius around the EC station to measure the daily rainfall. According to the total rainfall depth and the total evaporation of the whole period of investigation, a simple water balance was presented to show the total amount of water, which contributed to surface runoff and the recharge of groundwater.

All computations were based on daily averaged dataset, except the analysis made on the daily time courses. The gaps in the data correspond to the periods where weather data were not available.

4.2.3   Modeling the evaporation and surface conductance

A principal component analysis (PCA) was performed between the evaporative fraction (EF), z_{0m}/z, VPD, T_a and the moisture availability expressed by the Bowen ratio (β). As the estimation of z_{0m} was based on monthly dataset, all variables were averaged on a monthly basis. PCA expresses a set of variables as a set of linear combinations of factors that are not correlated between them; these factors represent an increasingly small fraction of the variability of the data. This method allows representing the original data (observations and variables) with fewer dimensions than the original, while keeping information loss to a minimum (Tutorial of XLStat, 2005). In simple word, PCA clusters all variables that are correlated to each other and having similar pattern in the same components. Therefore, we focused on the correlation of the variable and their similar pattern to evolve simple equations for the estimation of the monthly actual evaporation. The equation proposed by Jarvis and McNaughton (1986) for the estimation of the imposed transpiration to vegetation canopy by the atmosphere was then compared to the monthly evaporation to evolve the surface conductance. The imposed transpiration was expressed as follows:

$$E_{imp} = \frac{\rho_a c_p}{\lambda \gamma} g_c VPD \qquad (4.10)$$

4.3   Results

First, the seasonal dynamics of the climatic variables affecting the energy partitioning are discussed. Roughness length for momentum and vegetation dynamics, surface conductance, and the decoupling coefficient are discussed in sections 4.3.2 and 4.3.3. The seasonal energy partitioning is presented in section 4.3.4. The overall results and observations are used for the modeling in section 4.3.5.

4.3.1   Seasonal dynamic of meteorological parameters

a. Rainfall

Rainfall drives energy partitioning during the rainy season. According to Kabat et al. (1997) and Lebel et al. (1997), rainfall in the Sahel is typically generated by squall lines, arriving roughly every 3 days throughout the rainy season. This was more or less true for the first rainy season (2003), where the rainfall was relatively well distributed over the season. During the second rainy season (2004), the rainfall was irregular, and the times intervals between rainfall events were more than 10 days. The monitoring of rainfall started with two months delay in 2003 because of the non-availability of equipment. For these months, the gaps were filled with the measurements from the SONABEL (SOcieté NAtional Burkinabé de l'ELectricité) station in Kompienga, which is located about 20 km from the study station. Total rainfall in 2003 was about 1229 mm. In 2004, the rains started in April and stopped in October with a total of 825 mm. A remarkable decrease of 33 % of total rainfall from 2003 to 2004 can be observed, which may have resulted in large changes in the partitioning of surface fluxes. This effect is clearly visible in the seasonal dynamics of sensible and latent flux described in section 4.3.4.

b. Atmospheric variables

Daily average climatic variables from May 2003 to November 2004 are presented in Figure 4.2. Figure 4.2(a) shows the mean wind speed. It can bee seen that mean wind speed is relatively high during the dry season and ranged between 2 to 6   m s^{-1}. It decreases gradually from the onset to the end of the rainy season. Figure 4.2(b) shows the mean air temperatures and it follows the seasonality of rainfall, the lowest value being observed during the rainy seasons (about 22 °C) and the highest ones during the dry season (about 35 ° C). A weak decrease was also observed between December and January (dry season) which corresponds to the winter time. Figure 4.2(c) shows the pattern of VPD. The variables followed the seasonality of rainfall as well. VPD ranged 0.3 to 4.5 kPa in 2003 and 2004, respectively. The lowest value of VPD was observed during the rain season. With respect to R_s (Figures 4.2-d), it had the highest values during the dry season and lowest during the rainy season with high variability because of cloudiness.
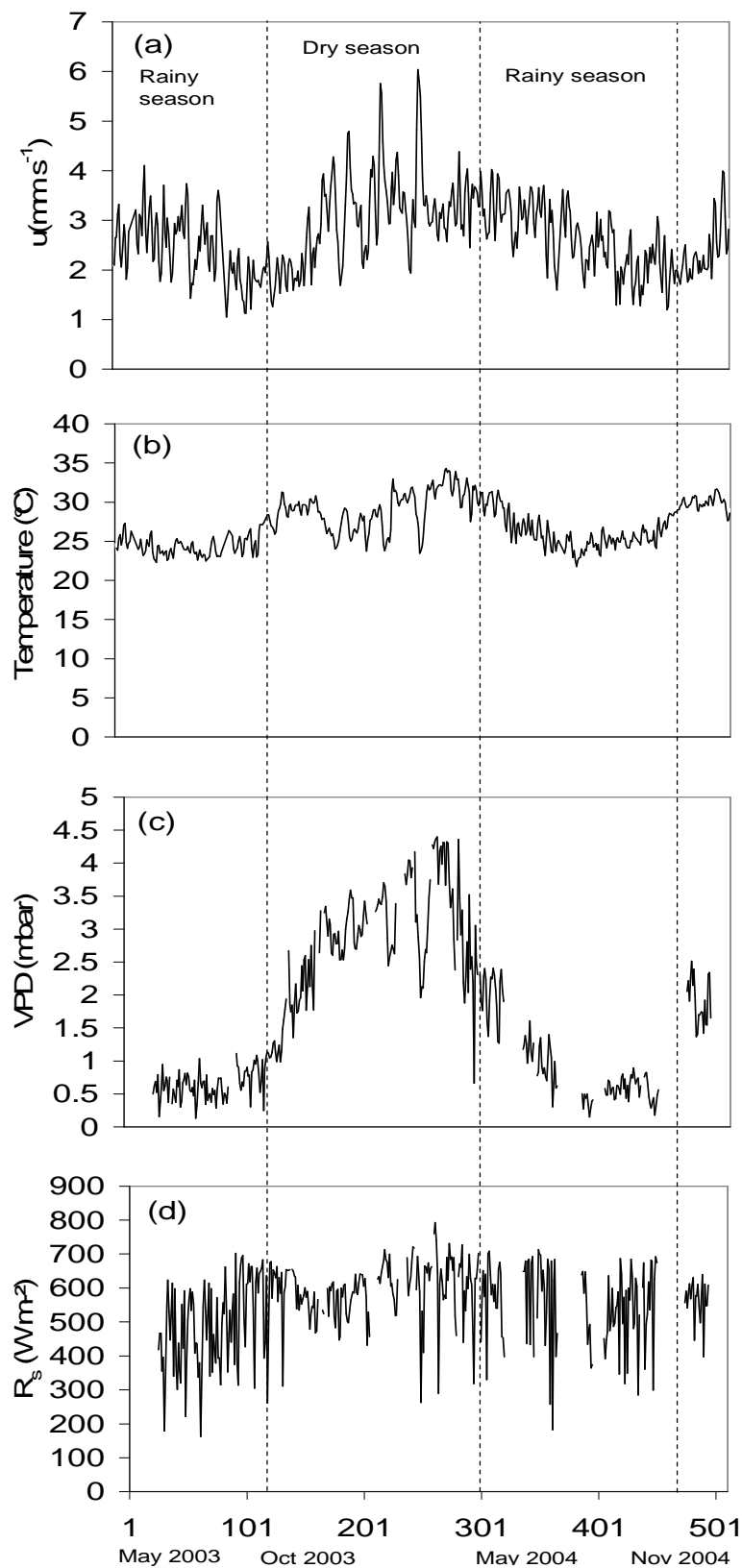
Figure 4.2: Average measured climatic variables from May 2003 to November 2004: (a) air temperature and rainfall; (b) relative humidity and vapor pressure deficit; (c) wind speed; (d) solar radiation

4.3.2 Roughness length for momentum and vegetation dynamics

According to Meijninger et al. (2000), z_{0m} for sparse vegetation varies between 0.10 to 0.20 m. These values are similar to the ones observed during the dry season (November to May), when the vegetation cover was more homogenous, but smaller than the values during the growth period (June to September) where $0.2 < z_{0m} \leq 0.45$. Figure 4.3 shows the seasonal trend of z_{0m} and gives a rough idea about the seasonal dynamics of vegetation cover. In fact, the seasonal vegetation fraction (α_v) retrieved from the USGS database had similar pattern and was correlated to the seasonal values of z_{0m} (Figure 4.4). This correlation shows that in area, where information are not available on the vegetation fraction, the roughness length for momentum can be used as a proxy. During the dry season, z_{0m} was relatively constant and was about 0.13 m. This relatively constant value of z_{0m} shows that there is hardly any resistance to wind. In this period, the crops were harvested; grasses completely dry and vegetation essentially consisted of sheanut trees. With the first rainfall, crops and grasses appeared and z_{0m} started to increase. Following the growth, z_{0m} continued to increase and reached the maximum between August and September, which corresponds to the maximum crop height (maturity). The maximum was 0.33 m and 0.41 m in 2003 and 2004, respectively. The difference is related to the type of the crops that farmers were growing around the EC station. Farmers grew more maize in 2003 and more sorghum in 2004, the latter is taller than maize. From September, z_{0m} decreased due to crop harvest and to farmers cutting down and collect the stems. This decrease in z_{0m} continued until November, when z_{0m} again reached the minimum of 0.13 m. The study area is continuously subject to these seasonal dynamics of the vegetation cover, which is also the main cause of the seasonality of surface fluxes. This result shows that roughness length for momentum is an important parameter in the dynamics of surface fluxes. From the literatures review on land surface models, it has been shown in some studies that they are not sensitive to roughness length for momentum. For instance, Instiful, (2004) found that z_{0m} is in third position in term of sensitivity of land surface models to environmental parameters and factors. This is because most of the micrometeorological studies are conducted over homogeneous vegetation and for relative a short duration. Therefore, the real dynamics

of z_{0m} cannot be assessed and will appear to be constant over time. In the present case, if the study had been conducted during the dry season, similar conclusions regarding the constancy of z_{0m} would have been obtained. More research is needed on the effect of the seasonal dynamics of z_{0m} on land surface models, especially in West Africa savanna. In fact, even if an area is not submitted to agricultural activities, as was the case in the trial site, seasonal bush fires could change the morphology of the vegetation and have significant effects on z_{0m}. We focus on this issue in Chapter 5.
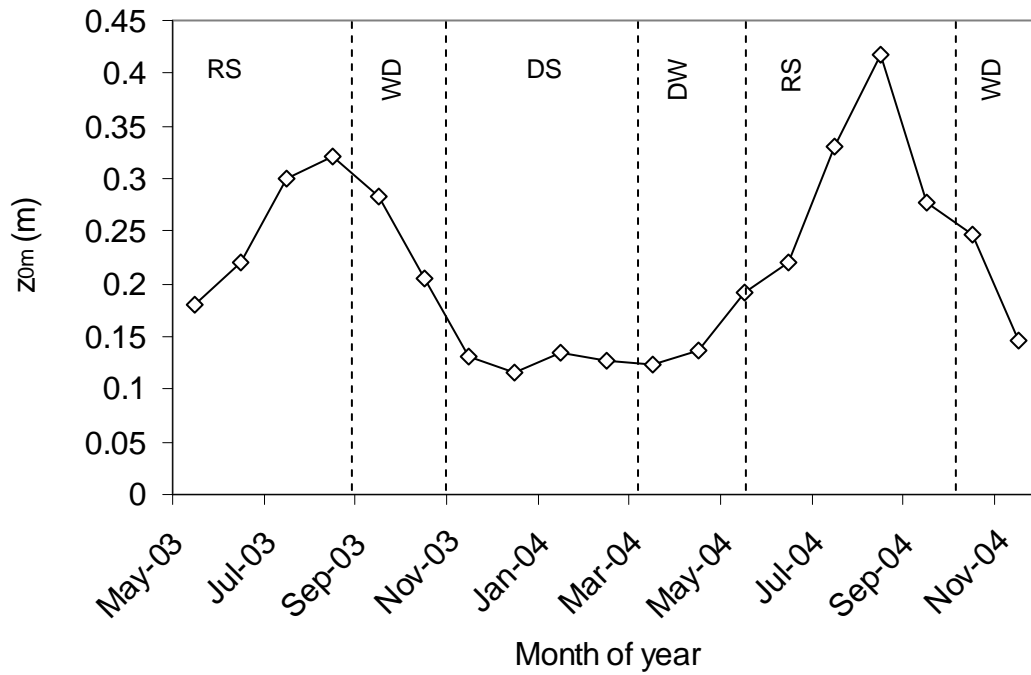

Figure 4.3:   Seasonal dynamics of the roughness length for momentum (RS: rainy season; WD: wet to dry transition period; DS: dry season; DW: dry to wet transition period)
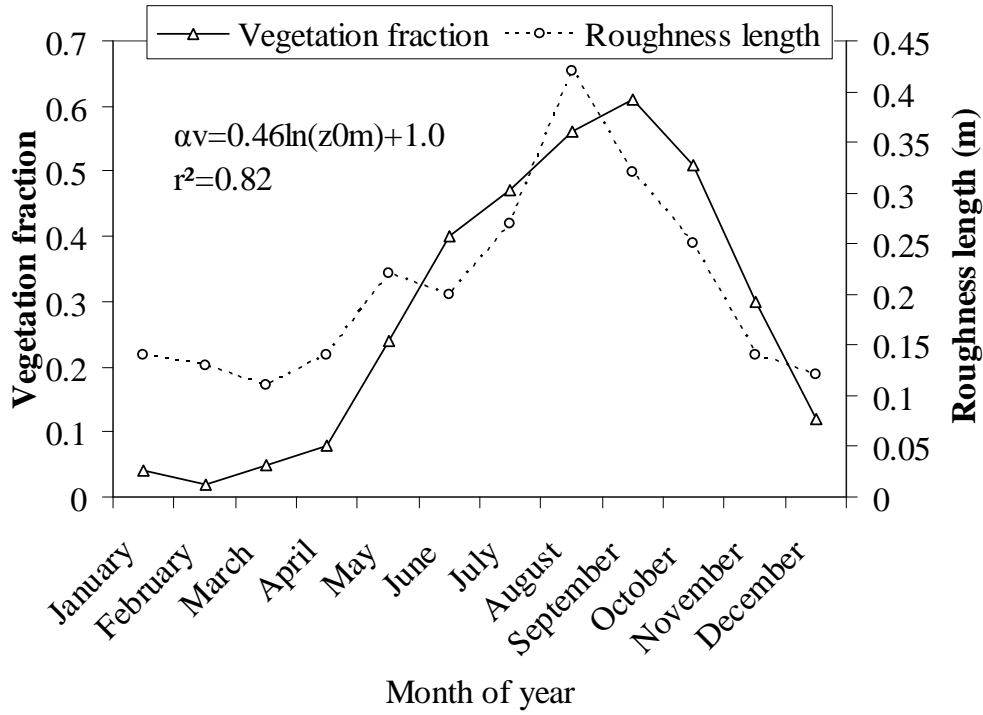
48

Figure 4.4:   Seasonal variation of the vegetation fraction (α_v) and roughness length for momentum (z_{0m})

4.3.3   Surface conductance and decoupling coefficient

According to Wilson and Baldocchi (2000), the variation of sensible heat flux, and the resulting effect on boundary layer processes, depends on both biological and climatological variables. The relative importance of biological and climate parameters in creating seasonal and inter-seasonal variability is a significant hydrological and meteorological question. If atmospheric demand is the primary control of variability, then heat flux between seasons could be estimated directly from R_n and VPD, while stomatal responses do not need to be treated in-depth. Alternatively, if biological responses are needed to adequately estimate the seasonality of heat fluxes, then an accurate presentation of stomatal response is necessary.

Figure 4.5 shows that g_c showed high variability during the rainy seasons and ranged between 6 to 86 mm s^{-1}. The falls and raises are related to the rainfall events. During the dry season, g_c was weaker and did not surpass 5 mm s^{-1}. The variability was very slight except the abrupt raise in April due the first rains. The monthly average shows that with the first rainfall events and the appearance of grasses and crops (rainy

season of 2003), g_c increased rapidly and reaches its maximum in August (39 mm s^{-1}).
At the same period in 2004, g_c was 38 mm s^{-1} which obviously shows the influence of
the abundance of soil moisture and the leaf area index (LAI) on the seasonal variability
of g_c. Similar results were reported by Kelliher et al. (1995), McNaughton and Jarvis
(1983) and Smith and Jarvis (1998). The average value was about 2.6 mm s^{-1} during the
dry season in 2004. This low value of g_c was related to the sparse vegetation cover (17
trees/ha) and the poor availability of soil moisture. For the dry season, g_c can be
considered as sheanut trees canopy conductance.

The decoupling coefficient (Ω) was calculated for dry canopies and ranged
from 0.18 to 0.4 for extremely dry periods (December to April) and 0.6 to 0.9 for the
wet period (June to September). These values suggest that during the dry periods, the
main driving parameters of surface fluxes were g_c and VPD according to the theory of
Smith and Jarvis (1998). During the transition periods (October to November or April to
May), g_c, VPD and R_n contribute to the variability of heat fluxes equally, since the
decoupling coefficient Ω was about 0.5.

With respect to the Priestley-Taylor coefficient, the highest values (0.7 to 1.2)
were observed during the rainy season and the transitions periods. The values greater
than 1 indicate that the actual evaporation rate was more than the potential one and was
observed between August and September when rains are more regular, VPD close to
zero. The weakest values of $\lambda E / \lambda E_{eq}$ (0.2 to 0.6) were observed during the dry season
(December to April). Also, there was a strong correlation between $\lambda E / \lambda E_{eq}$ values and
g_c. We observed a logarithmic increase of $\lambda E / \lambda E_{eq}$ with increase g_c with a significant
coefficient of determination $r^2 = 0.78$ (Figure 4.5). Similar relationship was found by
Linda et al. (2002) on grassland in Canada. However, a close analysis shows two visible
trends on Figure 4.4. $\lambda E / \lambda E_{eq}$ seems to be independent to g_c during and after the days
with significant rains (encircled points), which means that direct evaporation from soil
and intercept rains contribute significantly to the total evaporation. At the opposite, for
the days without rains (including days in the dry season) $\lambda E / \lambda E_{eq}$ shows an increase
trend with g_c indicating that vegetations contribute more in the total evaporation.

Therefore, we can conclude that the control of surface conductance on the evaporation is limited by moisture availability.
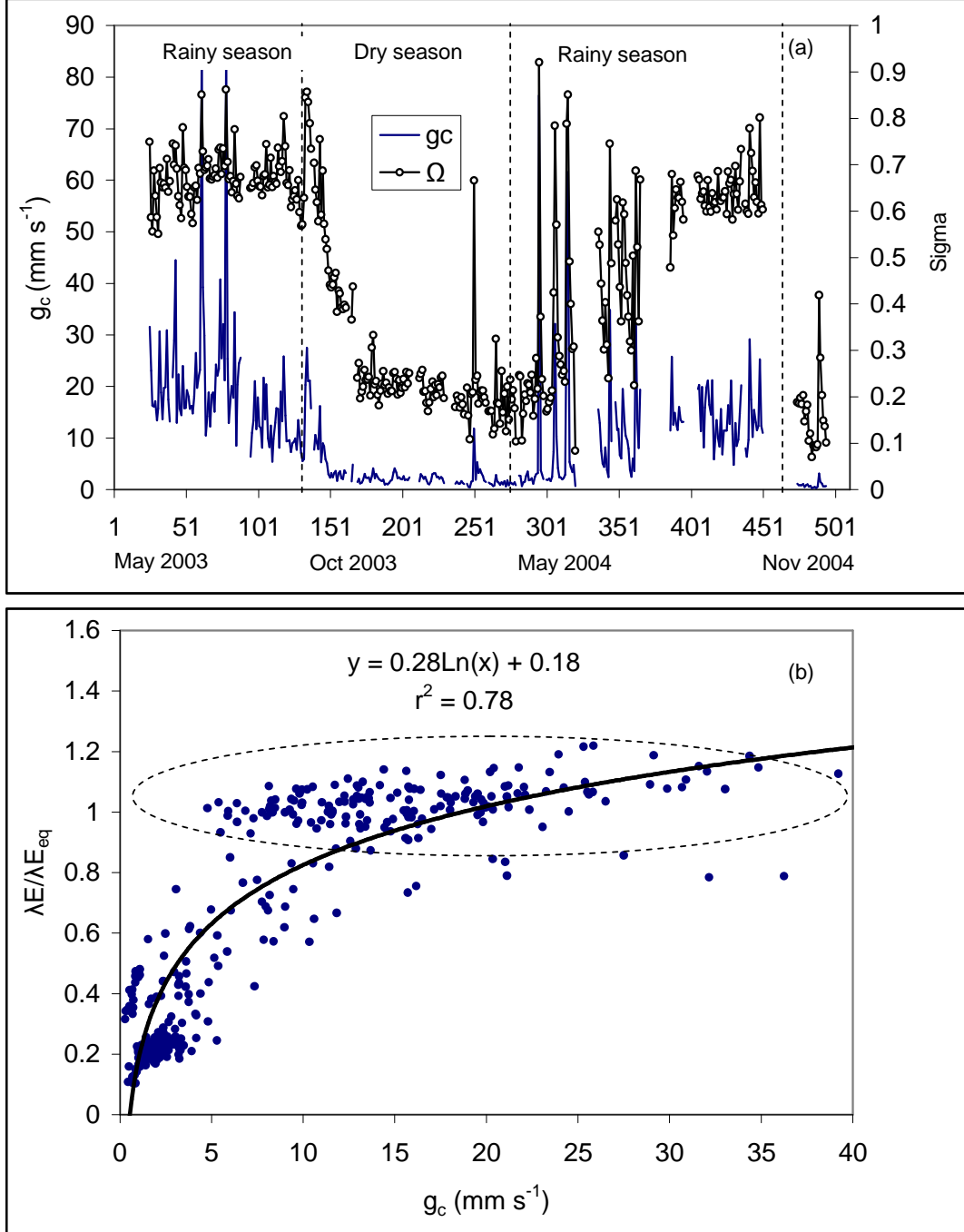

Figure 4.5:   Seasonal trend of surface conductance and its relationship with $\lambda E / \lambda E_{eq}$

For better understanding of the daily dynamics of the energy partitioning, the daily time course of g_c, g_a and Ω was plotted for three contrasting days. Figure

4.6(a1, a2, a3) presents the daily time course of g_c, g_a and Ω, respectively. For 30 July 2003 (rainy season) g_c increases rapidly from 7:00 to 9:00, at which time it reaches the maximum (about $25\,\text{mm}\,s^{-1}$), and decreases to the lowest value (about 12 $\text{mm}\,s^{-1}$ on average) between 12:00 to 17:00. The falls and raises in the trend indicated that both *VPD* and R_n affect its dynamics with a slight dominance for R_n. This is confirmed by the trend of the decoupling coefficient varying around the average value of 0.63. With respect to g_a, the variation is somewhat difference since it reaches the maximum between 9:00 to 10:00. Its magnitude was always higher as compared to g_c. The order of magnitude ranged from 1.92 to 3 times the g_c value during the day time. Similar trend was observed for 03 September 2004 (rainy season). Here, a rain of 33 mm was observed between 10:00 to 11:00, which resulted to a malfunctioning of the eddy covariance devices. This malfunctioning of the eddy covariance devices can also be observed on the trend of g_a by a decrease at 11:00. Normally, g_a should be higher as rains are always accompanied by violent winds in the savanna zone of West Africa. As shown on Figure 4.6(a3, b3, c3), during the dry season (09 March 2004), g_c, g_a as well as Ω rises to their peaks very early at 8:00 and decreases rapidly to its lowest values between 10:00 to 18:00 except g_a, which was relatively constant between 10:00 to 13:00. Here *VPD* appears to be dominant in the dynamics of g_c according to Ω, which was about 0.4 on average.
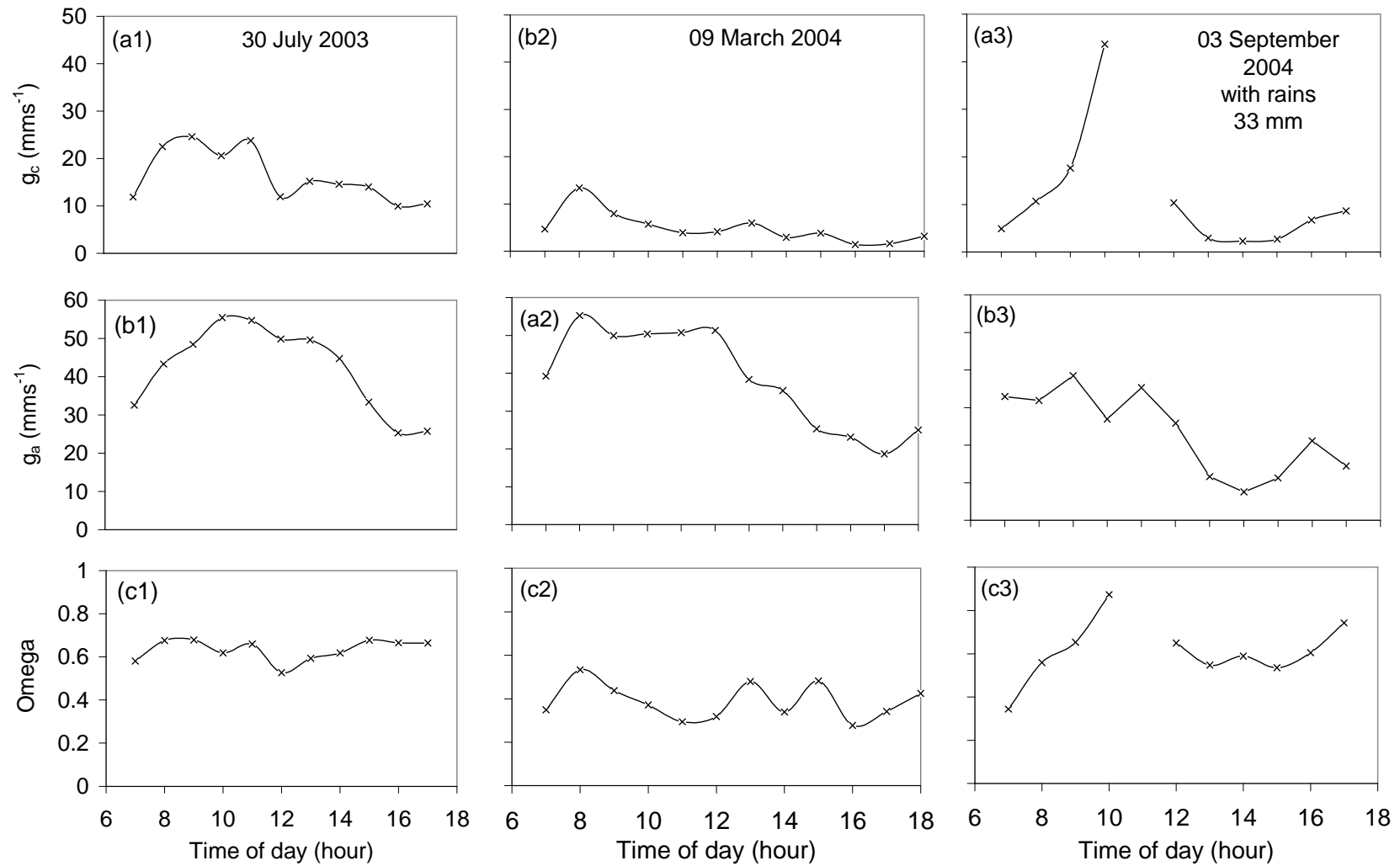
Figure 4.6:   Daily time courses of the surface conductance (g_c), aerodynamic roughness length (g_a) and decoupling coefficient (Ω)

4.3.4   Sensible and latent heat flux

Figure 4.6 shows the daily average of H and λE for the measurement period. The values are negatively correlated over both the rainy and the dry season. During the dry season, λE was relatively constant and was about 33 W m^{-2} in 2004 and 41 W m^{-2} in 2003 (from available data in February and March 2003). This low level of energy consumption was related to the low amount of water transpired by the trees due to poor soil moisture availability. During the same period, H was high but more irregular than λE. From December to early February, the weather is cool and this effect can be seen in Figure 4.7 showing a decrease in H for that period. From February to late April, H showed an increase trend and was similar to the daily mean temperature, with an average value of about 158 W m^{-2}. In 2003, the average value of H was about 176 W m^{-2} (from data of February and March 2003). Comparing both dry seasons, it can be seen that λE decreases significantly by 19.5 % and H increases by 10 % from 2003 to 2004. After the first rainfall events, the trend was reversed due to the consumption of available energy to evaporate water available at the surface of the soil and tree leaves. Evaporation showed an increase trend as crops and grasses grew, but were more sensitive to the occurrences of rains. Similarly, H decreased also with high variability according to the occurrence of rains. Here, the average values were 81 W m^{-2} and 176 W m^{-2} for H and λE, respectively. During the same period in 2003, the magnitude of H and λE was 65.5 W m^{-2} and 193.5 W m^{-2} on average, respectively. Comparing both rainy seasons, it can be seen that the average value of H significantly decreased with 20 %. Similarly, the average value of λE increased with 9 %. This inter-annual variability is associated with the important decrease of 33 % in rainfall from 2003 to 2004 as noted in section 4.2.1. The importance of moisture availability and the effect of g_c on the energy partitioning also become clear from the plot of the Bowen ratio (β) versus g_c.
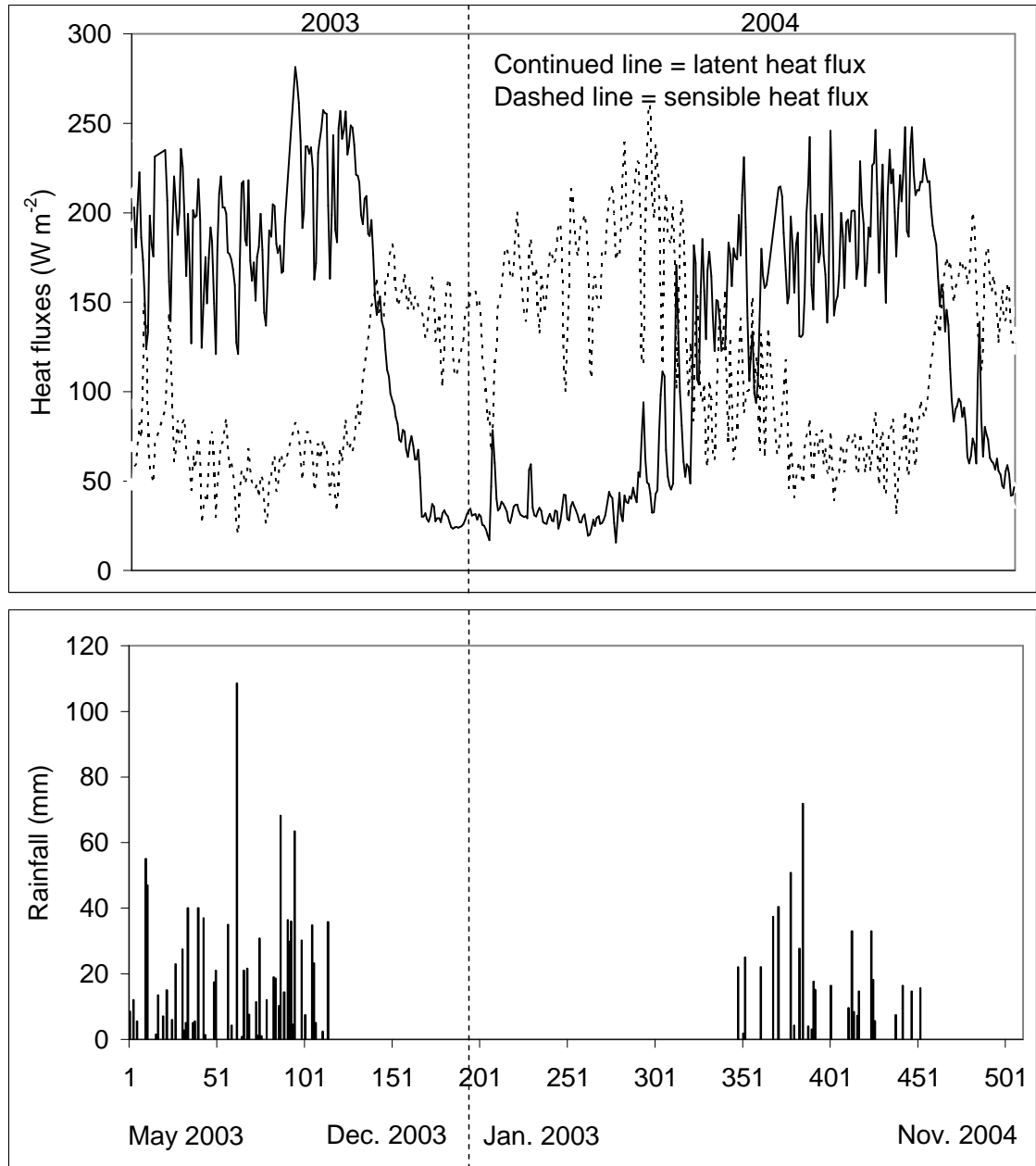
Figure 4.7:   Seasonal dynamics of the sensible heat flux (dashed line) and latent heat flux (continuous line), and rainfall for both season of measurement

Figure 4.8 shows an inverse decline of β when g_c decreases, with a significant coefficient of determination (r^2=0.93 and 0.80, respectively). However, cloudiness could also have contributed significantly to the process because of its effect on the incoming radiation and, especially, on net radiation. The peak values of λE were associated with clear days, mostly after a period of significant rainfall. The scattered feature of the points for lower values of g_c denotes the influence of the vapor pressure

55

deficit, which controls the dynamics of the canopy transpiration during days without rains.
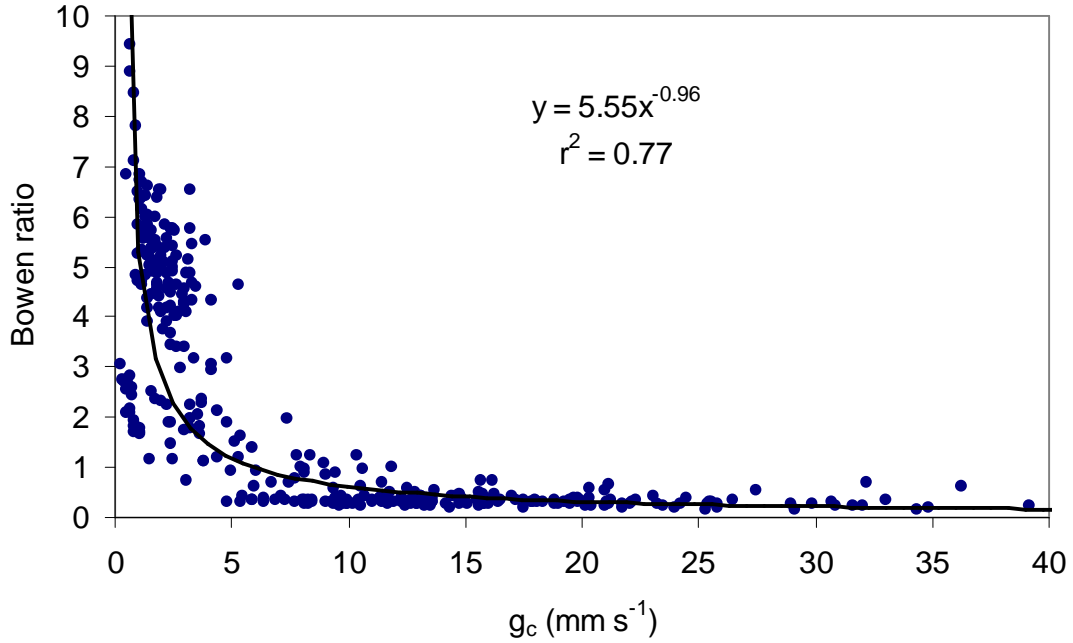

Figure 4.8:   Relationship between the Bowen ratio (β) and surface conductance (g_c)

The daily time course of the energy partitioning between H and λE are presented on Figure 9 for 30 July 2003 (rainy season), 09 March 2004 (dry season) and 03 September 2004 (rainy season). Figure 4.8 shows that R_n was very abundant during both dry an rainy season. The maximum R_n ranged from 500 to 800 W m^{-2}. In both rainy seasons, λE was the main consumer of the available energy as shown by the daily average on Figure 4.7. For the days without rains, H and λE follows similar pattern as R_n (Figure 4.9-a), which means it contributes effectively in the energy partitioning during daytime. Rains affect significantly the pattern of the energy partitioning because of the low vapor pressure deficit. As shown on Figure 4.9-c, effective dynamics are observed after the rains but both H and λE remain low even if the available energy is very abundant.
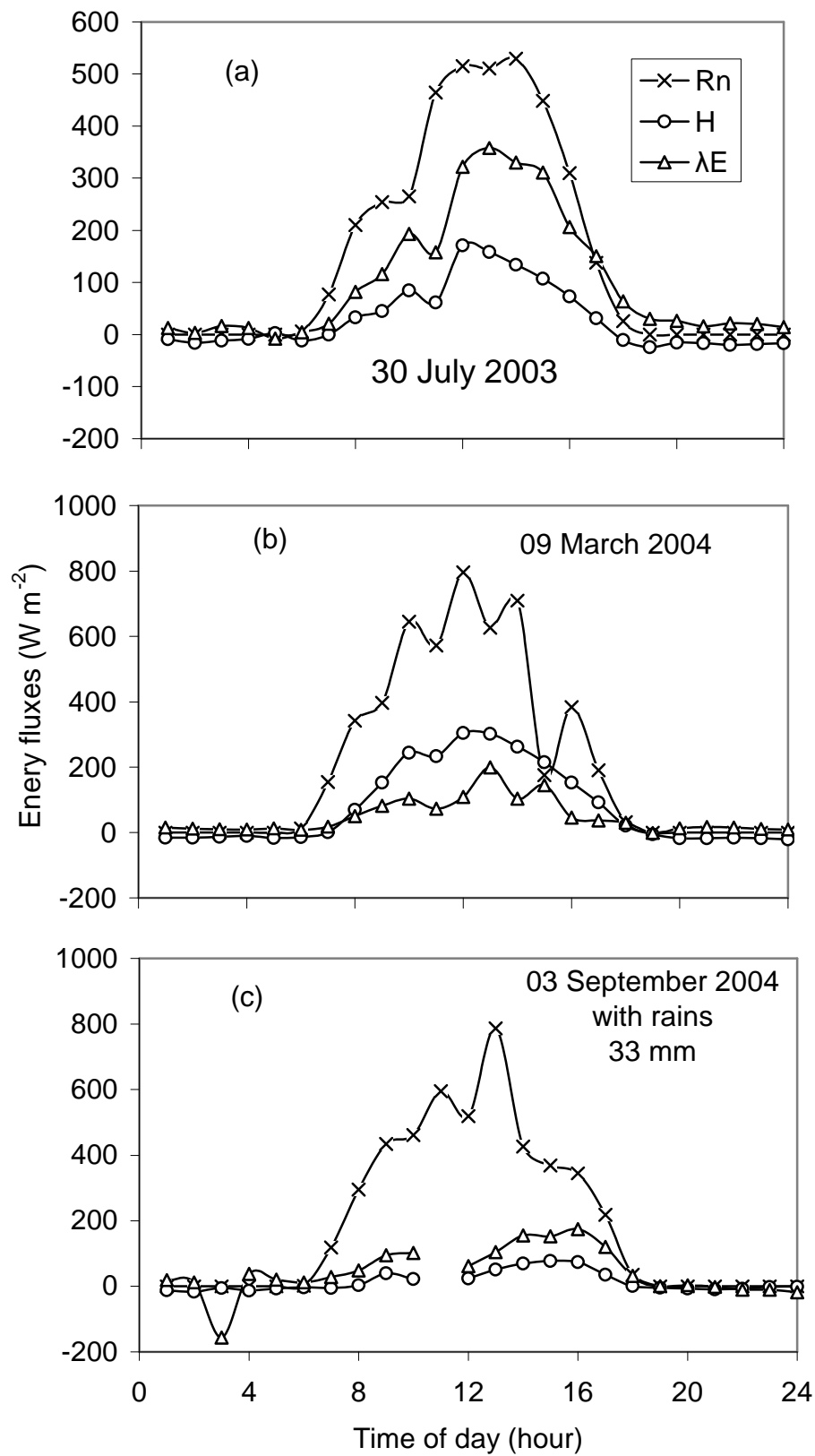
Figure 4.9:   Daily time course of the energy partitioning

In term of water balance, which is more interesting for hydrologist, the monthly actual evaporation estimated from the measured latent heat flux was plotted against the monthly rainfall for the whole period of investigation. During the rainy season of 2003, the annual rainfall was about 1229 mm against 351 mm evaporated, while annual rainfall was about 825 mm against 268 evaporated during the rain season of 2004. Therefore, 878 mm had contributed to the surface runoff, infiltration and percolation to groundwater during the rainy season of 2003. Similarly, 557 mm had contributed to the surface runoff, infiltration and percolation to groundwater during the rainy season of 2004.These simples water balance shows that more water was gained in the hydrological system, and could be interesting in the estimation of the total recharge of groundwater if information is available on the total surface runoff for the same period.
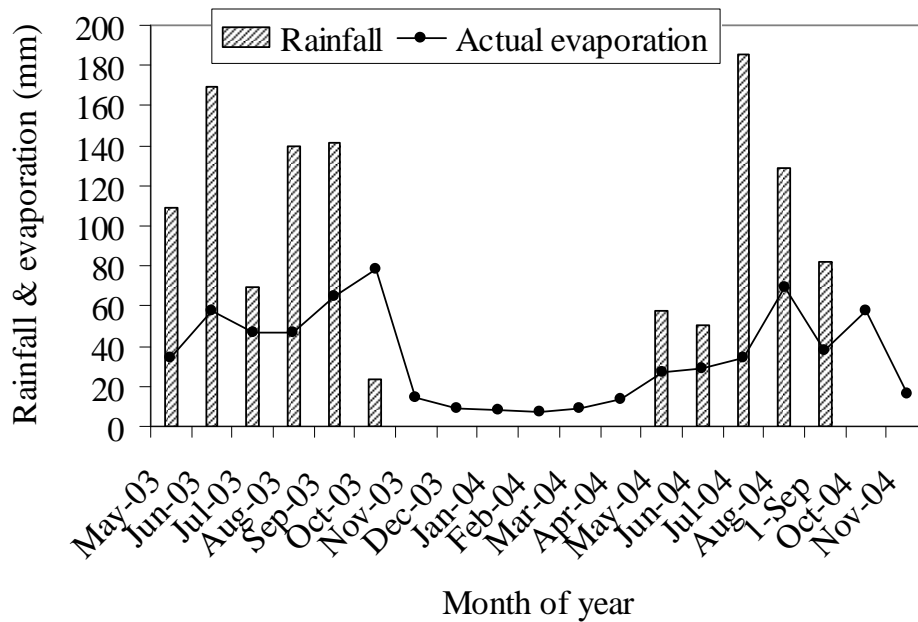

Figure 4.10:   Monthly actual evaporation against monthly rainfall for the whole period of investigation

Here, there is a causal relationship in the partitioning of the available energy between sensible heat and latent heat flux, which makes it difficult to give priority to the individual effects of the variables described in this study. However, it is clear that moisture availability is the starting point of all processes, since all variables were relatively constant during the dry season. Major changes start with the first rainfall

event in April, and the situation becomes stable when the soil surface becomes completely dry again in December. Therefore, it might be useful to compare correlations between the variables. This comparison is made in section 4.3.5 between the evaporative fraction (EF) and z_{0m}/z, and between the Bowen ratio (β) and VPD. The results of the comparisons lead to updated models for the estimation of E and g_c.

4.3.5 Principal Component Analysis (PCA) and modeling
a. Principal Component Analysis

The analysis shows that z_{0m} and EF are positively correlated and negatively correlated with the other variables. The correlation coefficients are presented in Table 4.2. Figure 4.11 clearly shows that z_{0m} and EF are positively correlated and closed to each other in the circle of unit radius (which means that they have a similar pattern). This correlation is particularly strong during the transition periods before crops and grasses reach their maturity. A similar correspondence between β and VPD is also shown. These are positively correlated, and this correlation is particularly strong during the dry season. Because of the depletion of soil moisture, most of the available energy goes to heating the ambient air which increases air temperature and, consequently, the vapor pressure deficit. In contrast, T_a contains information that is independent from VPD, β, EF and z_{0m}/z. Subsequently, the rates of increase or decrease in z_{0m} and EF from one period to another were calculated and compared. A similar procedure was followed for β and VPD. It was observed that the ratio of each couple of variables was similar with a mean bias error (MBE) of -0.09 for the first pair of variables (z_{0m} and EF) and MBE= 0.0015 for the second pair (β and VPD). Therefore, it can be concluded that any relative change in z_{0m} involves proportional relative change in EF. Similarly, any relative change in VPD involves proportional relative change in β. This conclusion is particularly relevant and can be easily modeled.

Table 4.2:   Correlation matrix between the different variables

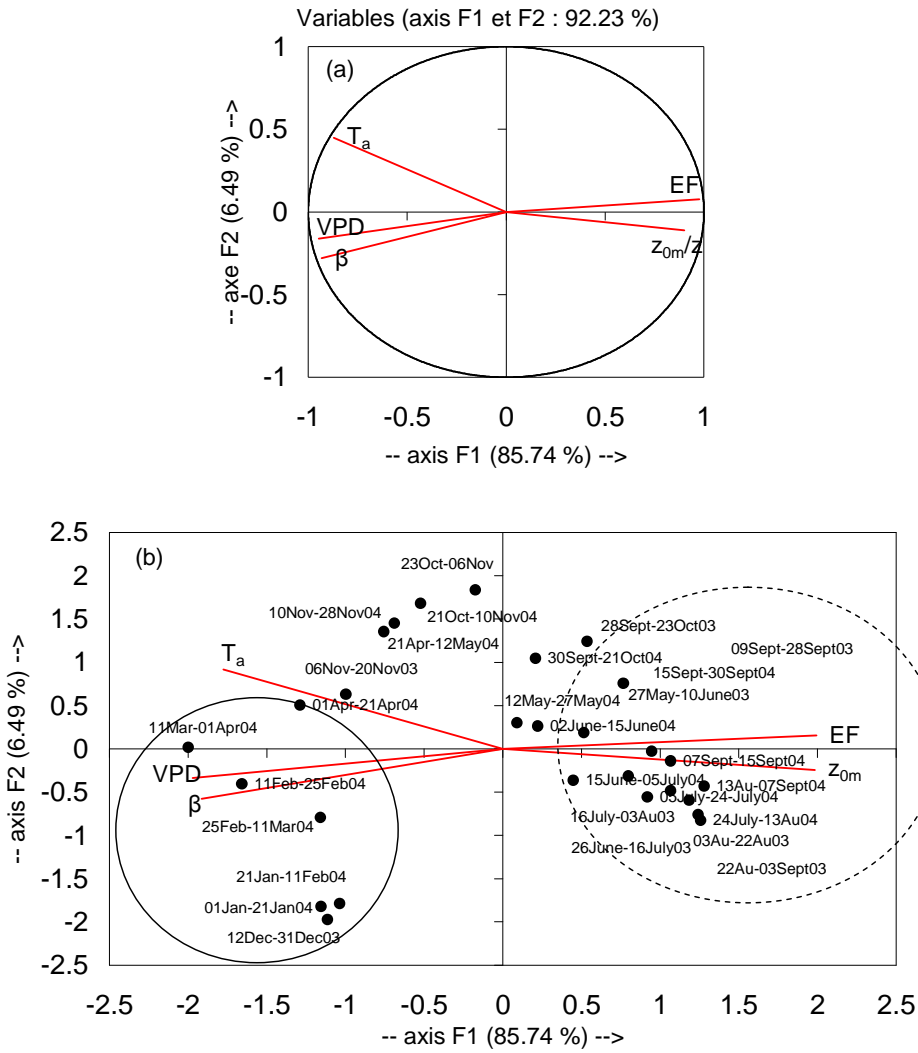|	z_{0m}	β	EF	T_a	VPD
z_{0m}	1	-0.769	0.846	-0.750	-0.808
β	-0.769	1	-0.928	0.714	0.893
EF	0.846	-0.928	1	-0.818	-0.917
T_a	-0.750	0.714	-0.818	1	0.760
VPD	-0.808	0.893	-0.917	0.760	1

Figure 4.11:   (a) Repartition of the variables in the circle of unit radius showing 92 % of the variability of the variables on axis F1 and F2. (b) Biplot of the variables and the corresponding measurement periods. The dash circles shows the correlation between *EF* and z_{0m}, and the period, where that correlation is stronger. Similar representation is shown for β and *VPD* in the continuous circle

b. Modeling

Roughness for momentum and evaporative fraction

The plot of EF versus z_{0m}/z shows two trends (Figure 4.12). The first trend (dry season and transition periods) shows an overall linear increase of EF with increasing z_{0m}/z. During that period, z_{0m}/z account for about 90 % of the variability of EF ($p < 0.0001$). When the crops and grasses mature (July to September), EF seems to be constant and independent of z_{0m}/z. EF ranged from 0.59 to 0.79 with a mean value of 0.73. This is understandable, because the environment tends to evaporate at it potential rate due to the high soil and canopy wetness. Therefore, the different periods are treated independently in the model.
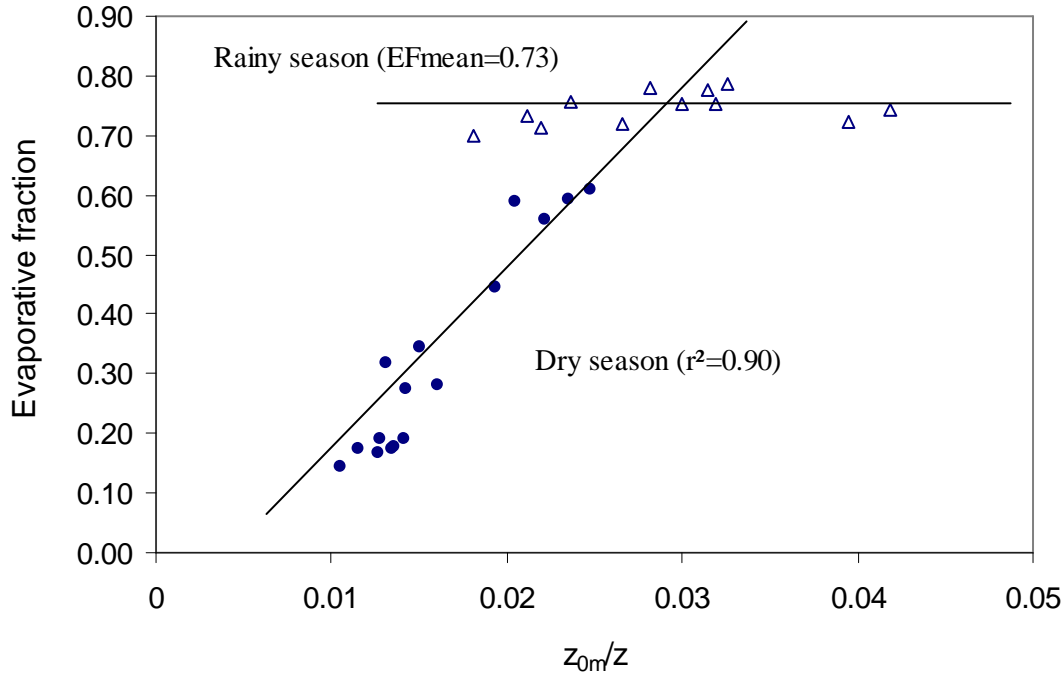

Figure 4.12:   Plot of the evaporative fraction versus the ratio z_{0m}/z

For the maturity period the equation is:

$$EF = 0.73 \qquad (4.11)$$

The evaporative fraction is:

$$EF = \frac{\lambda E}{H + \lambda E} \qquad (4.12)$$

Combining Eq. (4.11) and Eq. (4.12) results in:

$$E = 2.704 \times \frac{H}{\lambda} \qquad (4.13)$$

The energy balance equation gives:

$$H = R_n - G - \lambda E \qquad (4.14)$$

Eq. (4.13) and Eq. (4.11) give:

$$E = 0.73 \times \frac{R_n - G}{\lambda} \qquad (4.15)$$

Eq. (4.15) is similar to the De Bruin (1987) modified equation of the Makkink (1957) formula. The main difference is that the De Bruin equation is expressed as a function of R_s, whereas Eq. (4.15) is expressed as a function of the available energy. However, Eq. (4.15) can be easily rearranged and expressed as a function of R_s, since there is a close relationship between ($R_n - G$) and R_s.

During the dry season and the transitions periods, the evaporative fraction is expressed as follows:

$$EF = 38.645 \frac{z_{0m}}{z} - 0.291 \qquad (4.16)$$

The statistics for the coefficients show that the intercept ($p < 0.0001$) and the constant ($p < 0.001$) are both highly significant.

Combining Eq. (4.12), Eq. (4.14) and Eq. (4.16) gives:

$$E = \left(38.645 \frac{z_{0m}}{z} - 0.291 \right) \frac{R_n - G}{\lambda} \quad \text{or} \quad E = (EF) \frac{R_n - G}{\lambda} \qquad (4.17)$$

Surface conductance was inferred by comparing Eq. (4.10) and Eq. (4.17), since it is during the dry season and the transition periods that transpiration is strongly coupled to the atmosphere. Therefore, the following equation was obtained:

$$g_c = \frac{\left(38.645 \frac{z_{0m}}{z} - 0.291 \right)(R_n - G)\gamma}{\rho_a c_p VPD} \quad \text{or} \quad g_c = \frac{EF \times \gamma (R_n - G)}{\rho_a c_p VPD} \qquad (4.18)$$

The surface conductance during the rainy season could be inferred from Eq. (4.18) by replacing EF by 0.73.

Bowen ratio and vapor pressure deficit

Two trends for β versus VPD were also observed (Figure 4.13).

During the rainy season and the transition periods, an exponential increase in β with increasing VPD ($r^2 = 0.92$) was observed and the equation was expressed as follows:

$$\beta = 0.57VPD + 0.28 \qquad (4.19)$$

As such, about 92% of the variability of β is caused by VPD with an overall significance of $p < 0.0001$ ($SE = 0.09$). This high contribution of VPD to the variability of β is also understandable as they both express water stress in a given environment.

The Bowen ratio is:

$$\beta = \frac{H}{\lambda E} \qquad (4.20)$$

The combination of Eq. (4.19) and Eq.(4.20) gives:

$$E = \frac{1}{1.28 + 0.57VPD} \times \frac{R_n - G}{\lambda} \qquad (4.21)$$

When vegetation is coupled to the atmosphere, Eq. (4.10) and Eq (4.21) can be compared with:

$$g_c = \frac{(R_n - G)\gamma}{\rho_a c_p VPD[1.28 + 0.57VPD]} \quad \text{or} \quad g_c = \frac{(Rn - G)\gamma}{\rho_a c_p VPD(1 + \beta)} \qquad (4.22)$$

During the dry season (December to April), it was observed that β was independent from VPD, which can be explained by the scarcity of moisture. β was more or less constant ($\beta = 4.60$ on average), but an abnormal increase was observed in March ($\beta = 6.01$). This might be related to dust storms which affected most of the Sahelian countries in West Africa in that period. The storms lasted for about one week and might have affected the partitioning of energy flux or the sensitivity of the measurement devices. The general trend was used for this analysis, therefore:

$$\beta = 4.60 \qquad (4.23)$$

Combining Eq. (4.21) and Eq. (4.23) gives:

$$E = 0.179 \times \frac{R_n - G}{\lambda} \qquad (4.24)$$

This last equation could also be quickly obtained from Eq. (4.21) by replacing VPD by 0. Similarly, surface conductance can be estimated during the dry season from Eq. (4.22) by replacing β by 4.60.
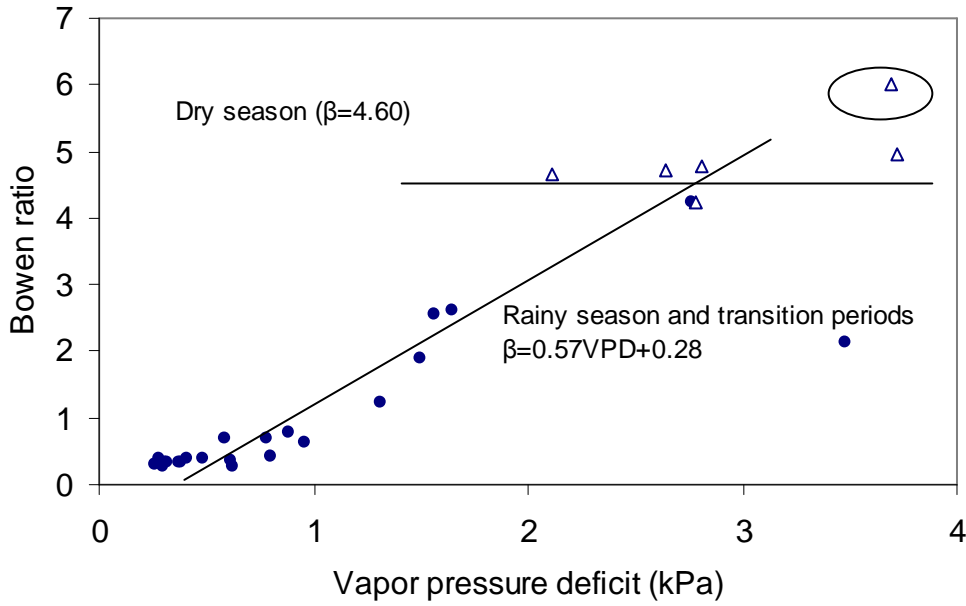
Figure 4.13:   Plot of the Bowen ratio versus vapor pressure deficit

Eq. (4.17) and Eq. (4.21) are two formulations that can be used to estimate actual evaporation on monthly basis. Both give good estimations when compared to the estimation of λE with the Penman-Monteith equation (Figure 4.14), but Eq. (4.21) seems to be more accurate, although all equations led to an underestimation. In fact, the estimation with Eq. (4.17) had a higher absolute MBE (-1.23 W m^{-2}) than the estimation with Eq. (4.21), where MBE=-0.45 W m^{-2}. Similarly, Eq. (4.18) and Eq. (4.22) expressed g_c as a function of the available energy, VPD and especially z_{0m}. This means that the stomatal conductance increases with increasing z_{0m} when the available energy is abundant and decreases with increasing VPD. The overall MBE for both equations was -1.56 mm s^{-1} and -0.84 mm s^{-1}, respectively (Figure 4.15). Both equations lead to an underestimation but once again the estimation with Eq. (4.22) gives more accurate results with regard to the absolute bias error. Similar results were reported by Alves and Pereira (1999), who gave explicit relationships between surface resistance ($1/g_c$) and R_n and between surface resistance and VPD. This clearly explains when R_n governs surface resistance and when VPD becomes determining. Another important aspect is that g_c can also be expressed as a function of EF and β, which expresses implicitly the relationship between g_c and moisture availability.
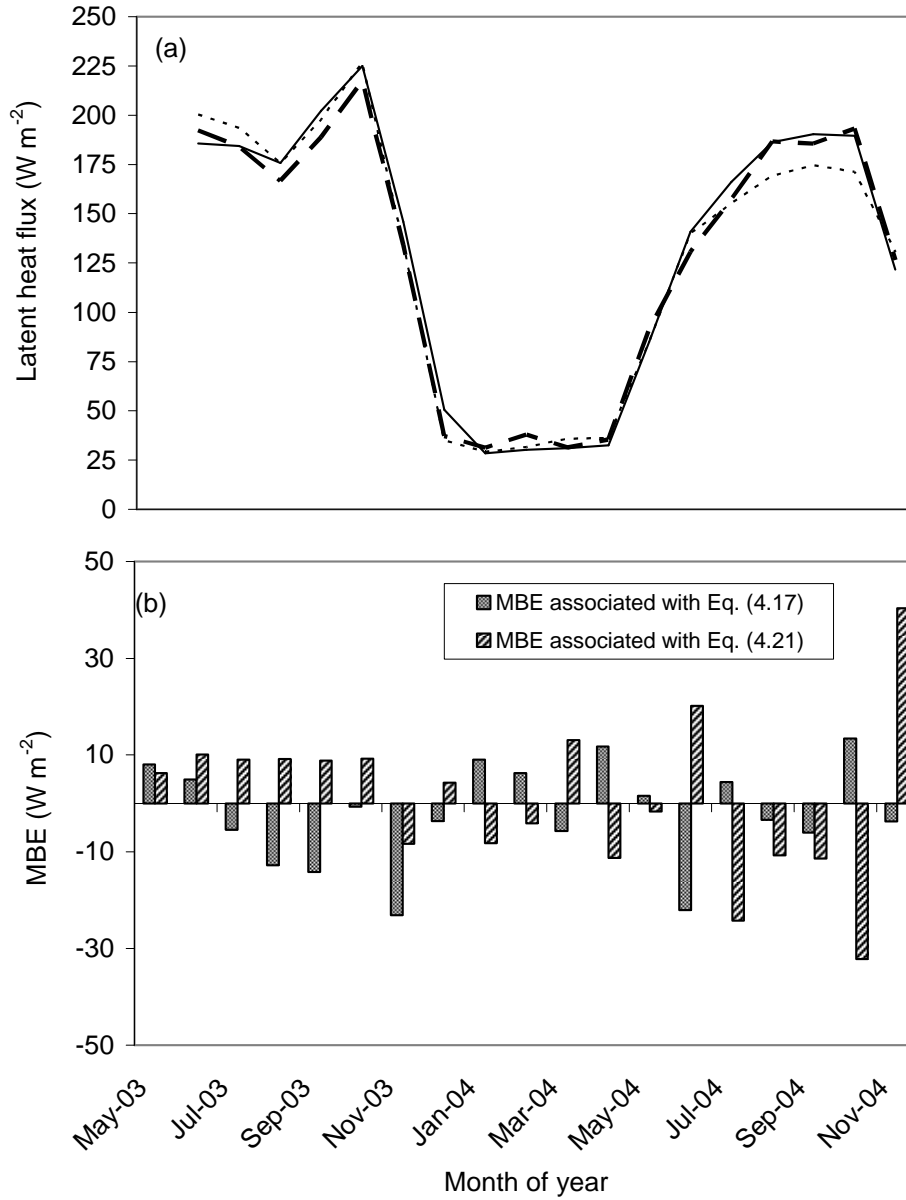
Figure 4.14: Comparison between the observed latent heat flux (continuous line) and the estimation with the new models. The bold dashed line corresponds to the estimation with Eq (4.17), and the light dashed line corresponds to the estimation with Eq. (4.21)

The designed empirical models could be useful and could be easily implemented to estimate actual evaporation in any environment. R_n, G, and VPD are easily measurable with weather stations, which are widely available in the region. If a special device (like an EC station) is not available to accurately measure z_{0m}, this value can be estimated from empirical formulas in the literature (see Brutsaert, 1982; Shaw and Pereira, 1982). In the particular interest of the GLOWA-Volta project, different

EC's and scintillometers have been installed across the Volta basin in different agro-ecological zones and constitute therefore a network of eddy flux measurements, which could be useful to validate the new formulations.
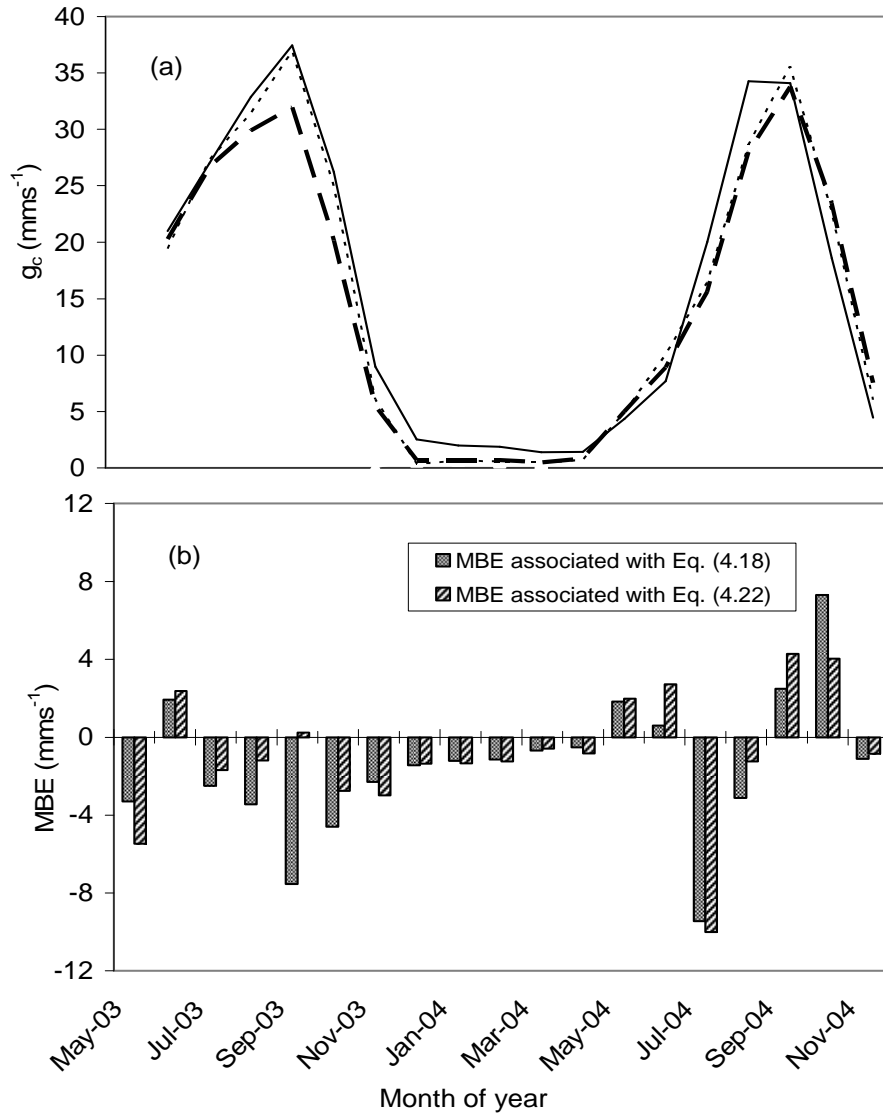

Figure 4.15: Comparison between the surface conductance (g_c) estimated with inverted Penman-Monteith equation (continuous line) and the g_c estimated with new models. The bold dashed line corresponds to the estimation with Eq. (4.22), and the light dashed line corresponds to the estimation with Eq. (4.18)

4.4   Conclusion

This first long-term evaluation of surface fluxes in the West African savanna shows that there is a clear pattern in the partitioning of available energy between sensible heat and latent heat flux. The multiple correlations between variables make it difficult to identify the exact individual contribution of each variable. However, the main driving factor is moisture availability, and all or parts of the other contributing variables in the process depend on this main factor.

During the dry season, the main driving factors reducing the latent heat flux was vapor pressure deficit, while net radiation was non-limiting. A vapor pressure deficit also has a significant effect on surface conductance and vice-versa. During the dry season, the major part of the available energy goes into heating the atmosphere, thus increasing the sensible flux. During the transition periods and the rainy season, the phenomenon is reversed and the latent heat flux becomes the main consumer of the available energy and soil moisture is no longer limiting. During these wetter days, vapor pressure deficit plays minor role, while net radiation becomes the main driving factor. All processes also depend on the abundance and the distribution of rainfall over the rainy season. Another important finding of this study is the clear and pronounced seasonal dynamic of roughness length for momentum. Usually, fixed values of roughness length for momentum are used in land-surface models, since some studies have shown that this variable has only minor effects on surface fluxes. This static treatment of roughness length for momentum seems to be less accurate in the case of savanna vegetation, where there is a drastic change in vegetation cover according to the seasons. Moreover, agricultural activities amplify this change. Similarly, seasonal bush fires, which completely change the morphology of the vegetation cover, could also significantly affect the roughness length for momentum.

The overall results of this study focus on the assumptions given by Smith and Jarvis (1998) regarding developed new equations for their estimation of actual evaporation and surface conductance in the particular case of savanna vegetation submitted to agricultural activities. The new formulations seem to be more consistent. However, independent data sets are not yet available to test the equations more thoroughly. Therefore, independent testing this should be the next step and the recently established flux network of the GLOWA-Volta Project could be useful for that. The

simpler equations developed here could be an alternative to many of the sophisticated models available in the literature. Inclusion of these equations in some of the well known Land Surface Transfer Models should be considered for weather and climate models for the West African savanna.

5 EFFECT OF SEASONAL DYNAMICS OF VEGETATION COVER ON LAND SURFACE MODELS[3]

5.1 Introduction

The performance of most of the land surface models (LSM) is particularly sensitive to the partitioning of the energy on the earth's surface. The LSMs fail when simulating the real seasonal dynamics of the surface fluxes over the semi-arid terrain, especially over the savanna vegetation in West Africa (Schüttemeyer, 2005). The reason for this failure is that the LSMs are mostly calibrated for temperate regions (midlatitudinal regions), where the feedback mechanisms in the boundary layer are more related to the soil wetness, whereas in semi-arid regions this feedback is related to the way stomata release water into the atmosphere (Niyogi et al., 2002; Schüttemeyer, 2005). Another reason is that when these models are based on data of the semi-arid regions, the relatively short observation time leads to a partial modeling or insight of the process of the dynamics of the surface fluxes. An illustration of this situation is the HAPEX-Sahel project (Goutorbe et al., 1994) and the SEBEX project (Sellers et al., 1997). The first project lasted for only three months of intensive observation of the surface fluxes.

In fact, the savanna region is one of the most sensitive areas in the world because of the climate pattern. This region is characterized by a relative short rainy season (May to October) followed by a long dry season (November to April), which implies a complete change in the soil moisture conditions and the morphology of the vegetation. During the rainy season, most of the LSMs accurately estimate the surface fluxes, because the soil wetness is similar to that in the midlatitudinal regions. At the end of the rainy season, the environment starts to dry out and this drying period is not taken into account in most of the models. Schüttemeyer (2005) tested the NOAH LSM in two different regions in Ghana, West Africa, and concluded that the mean bias error increased during the drying period due to the use of wrong values of surface albedo, temperature, leaf area index (LAI) and Zilintekinvich coefficient. The NOAH LSM is a joint product of the National Centers for Environmental Prediction (NCEP), the Oregon State University, the Air Force and the Hydrologic Research Lab and is based on the

---

[3] Material in this chapter is accepted for publication in Hydrology and Earth System Sciences (HESS) with S. Yonkeu, and N.C. van de Giesen as co-authors.

former Oregon State University land surface model (OSULSM) (Ek and Mahrt, 1991). Schüttemeyer (2005) modified the equation used in the model for the estimation of the surface resistance, to adjust it to a real situation of savanna vegetation for the drying period.

Another important parameter affecting the accuracy of the NOAH LSM is the ratio z_{0m}/z_{0h} (roughness length for momentum over the roughness length for heat). Most of the authors used a fixed value for this ratio, which could be one for the reasons of its failure to simulate accurately the surface fluxes over the savanna vegetation of West Africa. In fact, the roughness length for momentum is not constant over time and variation is more pronounced over a terrain under intensive agriculture because of the large change in the vegetation fraction and *LAI* according to season. A seasonal bush fire, especially during the dry season, also changes this variable in areas without any agricultural activities. Therefore, the objective of this study is to evaluate and to test the sensitivity of the LSMs to the dynamics of the vegetation cover with respect to z_{0m}. The NOAH LSM is used for this purpose because it constitutes a typical LSM, which couples the soil and the vegetation to the atmosphere by the surface exchange coefficient for heat (C_h). The sensitivity of the NOAH LSM with respect to z_{0m} could illustrate the behavior of most of the LSMs, because they all have a similar conception. First, the standard form of NOAH LSM (fixed value of z_{0m} for all periods) was evaluated and, the result then compared the result to the one using the seasonal values of z_{0m} calculated from the data collected in Kompienga (East Burkina Faso: 11° 07' N; 0° 31' E) from May 2003 to November 2004. The results cover almost two years, including one relatively wet (2003) and one relatively dry (2004) year. They can contribute to obtaining more insight and to better understanding of the real dynamics of the surface fluxes, and to refining the land surface models in this environment. The research was conducted within the framework of the GLOWA-Volta (van de Giesen et al., 2002) and VinVal projects.

5.2   Model description

The NOAH LSM model is based on the principle of the NCEP meso-scale evaporation model. There are two major concepts: the multi-layer soil and the simple canopy layer

concept. The multi-layer soil concept is based on the model of Mahrt and Pan (1984), and the moisture used for the canopy transpiration is extracted from the different layers using a weighting function including the root depth and a uniform root distribution. The water and heat budget in the soil is based on the Richards equation coupled to the Fourier law of diffusion. The surface skin temperature is determined following Mahrt and Ek (1984) by applying a single linear surface energy balance equation representing the combined ground/vegetation surface. The canopy layer concept is based on the model of Pan and Mahrt (1987), which has been extended by Chen et al. (1996) to include the complex canopy resistance approach of Noilhan et Planton (1989) and Jacquemin and Noilhan (1990). This is an empirically based approach for canopy resistance following the original model of Jarvis (1976) and Stewart (1996).

The subgrid variability is taken into account with a Reynold's number-dependent formulation for the ratio of roughness length for momentum (z_{0m}) in [m] and heat (z_{0h}) in [m]. The formulation proposed by Zilitinkevich (1995) is used in NOAH and is expressed as follows:

$$kB^{-1} = \ln\left(\frac{z_{0m}}{z_{0h}}\right) \tag{5.1}$$

with $B^{-1} = C\sqrt{\text{Re}^*}$ and $\text{Re}^* = \frac{u^* z_{0m}}{\nu}$

where k is the von Kármán constant ($k = 0.41$), ν is the kinematic molecular viscosity [-], Re^* is the roughness Reynolds number [m^2 s^{-1}], u^* is the friction velocity [m s^{-1}], and C is the coefficient ranging from 0.2 to 0.4. According to Schüttemeyer (2005), a value of $C = 0.6$ is suitable for the savanna region of West Africa.

The canopy resistance is modeled as a function of the atmospheric forcing and the soil moisture availability. The total evaporation (E) is the sum of the direct evaporation from the bare soil (E_b) in [mm], the wet canopy evaporation (E_c) in [mm] and the dry canopy transpiration (E_t) in [mm]. E_b is calculated as follows:

$$E_b = (1 - \alpha_V)\beta_b E_p \tag{5.2}$$

with

$$\beta_b = \frac{\Theta_1 - \Theta_{wp}}{\Theta_{fc} - \Theta_{wp}} \qquad (5.3)$$

where E_p is the potential evaporation [mm] calculated based on Mahrt and Ek (1984).

Θ_{fc} and Θ_{wp} are the soil water content at field capacity and wilting point, respectively.

α_V is the green vegetation fraction for the partitioning of the total evaporation.

The evaporation of the water intercepted by the canopy is computed as follows:

$$E_c = \alpha_V E_p \left(\frac{W_c}{S} \right)^n \qquad (5.4)$$

where W_c is the intercept canopy water content [mm], S is the maximum allowed W_c capacity ($W_c = 0.5$ mm), and $n = 0.5$.

The dry canopy transpiration is determined by:

$$E_t = \alpha_V E_p B_c \left[1 - \left(\frac{W_c}{S} \right)^n \right] \qquad (5.5)$$

with

$$B_c = \frac{1 + \dfrac{\Delta}{R_r}}{1 + R_c C_h + \dfrac{\Delta}{R_r}} \qquad (5.6)$$

where C_h is the surface exchange coefficient for the heat and moisture [m s^{-1}], Δ is the slope of the saturated specific humidity curve [mbar K^{-1}], R_r is a correction coefficient and is a function of the surface air temperature [W m^{-2} mbar^{-1}], the surface pressure, and C_h. There are two possible formulations of C_h (Chen et al. 1997). We present here the formulation based on the Obukhov length expressed as follows:

$$C_h = \frac{k^2 / R}{\left[\ln\left(\dfrac{z}{z_{0m}}\right) - \psi_m\left(\dfrac{z}{L}\right) + \psi_h\left(\dfrac{z_{0m}}{L}\right)\right] \times \left[\ln\left(\dfrac{z}{h_{oh}}\right) - \psi_m\left(\dfrac{z}{L}\right) + \psi_h\left(\dfrac{z_{0h}}{L}\right)\right]} \qquad (5.7)$$

where z is the measurement height [m], L is Monin-Obukhov length [m] and $R = 1.0$. ψ_m and ψ_h are the similarity theory-based stability functions for the momentum and heat, respectively. Paulson (1970) integrated a set of analytical expressions to specify a non-dimensional wind speed and potential temperature gradients as a function of $\dfrac{z}{L}$. Following Sun and Mahrt (1995), these stability functions are expressed as follows:

$$\psi_m = \begin{cases} -5\xi & 0 < \xi < 1 \\ 2\ln\left(\dfrac{1+x}{2}\right) + \ln\left(\dfrac{1+x^2}{2}\right) - 2\tan^{-1}(x) + \dfrac{\pi}{2} & -5 < \xi < 0 \end{cases} \qquad (5.8)$$

$$\psi_h = \begin{cases} -5\xi & 0 < \xi < 1 \\ 2\ln\left(\dfrac{1+x^2}{2}\right) & -5 < \xi < 0 \end{cases} \qquad (5.9)$$

with

$$\xi = \frac{z}{L} \text{ and } x = (1 - 16\xi)^{1/4} \qquad (5.10)$$

R_c is the canopy resistance and is based on the "big-leaf" approach developed by NP89 following the original approach of Jarvis (1976) and Stewart (1988). It is computed as follows:

$$R_c = \frac{R_{c\min}}{LAI \times F_1 \times F_2 \times F_3 \times F_4} \qquad (5.11)$$

where

$$F_1 = \frac{R_{c\min}}{R_{c\max} + \dfrac{f}{1+f}}$$

(5.12)

with

$$f = 0.55 \frac{R_g}{R_{GL}} \frac{2}{LAI}$$

(5.13)

where $R_{c\min}$ and $R_{c\max}$ is the minimum and maximum canopy resistance[s m^{-1}], respectively. R_g is the global radiation at the surface [W m^{-2}], R_{GL} is site dependent parameter [W m^{-2}], and LAI is leaf area index [-]

F_2 is based on the new formulation of Schüttemeyer (2005) and is computed as follows:

$$F_2^{-1} = \exp(-g_D VPD)$$

(5.14)

where g_D is an optimised parameter for the savanna conditions [g kg^{-1}] and VPD is the air pressure deficit [mbar].

$$F_3 = 1 - a_T \left(T_{ref} - T_a \right)^2$$

(5.15)

where a_T is thermal coefficient [-], T_{ref} is the reference temperature and T_a is the air temperature [C].

$$F_4^{-1} = \begin{cases} 0 & \varpi < \Theta_w \\ \dfrac{\varpi - \Theta_w}{\Theta_{ref} - \Theta_w} & \Theta_w < \varpi < \Theta_{ref} \\ 1 & \varpi > \Theta_{ref} \end{cases}$$

(5.16)

where $\varpi = \sum_{i=1}^{z} R_m$, R_m is the root density [m m^{-3}]calculated according to Zeng et al. (1998) and m is the number of soil layers [-]. Θ_w and Θ_{ref} are soil moisture at wilting point and field capacity [m^{-3} kg^{-1}], respectively.

The forcing data used in the model are summarized in Table 5.1 together with the coefficients and parameters. The vegetation type was set to savanna and the same vegetation fraction set by Schüttemeyer (2005) for Tamale was used. The soil type was set to sandy loam according to Ungaro et al. (2004). More details on the model can be found in Schüttemeyer (2005), Chang et al. (1999), and Cheng et al. (1997).

5.3 Method

The NOAH LSM was run off-line and the simulated sensible and latent heat flux were validated with hourly eddy fluxes measured at 10 m height above the ground surface. The forcing data were obtained from a nearby automatic weather station, at 2 m above ground surface. The sample period was 5 seconds and the average value of all variables was stored every 20 min. The ground heat flux and net radiation were not directly measured, therefore the analysis focused on the sensible and latent heat flux on an hourly basis. The time step for the integration was set to one hour. Eddy fluxes and the atmospheric forcing data were available from May 2003 to November 2004 with some gaps because of technical problems with the station. Therefore, the model was run for those periods, where data was available (the period between downloads). For each period, the model was run with a corresponding seasonal value of z_{0m} calculated according to Martano (1999) with a fixed value z_{0m} as used in the standard form of NOAH LSM. This fixed value of z_{0m} was set to 0.216 m, the average of the whole seasonal z_{0m}. The results for each run were compared on a seasonal basis, and on a daily basis for two selected periods during the drying period (DOY348 to DOY365), and the rainy season (DOY227 to DOY250). The seasonal values of z_{0m} are presented in Table 5.2. In order to test the sensitivity of the model to the initial moisture in the soil and to canopy water content, E_b and E_c were neglected during the completely dry season (from December to late April), and the results were compared to the case when all components of evaporation were taken into account.

The surface downward longwave radiation was not directly measured. It was estimated using air temperature and relative humidity following Idso and Jackson (1969) for clear sky conditions (see Schüttemeyer, 2005).

Table 5.1:   Parameters used in NOAH LSM and values

Designation	Parameters & coefficients	Value	Units
General parameters			
Vegetation fraction	α_V	See Table 5.2	[-]
Albedo	α		[-]
Maximum canopy interception capacity	S	0.50	mm
Roughness length for momentum	z_{0m}	See Table 5.2	m
Roughness length for heat	z_{0h}		m
Soil moisture at field capacity	θ_{fc}	0.32	$m^3\ kg^{-1}$
Soil moisture at wilting point	θ_{wp}	0.01	$m^3\ kg^{-1}$
Soil porosity			%
Maximum canopy resistance	R_{cmax}	5000.00	$s\ m^{-1}$
Minimum canopy resistance	R_{cmin}	18.00	$s\ m^{-1}$
Leaf area index	LAI	3.00	[-]
R_{GL}		30 for trees and 100 for crops (Jacquemin and Noilhan, 1990)	$W\ m^{-2}$
g_D		36.7 (Huntingford et al., 1995) for savannah	$g\ kg^{-1}$
Thermal coefficient	a_T	0.0016 (Ek and Holtslag, 2004)	K^{-2}
Reference temperature	Tref	298 (Jacquemin and Noilhan, 1990)	K
Root distribution over 4 layers (Schüttemeyer, 2005)	27; 37; 27; 9; 34; 27, 14		%
Atmospheric forcing data			
Air temperature	T_a		K
Relative humidity	R_h		%
Surface pressure	P_s		mbar
Wind speed	u		$m\ s^{-1}$
Surface downward longwave radiation	R_{sL}		$W\ m^{-2}$
Solar radiation	R_s		$W\ m^{-2}$
Precipitation	P		mm

Table 5.2: Seasonal vegetation fraction (α_V) and albedo (α) and roughness length for momentum (z_{0m})

Month of the year	Vegetation fraction	Albedo	z_{0m}
January	0.04	0.22	0.14
February	0.02	0.27	0.13
March	0.05	0.3	0.11
April	0.08	0.25	0.14
May	0.24	0.24	0.22
June	0.4	0.24	0.20
July	0.47	0.26	0.27
August	0.56	0.25	0.42
September	0.61	0.26	0.32
October	0.51	0.22	0.25
November	0.3	0.23	0.14
December	0.12	0.23	0.12

5.4 Results and discussion

The results from the model were compared to the observed values for sensible heat and latent heat flux on a seasonal and daily basis. The sensitivity of the model with respect to the roughness length for momentum is discussed as well as the sensitivity to the initial soil moisture in the soil layer. Recommendations are given for refining the model to a savanna environment under intense agriculture.

5.4.1 Comparison at seasonal basis

a. Latent heat flux

NOAH LSM reasonably reproduces the seasonal pattern of λE but underestimates it most of the time as shown by the seasonal pattern of the mean bias error (MBE) (Figure 5.1). When a fixed value of z_{0m}=0.216 m was used for the simulation, the average MBE of -35 W m^{-2} and -40 W m^{-2} was obtained during the rainy season of 2003 and 2004, respectively. During the transition period (drying up and wetting periods), the average MBE was -5 W m^{-2}. Similarly, during the dry period the average MBE was -19 W m^{-2}. The absolute value of the MBE is relatively important during the rainy season in contrast to the transition period (drying and wetting period). The model underestimates λE in the rainy season and might be related to the measurement device. In fact, in eddy covariance systems, air moisture content is measured with a Krypton hygrometer, which

has a pathway of 1 cm between the lenses. Sometimes, under rainy conditions, the lenses can be wetted completely by rain drops, which can lead to an overestimation of λE. Likewise, dew can cause a similar effect and can also lead to an overestimation of λE. This fact becomes clear when λE is analyzed on a daily basis (see section 5.4.3). The weakness of the MBE in the transition periods might be related to the modification by Schüttemeyer (2005), who adjusted the estimation of the surface resistance to the climatic conditions of the West African savanna during those periods. However, as the work of Schüttemeyer was limited to only one drying period (from August 2003 to January 2003), the improvement seems to be limited to that period and does not take into account the situation during the dry period (January to April), where the MBE increased again. When all components of the evaporation where taken into account, the model led to an overestimation of about 58 % of the observed λE in December (DOY348 to DOY365). Similar observations were found on a daily basis for the same period, where the MBE was 34 W m^{-2} (see section 5.4.2). Similarly, the model overestimated the observed λE by 38 % between January and February. This observation seems to be related to the static treatment of the initial moisture conditions in the soil layer. Ek and Holtslag (2004) came to similar conclusions in their study at Cabauw, Netherlands. According to those authors, a change of moisture in the soil layer by a few percent can have a notable effect on the surface fluxes, i.e, on observed as well as modeled. Therefore, more attention should be given to soil moisture conditions. Instead of a static treatment, a seasonal pattern should be taken into account to reduce this error.

When the analysis using the seasonal values of z_{0m}, was repeated a relatively weak improvement of the absolute MBE during the rainy and dry season (-28 W m^{-2} and -37 W m^{-2} during the rainy season of 2003 and 2004, respectively, and -16 W m^{-2} during the dry season) was obtained. In contrast, the absolute value of the MBE increased during the transition periods (MBE=-9 W m^{-2}). Therefore, it can be conclude that, the simulation of λE was not very sensitive to the change in z_{0m} on a seasonal basis.
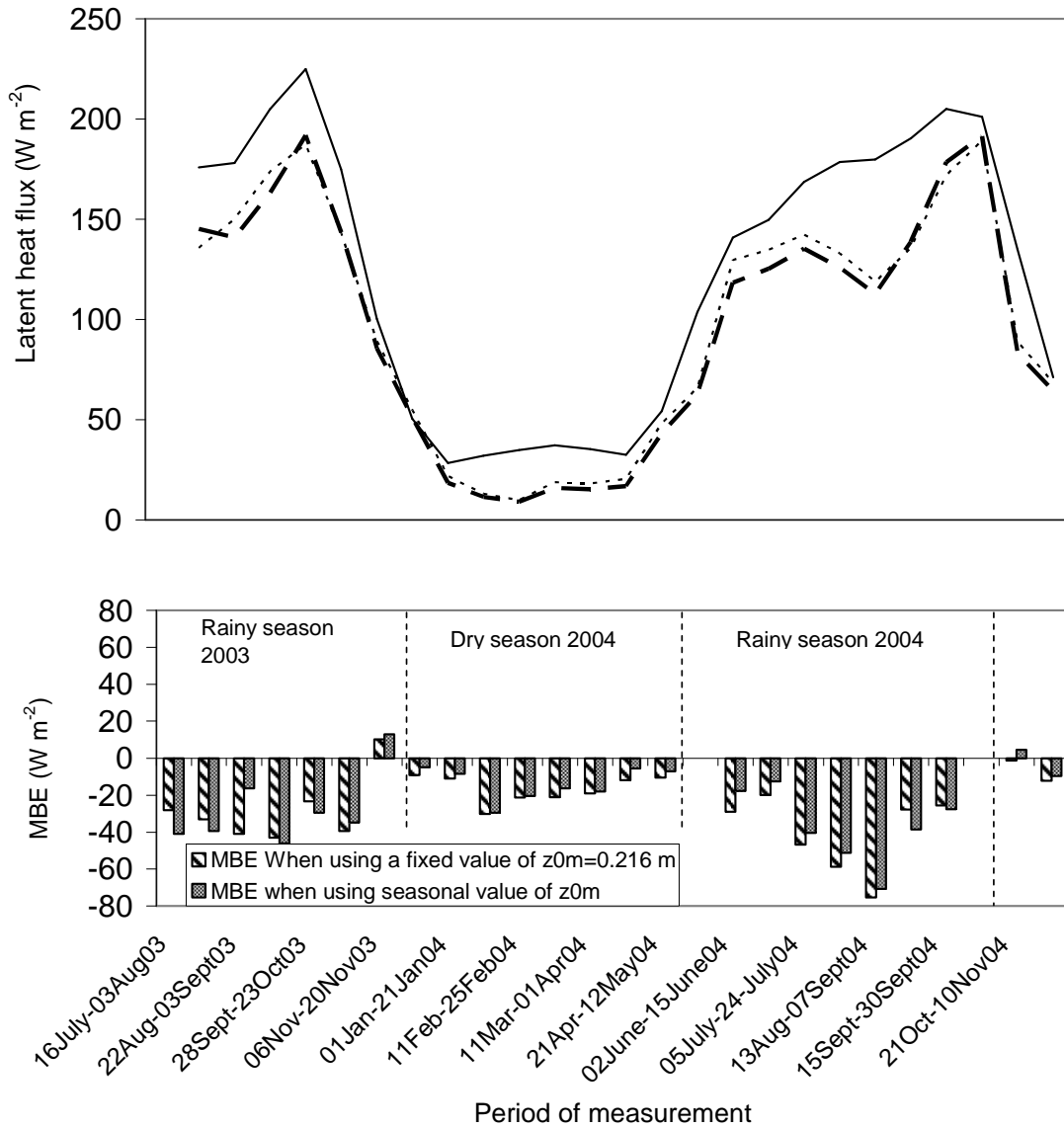
Figure 5.1:   Comparison between the observed and simulated latent heat flux on a seasonal basis. The stick line corresponds to the measured latent flux, the bold dashed line corresponds to the simulated latent heat using a fixed value of z_{0m}, while the light dashed line corresponds to the simulated latent heat flux using the seasonal values of z_{0m}

b. Sensible heat flux

A similar analysis for the case of λE was performed. In the simulation, a fixed value of z_{0m} =0.216 m was first used and then a season-dependent value corresponding to each period. As shown in Figure 5.2, the simulated H fits the observed H quite well. The MBE is low during the rainy season for both cases with an overall underestimation

during the rainy season of 2003 (MBE of - 0.82 W m^{-2} and -1.6 W m^{-2} in the case of a fixed value of z_{0m} and a seasonal value of z_{0m}, respectively). Similarly, the model led to an overall overestimation during the rainy season of 2004. This underestimation in 2003 and the overestimation in 2004 could be related to the distribution of the rainfall during both rainy seasons. In fact, during the rainy season of 2003, the rainfall was distributed well, so that the value of the surface albedo and the vegetation fraction was stable and reflected the real situation in the field. In contrast, rainfall was very irregular during the rainy season of 2004, so that the surface albedo and the vegetation fraction changed appreciably between the two rainfall events. Therefore the value of the surface albedo and the vegetation fraction may not reflect the real field conditions.

The model also underestimated the observed H between October and November 2003 corresponding to the beginning of the drying period (Figure 5.2) and might be related to use of incorrect surface albedo and the vegetation fraction value. In the drying and the completely dry period, the model led to an overall overestimation of the sensible heat flux (MBE =4 W m^{-2} for both cases). This overestimation could also be related to the incorrect value of the surface albedo, the vegetation fraction and the coefficient of Zilitinkevich, which have a direct effect on sensible heat flux, net radiation and latent heat flux though the calculation of the ratio z_{0m}/z_{0h}. Therefore, the simultaneous analysis of these three variables could be a first step in understanding this process (Schüttemeyer, 2005). In fact, these three variables are related to each other according to the principle of the energy balance closure.

Here, it was also observed that the use of the seasonal value of z_{0m} does not have a strong effect on the simulation of the sensible heat flux. However, z_{0m} becomes more relevant when analyzing LE and H on a daily basis. This is the focus of the next section 5.4.2.
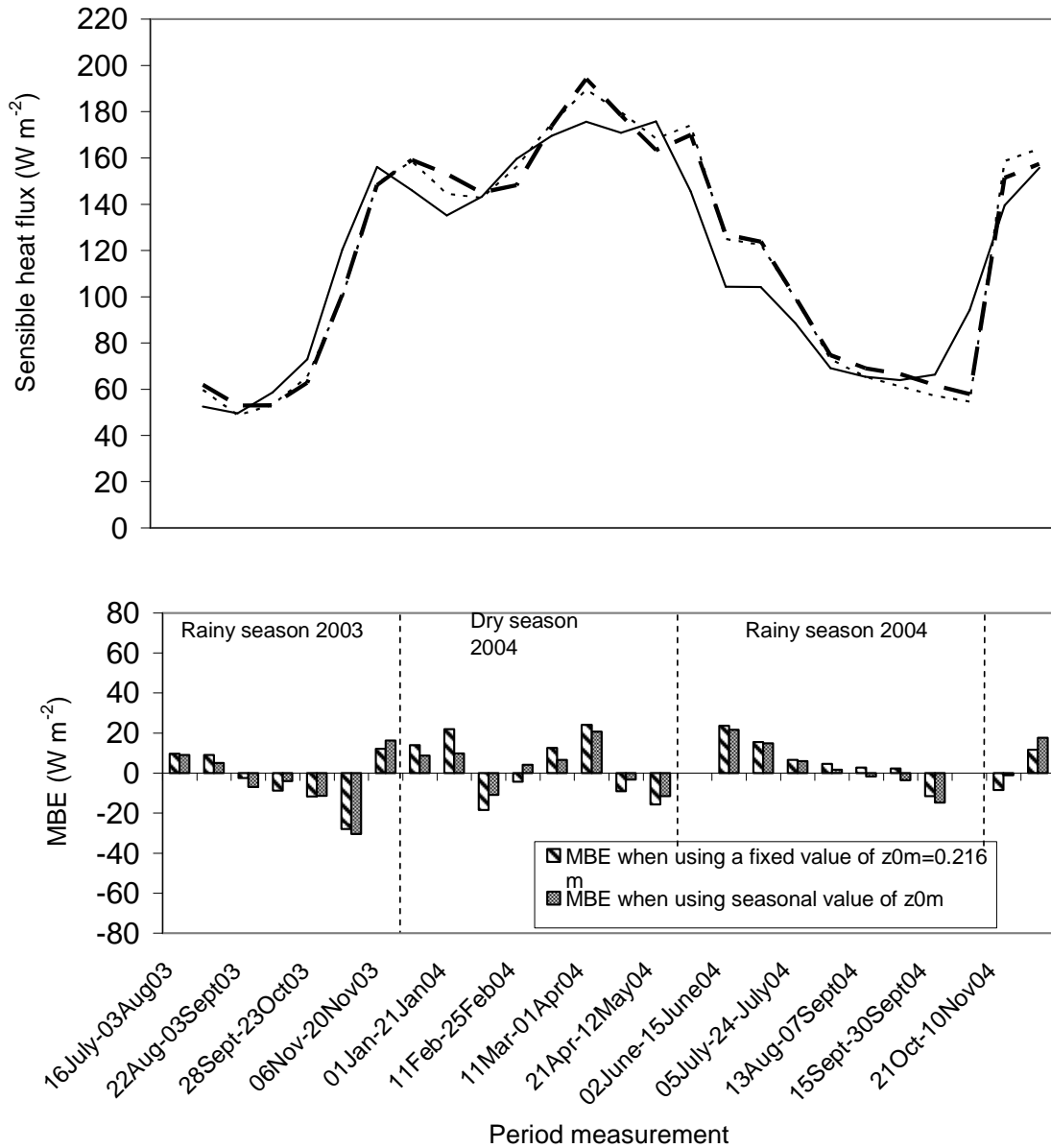
Figure 5.2:   Comparison between observed and simulated sensible heat flux on a seasonal basis. The stick line corresponds to the measured sensible heat flux, the bold dashed line corresponds to the simulated sensible heat using a fixed value of z_{0m}, while the light dashed line corresponds to the simulated sensible heat flux using the seasonal values of z_{0m}

5.4.2   Comparison on a daily basis (drying period)

a. Latent heat flux

The period from DOY348 to DOY365 (December 2003) was selected to show the relevance of changes in z_{0m}. For this, only the dry canopy transpiration was considered, and the result was compared to the case all components of the evaporation were

considered. Figure 5.3 shows that λE simulated using the season-dependent value of z_{0m} =0.115 m corresponding to the selected period produces a more accurate estimation of λE than the fixed value of z_{0m} 0.216 m, although both led to an underestimation. The overall MBE related to the use of z_{0m} =0.115 m was -5 W m^{-2} and -10 W m^{-2} for z_{0m} =0.216 m. This was found to be related to the surface exchange coefficient for heat (C_h). In fact, it was noticed that small values of z_{0m} led to higher C_h value and, therefore, to a higher potential evaporation. As the calculation of dry canopy transpiration is directly related to the potential evaporation by the weighting coefficients, the small values of z_{0m} will always leads to higher values of the actual evaporation during the dry season, while the other components are neglected. This conclusion is somehow contradictory to the definition of roughness length for momentum.
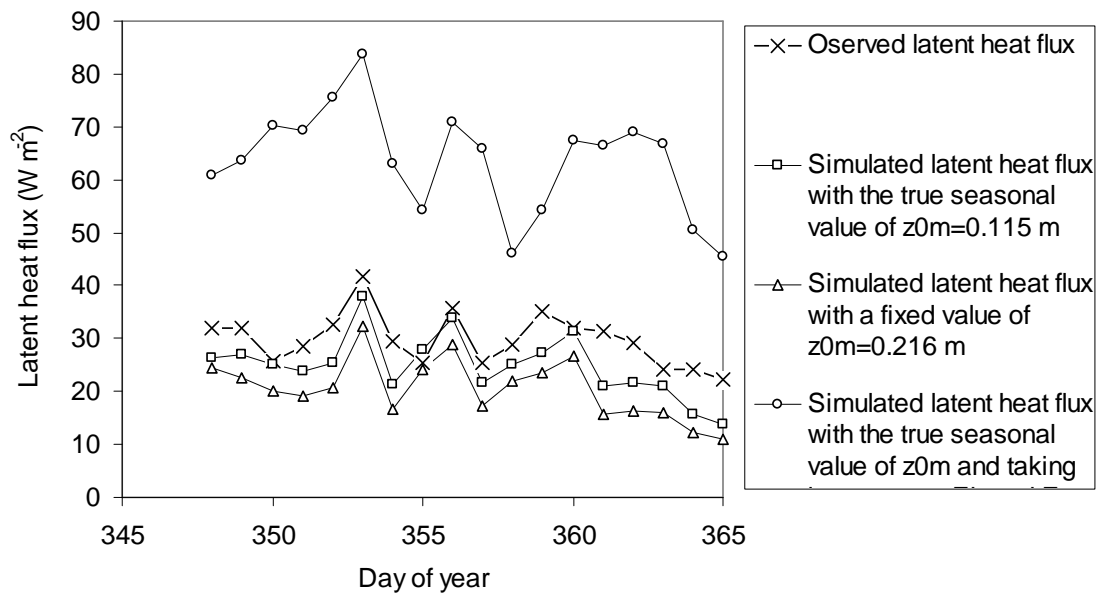

Figure 5.3:   Comparison between observed and simulated latent heat flux on a daily basis from DOY348 to DOY365 (drying period)

In fact, in the particular case of the vegetation cover, higher values of z_{0m} mean denser and taller vegetation in contrast to small values of z_{0m}, which should correspond to less a dense and lower vegetation. A higher z_{0m} should lead, in principle, to a higher actual evaporation for similar vegetation and climatic conditions.

b. Sensible heat flux

The sensible heat flux produced similar results to those for the latent heat flux. The season-dependent value of z_{0m}=0.115 m gives a more accurate estimation of the sensible heat flux (MBE=8 W m^{-2}) than the fixed value of 0.216 m (MBE=13 W m^{-2}) (Figure 5.4). Both overestimate the sensible heat flux. The heat exchange coefficient also contributed to this overestimation.
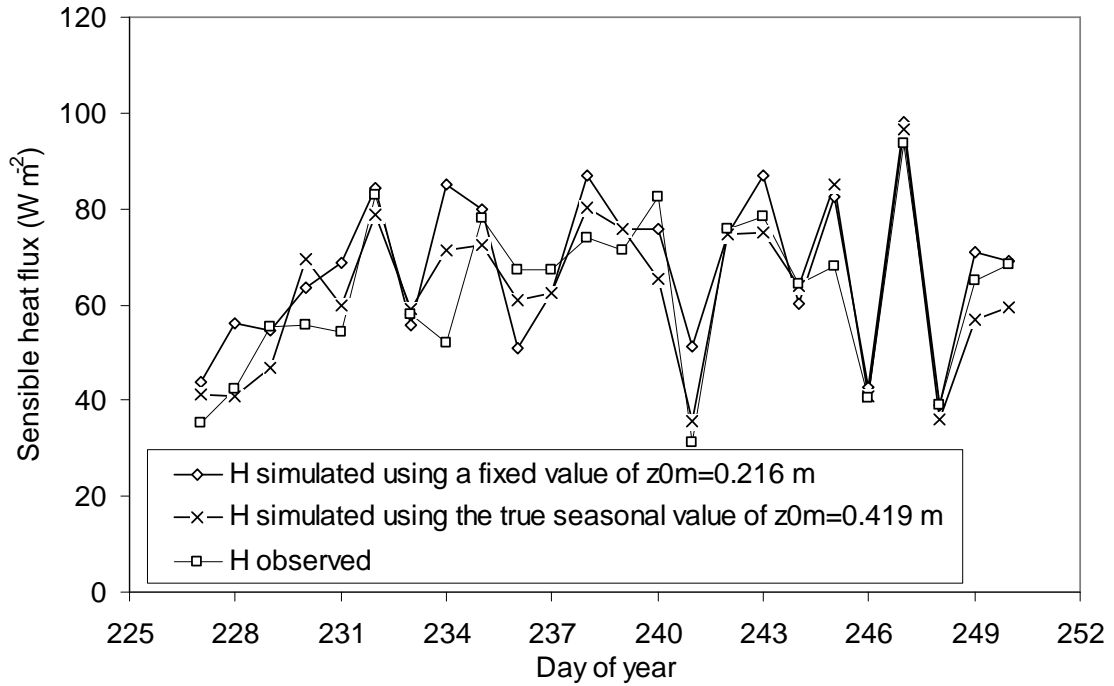

Figure 5.4:   Comparison between the observed and simulated sensible heat flux from DOY348 to DOY365

5.4.3   Comparison on a daily basis (wet period)

For this part of the analysis, all components of the actual evaporation were considered in the analysis. As during the dry season, the season-dependent value of z_{0m} gives a more accurate estimation of λE as well as H. For λE, the model underestimates the observed value for reasons explained in section 4.1 with MBE of -65 W m^{-2} for z_{0m}=0.419 m (seasonal value) and -71 W m^{-2} for z_{0m}=0.216 m (fixed value) (Figure 5.5).
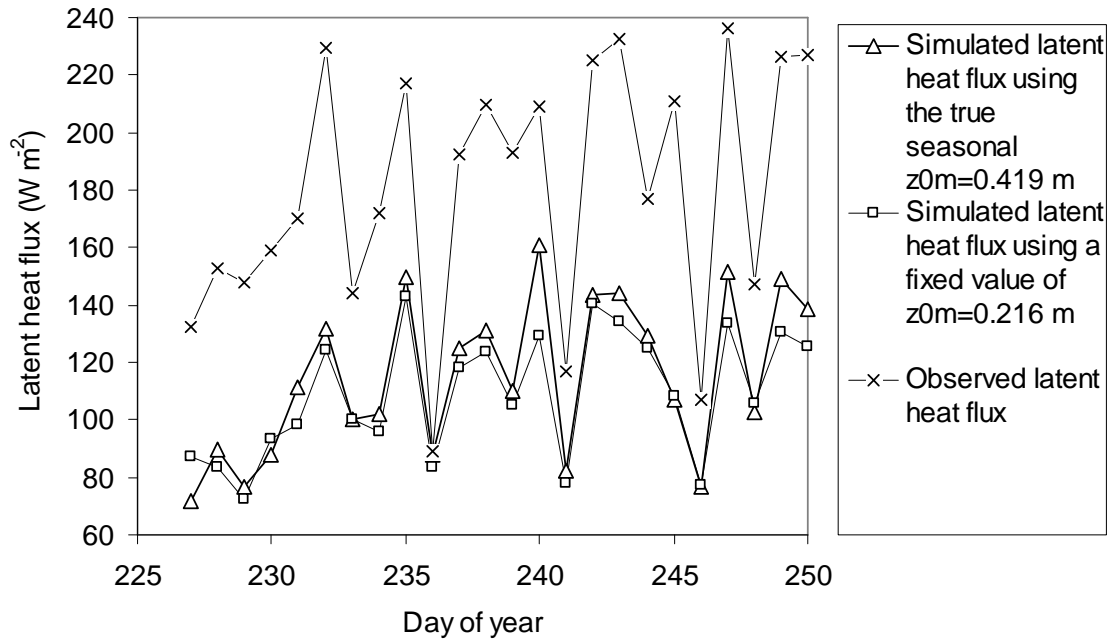
Figure 5.5:   Comparison between the observed and simulated latent heat flux from DOY 227 to DOY 250 (wet period)

With respect to the sensible heat flux, the model overestimates with MBE=0.3 W m^{-2} for z_{0m}=0.419 m (seasonal value) and 5 W m^{-2} for z_{0m}=0.216 m (fixed value) (Figure 5.6). The fact that small values of z_{0m} produce a higher evaporation (see section 5.4.1) seems to be compensated by the other components of evaporation. In fact, during the rainy season, the major part of the actual evaporation is the contribution of direct evaporation from the soil and the evaporation of water intercepted by tree leaves.

In all cases, there was no significant improvement when the simulated fluxes using seasonal values of z_{0m} were compared to those using a fixed value for all periods. However, the true value of z_{0m} (seasonal value) seems to be necessary to enhance the performance and the accuracy of the land surface models. The MBE was always weaker when a seasonal value of z_{0m} was used and appreciably so on a daily basis. Therefore, great attention should be paid to this parameter, and there is a need to take into consideration the seasonal dynamics in the case of a savanna area with intensive agriculture. Even if the area is not subject to agricultural activities, a seasonal bush fire could appreciably change the roughness length for momentum, which stresses the relevance of a deeper analysis of the effect of z_{0m}.
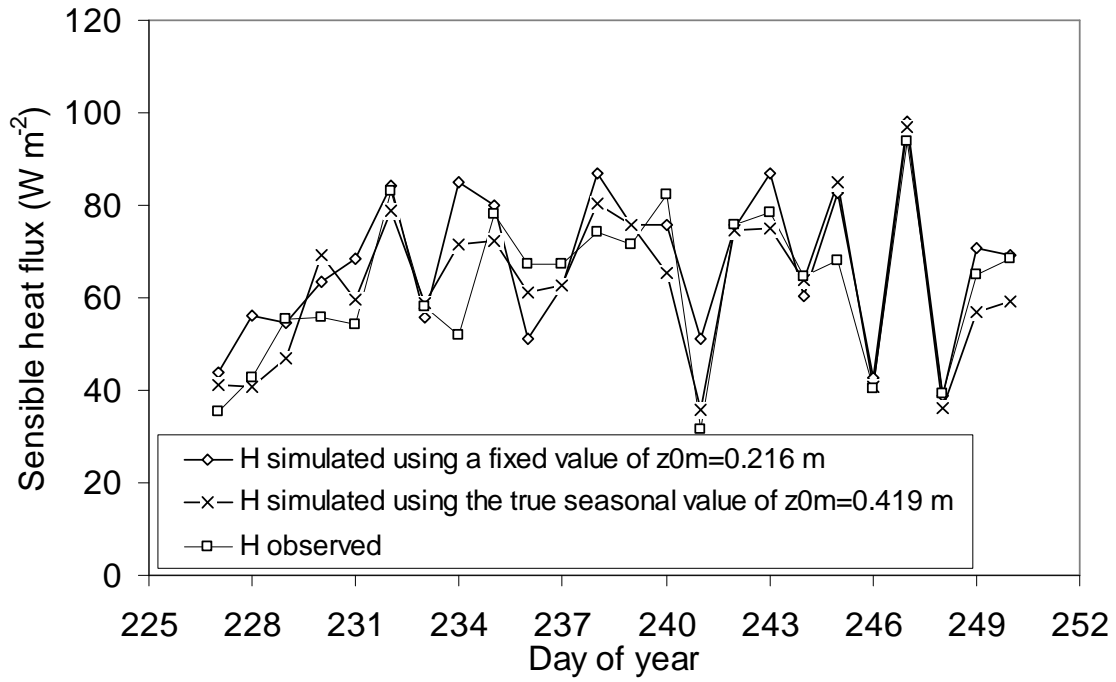
Figure 5.6:   Comparison between the observed and simulated sensible heat flux DOY 227 to DOY 250 (wet period)

5.4.4   Cause of insensitivity and proposed improvement

As previously pointed out, the insensitivity of the NOAH LSM to z_{0m} is probably related to the formulation of the part of the model that couples the soil and the vegetation to the atmosphere. This coupling is by the coefficient B_c explicitly expressed in the dry canopy transpiration (see Eq. 5.5). B_c is a function of the surface exchange coefficient for heat (C_h), which in turn is explicitly expressed as a function of z_{0m}. Therefore, B_c was calculated step by step to highlight the part of the formulation that makes it insensitive to z_{0m}.   This procedure was started by the surface exchange coefficient (C_h), which was independently calculated with Eq. (5.7) using the seasonal values of z_{0m} and a fixed value of 0.216 m. Figure 5.7 shows that there is a clear difference   between   both   cases.   The   relative

MBE ($\dfrac{C_h(z_{0m}=0.216)-C_h(seasonal)}{C_h(z_{0m}=0.216)}\times100$) was negative during both rainy seasons

and positive during the transition periods and dry the season. The higher peaks were

observed in August (a period of maximum growth and maximum z_{0m}) and were 25 % and 38 % during the rainy season of 2003 and 2004, respectively. During the dry season and the transition periods, the maximum MBE was 56 % and in March (the driest period corresponding to the weakest value of z_{0m}=0.115 m). Similar observations and relative MBE were found for the surface resistance (R_c) estimated by inverting the Penman-Monteith equation (Monteith, 1965). The inverted equation was preferred because it gave more accurate estimations than the formulation based on NP89. This was related to the use of constant value for moisture in a soil layer, because long-term measurements were not available. In fact, Huntingford et al. (1994) mentioned that in the Sahelian savanna, nothing is to be gained by using more complicated models than a Big Leaf Model based on inverting the Penman-Monteith equation.

When B_c was calculated, it was seen that the net difference observed in C_h and R_c was significantly reduced. The relative MBE value were now positive and weaker during the rainy seasons (0.82 % and 1.33 in 2003 and 2004, respectively), and negative during the dry season and the transition periods (the higher absolute value was 7 % and was found in March) (Figure 5.8). The weakness of the relative MBE and its inversion were found to be related to the product $R_c \times C_h$ in the denominator of the equation expressing B_c. This product annihilates the effect of the use of seasonal values and the fixed value of z_{0m} on C_h and R_c (Figure 5.8). Therefore, the product $R_c \times C_h$ is the major cause of the insensitivity of NAOH LSM to z_{0m}.
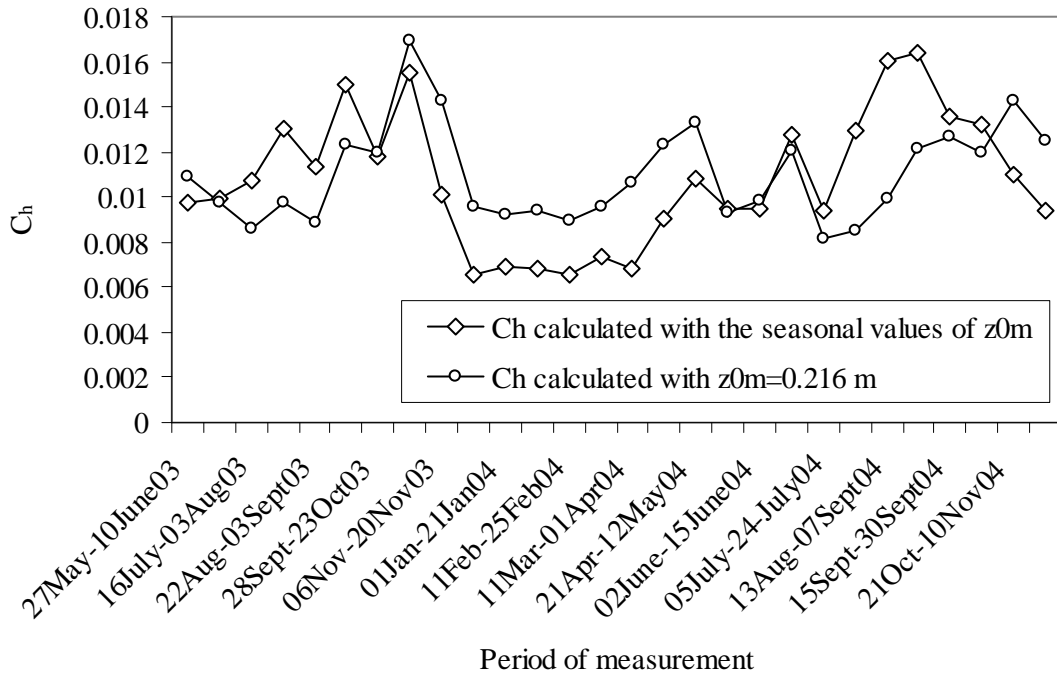
Figure 5.7:   Comparison between the surface exchange coefficients for heat calculated with the seasonal values of z_{0m} and with a fixed value of 0.216 m

The proposed formulation is based on a principle similar to that used in the Penman-Monteith equation. The principle is that the dry canopy transpiration decreases with increasing surface resistance (R_c). Therefore, the new formulation is expressed as follows:

$$B_{cnew} = \alpha \left(\frac{1 + \dfrac{\Delta}{R_r}}{1 + (R_c + C_h) + \dfrac{\Delta}{R_r}} \right) \qquad (5.17)$$

where α is the coefficient of adjustment of B_{cnew} to B_c. The value of α was set to 22.31 [s m^{-1}] and the optimum value obtained using the least square minimization approach. This value of α overestimated the original B_c during the rainy season (MBE=0.13 m s^{-1}) and underestimated during the dry season (MBE= - 0.19 m s^{-1}). The overall MBE was -0.11 m s^{-1} on a season-basis. Important is to notice here is that B_{cnew} clearly produces differences between the seasonal based z_{0m} and fixed value of

0.216 m (Figure 5.9). When B_{cnew} was introduced in the NOAH LSM program, its performance was improved. The bias error was greatly reduced when compared to the bias error of the original model (Figure 5.10). Therefore, the adoption of the proposed formulation of B_c can be recommended.
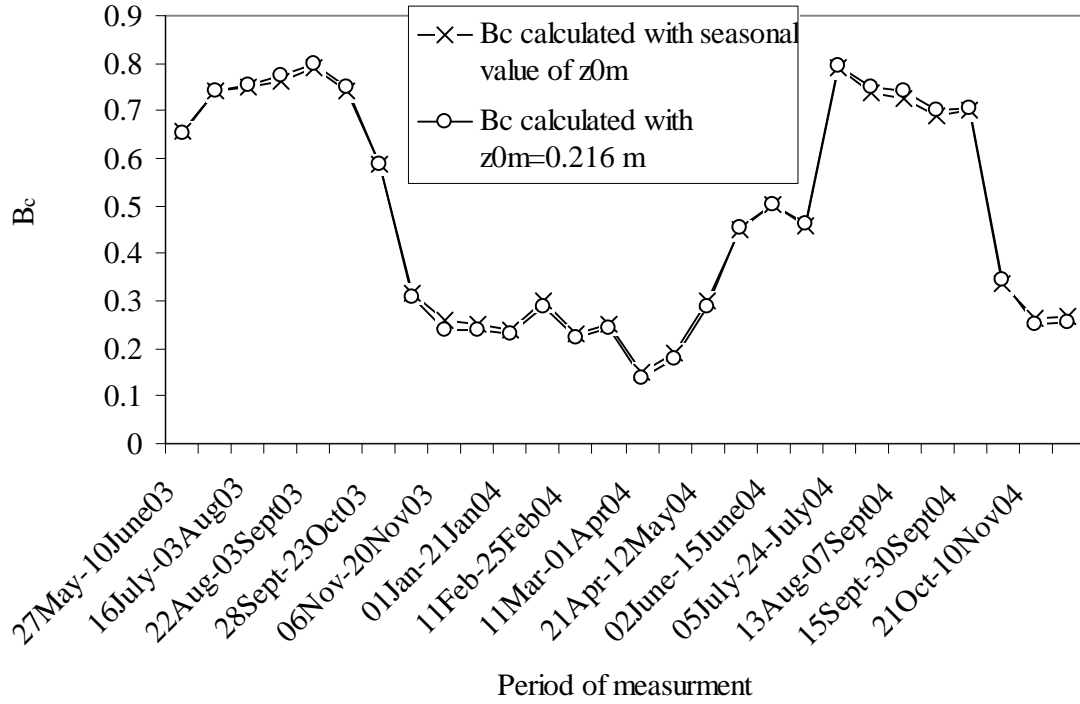

Figure 5.8:   Comparison between B_c calculated with the original formulation using a fixed and seasonal true value of z_{0m}
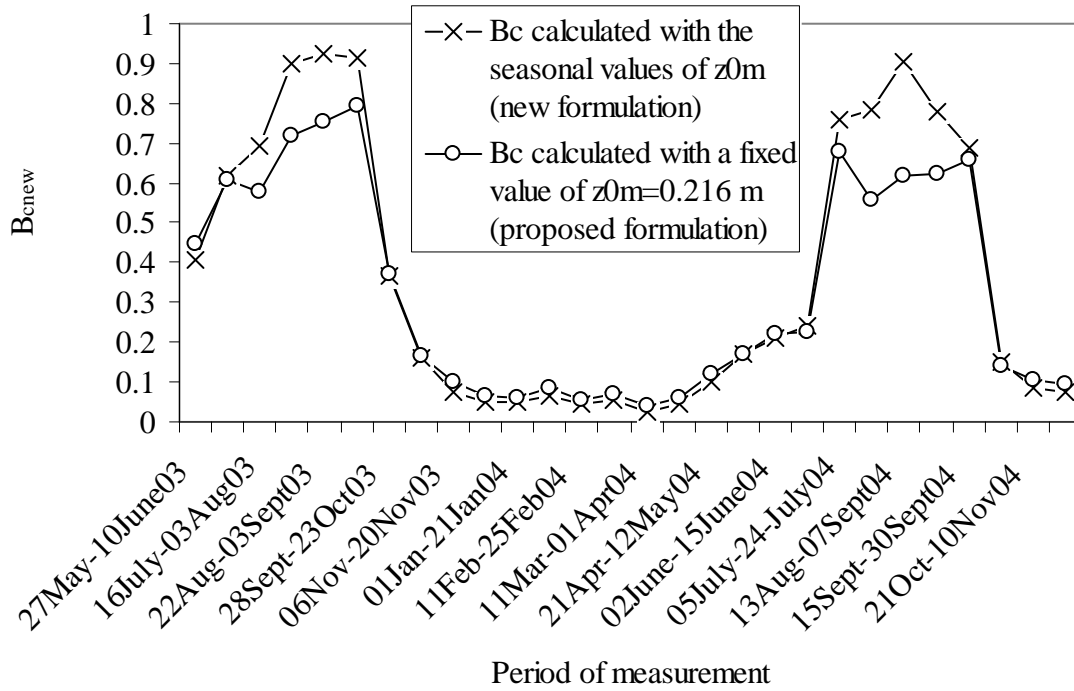
Figure 5.9: Comparison between B_c calculated with the proposed formulation using a fixed and seasonal true value of z_{0m}

5.5   Conclusion and recommendations

The first finding in this study was that the NOAH LSM was not sensitive to the change of roughness length for momentum neither on a seasonal basis nor on a daily basis. Therefore, when this model is kept in the standard form, a suitable fixed value of z_{0m} could be sufficient to simulate reasonably the seasonal dynamics of the surface fluxes over the savanna region in West Africa. However, this analysis shows that the different values of z_{0m} should give, in principle, different outputs for the surface fluxes. This was justified by the significant difference observed in the surface exchange coefficient for the heat and the surface resistance when applying the seasonal and a fixed value of z_{0m}. The results of the investigation show that the insensitivity of the NOAH LSM with respect to z_{0m} was related to the formulation of the coefficient B_c, which couples the dry canopy transpiration to the atmosphere. In the formulation of B_c, the product $C_h \times R_c$ was found to be the main cause for this. A new formulation of B_c is proposed to remediate the insensitivity, which appreciably improves the performance of the model.

Further problems arose with respect to the underestimation of observed latent flux, especially during the rainy and dry period. The use of a constant value for soil moisture, leaf area index and minimum resistance appeared to be the reason of these findings. It is recommended to introduce a seasonal variation of the variables as a first improvement. More research should be undertaken to formulate the relationship between the minimum resistance and the seasonal moisture variability, because the savanna vegetation is very sensitive to any variation in soil moisture. Similar recommendations are given by Schüttemeyer (2005). If seasonal data are not available, some simplifications could be made for the case of savanna zone submitted to intensive agriculture. The first simplification could be the subdivision of the annual cycle in three large ranges: the rainy season (June to October), the transition periods (October to December, April to June) and the completely dry period (January to April), where a constant value of soil moisture, leaf area index, the minimum resistance, albedo and the roughness length for momentum could be adequate for each period. This recommendation is justified by the fact that on farmland, two homogenous situations are generally encountered. During the growing periods, the terrain dominated by crops and sparse trees, the crop minimum resistance could be used, and the leaf area index and the roughness length momentum can be related to the development stage of crops. Well defined relationships between crop height, leaf area index and roughness length are available in the literature (Brutsaert, 1982, Oguntunde, 2004). The initial moisture condition of the soil layer can also be kept constant because of the regular rain during that period. The second homogenous period is the period after the harvest. The terrain is then dominated by bare soil and sparse trees. During that period, the tree minimum resistance could be used. Roughness length for momentum, leaf area index and soil moisture could also be kept constant. For all these periods, some point measurements of the needed variables could be carried out, and more time consuming long-term investigations can be avoided. For the transition periods, the recommendations of Schüttemeyer (2005) are suitable. Similar recommendations are also made fro terrain without agricultural activities.

Another important point is the use of all components of the actual evaporation during the drying and the completely dry period. This led to an overestimation of the observed fluxes when the standard form of the NOAH LSM but as soon as the direct

evaporation from the soil and the wet canopy was neglected, some adjustment of the dry canopy transpiration became necessary. This overestimation was greatly reduced when the proposed formulation of B_c was introduced.

The estimation of the canopy resistance of the inverted Penman-Monteith equation seems to be more realistic, because the formulation based on NP89 leads to an underestimation during the dry period and to an overestimation during the rainy season.
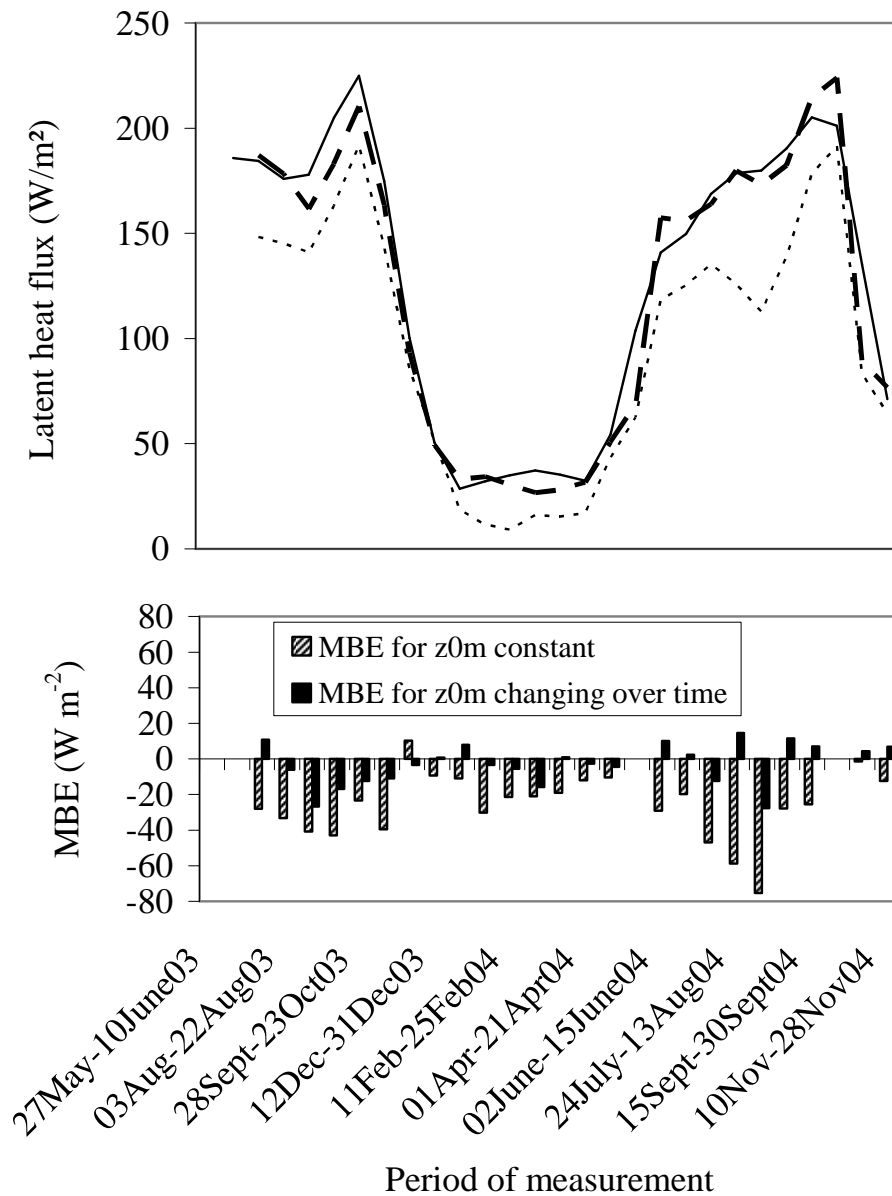

Figure 5.10: Comparison between the performance of the standard (light dashed line) and the improved NOAH LSM (bold dashed line). The continuous line corresponds to the observed latent heat flux

6 SEASONAL AND DIURNAL DYNAMICS OF SURFACE ALBEDO: IMPACT ON ACTUAL EVAPORATION AND MODELING

6.1 Introduction

Especially during the 1980s and 1990s numerous reports of rapid and widespread loss of the vegetation cover in West Africa appeared, also concerning the biophysical impacts of deforestation and desertification in the region (Gornitz, 1985; Sayer et al., 1992; FAO, 1993; WRI, 1988). This loss of vegetation in the tropical humid and dry regions (especially in Burkina Faso) caused by land-use such as logging, overgrazing, or intensive cultivation is thought to produce an increase in the land-surface albedo and a decrease in surface roughness. Many studies have shown that this increase and decrease lead to an increase in the atmospheric turbulences at the soil surface and in drought in regions such as the Sahel (Charney et al., 1975; Nicholson et al., 1998; Douglas and Ottke, 2002). In the particular case of Burkina Faso, agricultural activities consisting of systematic clearing of all unnecessary trees are the main cause of the loss of the vegetation cover. The remaining trees are mainly *Vittelaria paradoxa* (sheanut tree) with a cover of 90 % in the dry season. During the rainy season, crops (e.g. *Sorghum vulgare)* dominate the vegetation cover. This situation is thought to induce a large seasonal and daily variability of surface albedo and energy flux distribution, and will ultimately impact the actual evaporation rate and in turn, the regional climate.

Knowledge of the surface albedo is critical in many models such as crop growth models, eco-hydrological models (SVAT) and General Circulation Models (GCM). An error in the albedo may lead to uncertainties in computing net radiation and energy fluxes, and in the simulation of global surface temperatures (Sellers et al., 1996; Yin, 1998). Therefore, a comprehensive understanding and realistic numerical projection of the surface albedo would represent a major step forward in improving climate modeling. Furthermore, knowledge of the surface albedo, as a key parameter of surface solar radiation and energy budgets, is necessary for the mechanistic accounting of many lights and temperature-driven processes such as evaporation, photosynthesis, autotrophic and heterotrophic respiration (Yin, 1998; Giambelluca et al., 1999; Iziomon and Mayer, 2002). Hence, there is a necessity to accurately estimate the surface albedo by ground-based measurement.

A review of the literature reveals that surface albedo has been studied carefully in many parts of the world, but the outcomes of those studies are not comparable (Oguntunde, 2004). For West Africa, especially the savanna zone, the albedo data are very rare; the most important studies were conducted by Courel and Rasool (1984), Douglas and Ottke (2002), Allen et al. (1994) and Oguntunde (2004). The first two studies were done at a large scale and were based on the correlation of long-term term annual precipitation, land-cover change and surface albedo, whereas the second two gave more insight into the seasonal and daily dynamics of the surface albedo over natural vegetation or according to the phenological stage of a crop on a particular site (Niger and central Ghana, respectively). The literature review also reveals that ground-based measurements and data on the daily course of surface albedo are very rare in West Africa. Most of the measurements are based on regional aircraft flights or satellite imagery and are limited in time and space. There is little consensus about the effect of cloudiness on the daily albedo or the seasonal course. Therefore, in this study a long-term investigation of sheanut, bare soil and sorghum field surface albedo was conducted from January to October 2004. These ecosystems are very representative of the ecosystems of the savanna zone of Eastern Burkina Faso in particular and the savanna zone of West Africa in general. The first objective of this research focused on the effect of the seasonal and daily dynamics of surface albedo (ground-based measurement) and on the actual evaporation. Furthermore, the daily course was measured and its relation with solar angle, cloudiness and potential effect on actual evaporation was established. Selected empirical models available in the literature were adopted so as to simulate the measured albedo. This research is part of the GLOWA-Volta (van de Giesen et al., 2002) and VinVal projects

6.2   Trial site

The trial site is located in the East part of Burkina Faso (11° 07' N; 0° 31' E). The area is very flat with a slope of about 2 % on average. Agriculture is very intensive. The site is characterized by a Sudan climate and vegetation with a monomodal rainfall pattern. The soils are mainly sandy (Lixisoils). Sheanut trees were dominant in the site, had an average height of 8 m, and were separated by an average distance of 15 m. The density of sheanut trees was about 17 trees/ha. During the rainy season, sorghum, millet, maize

and groundnut were cultivated between the sheanut trees, and their growth alters the roughness length for momentum over time. This system of trees and crops can be found everywhere in the savanna in West Africa. Crop density was about four plants per square meter. The field scale uniformity can be observed on Figure 6.1 showing the location of the station on the Landsat image.
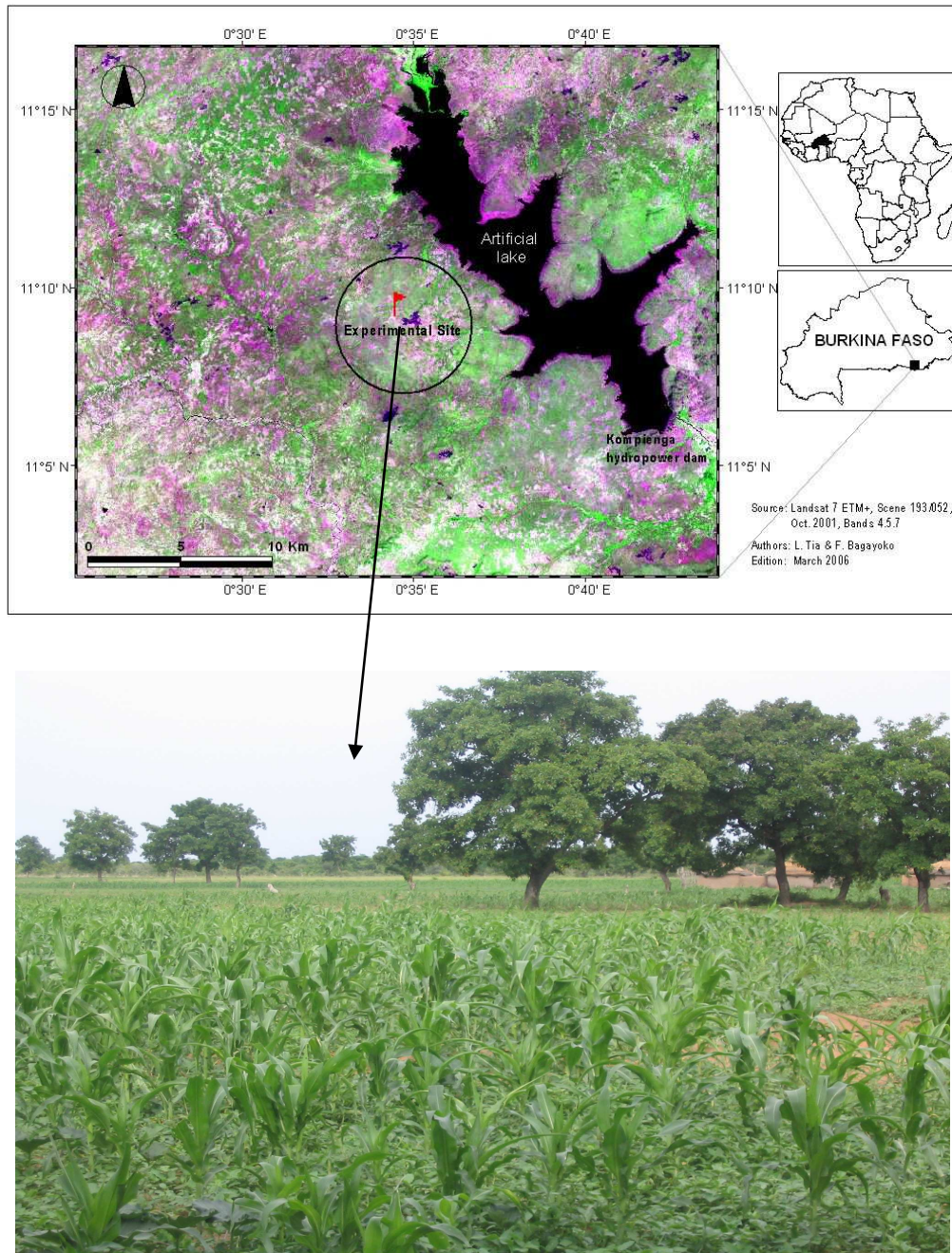

Figure 6.1:   Landsat image showing the location of the experimental site and a picture giving an impression of the field scale uniformity

95

6.3 Methods and materials

Surface albedo was measured every three weeks on a selected sheanut tree and the area around the EC station from January to October 2004. The technique consisted of measuring the incoming and the reflected radiation at 1.5 *m* above the selected area with a pyranometer (model: SP LITE, Kipp & Zonen, Delft, The Netherlands). The properties of the pyranometer are presented in Table 6.1. The pyranometer was mounted on a rod and the signal read with a multimeter. After seeding, sorghum crop albedo and growth were monitored.

Table 6.1:   Properties and specification of the pyranometer

Specifications	Properties
Sensor type	Silicon photovoltaic
Field of view	180°
Response time	< 1 sec
Sensitivity	77.0 µV/w/m²
Tilt response	No error
Non linearity	< ± 1 %
Nominal signal range	0 - 0.2 V
Spectral bande range	0.4 - 1.1 µm
Operating temperature	-30 to + 70 °C
Sensitivity to temperature	0.15 %/°C

Source: Kipp & Zonen pyranometer instruction manual

In order to estimate the effect of cloud cover on surface albedo, the hourly surface albedo was measured on selected days (DOY189, DOY190, and DOY273) from 7:00 to 18:00 corresponding to different sun angles under both clear and clouded sky conditions. To estimate the effect of surface albedo on the actual evaporation, the average *EF* value over two weeks was plotted against the measured surface albedo. The evaporative fraction was calculated as follows:

$$EF = \frac{\lambda E}{H + \lambda E} \tag{6.1}$$

where λE and H are latent heat and sensible heat flux [W m^{-2}], respectively. Sensible heat and latent heat flux were processed from the raw data measured with the *EC* station at 10 m height above the ground surface. The details on the setup and the

treatment of the raw data are available in Elbers (2002). The use of the evaporative fraction instead of actual evaporation is justified by the fact that it is easier to compare two normalized parameters.

Surface albedo was monitored on selected days (DOY 189, DOY 190, DOY 273) from 7:00 to 18:00 and was plotted versus the sun angle and the evaporative fraction (EF) to estimate the effect of sun angle on surface albedo, and the effect of surface albedo on EF.

Finally, two existing models based on Yin (1998) (for sheanut albedo) and Oguntunde (2004) (for crop albedo) were adopted to simulate the seasonal trend of surface albedo.

6.3.1   Modeling of sheanut albedo

The model proposed by Yin (1998) is of particular importance because it takes into account the characteristics of the canopy, its growth, the seasonal stress and the sun angle, all which affect the seasonal and diurnal dynamics of surface albedo. Initially the model was established to estimate the albedo of vegetated land surface in the temperate region where the canopy and the underlying soil are sometime covered by melting snow. As it never snows in the study area, this aspect was ignored. The principle of this model is that, in the absence of snow, the albedo of vegetated land may be viewed as the manifestation of canopy element-determined basic stand property after modification by various factors over time and location. Mathematically, this model is expressed by a series of functional multipliers as follows:

$$\alpha_v = \alpha_{v0} \times f_{HF} \times f_a \times f_{ss} \times f_p \times f_{mp}$$

(6.2)

where α_v is canopy surface albedo, α_{v0} is the base albedo and the value of α_v when the product of the multipliers equals unity, f_{HF} is a function of vegetation height, f_{ss} is a function of the seasonal biological stress, f_a is a function of relative leaf age, f_p is a function of climatic factors and f_{mp} is a function of the optical air mass factor and takes into account the dependence of surface albedo on solar zenith angle. The later functional multiplier was reformulated so that the solar zenith angle is clearly represented.

a. Definition of base albedo

According to Yin (1998), the base albedo depends on the reflectivity of the reflecting elements (leaves) and on the surface porosity of the canopy, which regulates the penetration and absorption of solar radiation. The reflectivity and porosity of the canopy have been found to be indexed by leaf life span and leaf size, respectively (Chabot and Hicks, 1982; Reich et al., 1991; Reich et al., 1992). Therefore, the formulation of the surface albedo varies asymptotically with leaf life span and leaf size as follows:

$$\alpha_{v0} = \frac{\alpha_{v0\max}}{1+\left(\dfrac{\alpha_{v0\max}}{\alpha_{v0c}}-1\right)\exp\left\{k_F\left[W+2.86F_l\left(1-k_Y Y_l - k_s S_l\right)\right]\right\}} \qquad (6.3)$$

where W is relative stem cover (including branch and twig; it varies between 0 and 1 with 1 for closed canopies); F_l is canopy leaf cover, which varies between 0 and 1 with 0 if leafless and 1 in full foliage, 2.86 is the ratio of average leaf area to stem area indices for closed canopies, Y_l and S_l are the mean life span and size (cm²) of canopy leaves, respectively, $\alpha_{v0\max}$ is the asymptote α_{v0c} value for canopies with large/long-lived leaves, α_{v0c} is the α_{v0} value free of canopy, k_F, k_S and k_Y are rate coefficients. The ratio 2.86 converts the stem and leaf covers to the same unit in terms of surface area. Analyzing closely the formulation of this asymptotic variation with leaf life span and leaf size, one can replace the vegetation leaf cover (F_l) by the leaf area index (LAI), which seems to be more representative and easier to measure for a single and isolated tree as in this work. Likewise, the relative stem cover (F_l) can be inferred from LAI and is taken as 10% of this value (White et al., 2000).

Therefore, Eq. (6.3) can be expressed as follows:

$$\alpha_{v0} = \frac{\alpha_{v0\max}}{1+\left(\dfrac{\alpha_{v0\max}}{\alpha_{v0c}}-1\right)\exp\left\{k_F\left[0.1LAI+2.86LAI\left(1-k_Y Y_l - k_s S_l\right)\right]\right\}} \qquad (6.4)$$

3.2.1 Definition of functional multipliers

According to Jarvis et al. (1976), the canopy albedo decreases with vegetation height and levels off as the vegetation reaches a certain height and the crown size is stabilized. Initially, this functional multiplier was expressed as follows:

$$f_{HP} = k_H^{\left\{\left(\frac{H_l}{H_l+1}\right)^{F_l}\right\}}$$

(6.5)

where H_l is forest height [m] and f_{HP} is bound between unity at $H_l = 0$, k_H (the asymptote with H_l approaching infinity or in the absence of foliage) and F expressing canopy leaf cover. Here, this later coefficient was replaced by the LAI.
Therefore Eq. (6.5) becomes:

$$f_{HP} = k_H^{\left\{\left(\frac{H_l}{H_l+1}\right)^{LAI}\right\}}$$

(6.6)

The leaf age multiplier is given by:

$$f_{a_l} = k_{a_l}^{a_l + \sin\left[\left(a_l - k_{a_l \max}\right)2\pi + a\cos(-0.5/\pi)\right]}$$

(6.7)

where a_l is the relative age of the leaf (it varies between 0 and 1 with 1 at life expectancy and 0 for no leaf), $k_{a_l \max}$ is the a_l value that maximizes the exponent in Eq. (6.7), and k_{a_l} is the f_{a_l} value when the power factor is unity.
The seasonal biological stress is expressed by:

$$f_{SS} = k_{SS}^{\sin[(dr - k_{d \max})2\pi + \pi/2]}$$

(6.8)

where d_r is the relative stress-calendar day (it varies between 0 and 1). It is expressed as follows:

$$d_r = \begin{cases} (1 + d_c - d_0)/365 & if \quad d_c \geq d_0 \\ \left[1 + (1 + d_c - d_0)\right]/365 & if \quad d_c < d_0 \end{cases} \tag{6.9}$$

where d_c is calendar days and d_0 the starting date of the stress calendar. d_0 was set to start at DOY274 (01 October) and to end at DOY120 (30 April). $k_{d\,max}$ is the d_r value that maximizes the exponent in Eq. (8), k_{SS} is the f_{SS} value at unity power factor. The climate multiplier is defined with a step function I_{p0} and is a function of the LAI :

$$f_p = k_{p0}^{I_{p0}(1 - LAI/100)} \tag{6.10}$$

where I_{P0} denotes severe drought, as indicated by a lack of precipitation for two consecutive months or longer (0 or 1 with 1 for dates falling within that duration, and 0 otherwise), k_{P0} is the f_p value for $LAI = 0$. Here, I_{p0} was kept to 1, because the effect of drought might be taken into account in the seasonal dynamics of the LAI . The trend of the measured LAI confirms this fact.

The optical air mass factor is intended to take into account the dependence of surface albedo to solar zenith angle and is expressed as follows:

$$f_{mp} = k_m^{1 - m_a(1 - k_p P_a)/\left[3.55(1 - k_p)\right]} \tag{6.11}$$

where m is the daytime mean optical air mass at sea level and is a function of the solar zenith angle (see Yin, 1997), P is the relative station atmospheric pressure ($= \exp(-A/8000)$), A being the elevation of the station, k_m is the f_{mp} value at the top of the atmosphere and is set equal to 1 for the reference point of $m_a = 3.55$ and $P_a = 1$, k_p is a coefficient of correction (see Table 6.2).

Yin (1998) gave the best-fit values of the different coefficients used in the model for two types of canopy (broadleaved and needle-leaved canopy). Table 6.2 shows these best-fit coefficients, and the gaps correspond to the functional multipliers,

which were statistically insignificant. It was assumed that the sheanut tree is a broadleaved evergreen. Therefore, the seasonal stress and leaf age multiplier, which were tested to be statistically insignificant for broadleaved deciduous coniferous forest, must be considered. Some of the best-fit values of coniferous forest did not match with sheanut tree and were recalibrated. These are $\alpha_{v0\max}$ and k_m, which were set to 0.320 and 1.915, respectively.

6.3.2 Modeling of crop albedo

The model proposed by Oguntunde (2004) was used. This model is based on the original formulation of Uchijima (1976), which was reformulated by Jensen and Rahman (1987). It takes into account diurnal dynamics, variability of crop albedo at different phenological stages as well as the albedo of the underlying soil surface, and is expressed as follows:

$$\alpha_{ca} = \alpha_c - (\alpha_c - \alpha_u)\exp(-k_e LAI) \tag{6.12}$$

where α_c is the albedo of a fully developed crop canopy, α_u is the albedo of the underlying soil surface, k_e is the extinction coefficient and LAI is the leaf area index. The crop canopy albedo α_c is given as:

$$\alpha_c = f_c \alpha_{cS} + f_l \alpha_l \tag{6.13}$$

where α_l is the single leaf albedo, α_{cS} represents the albedo of a semi-infinite canopy, f_c and f_l are weighting factors for canopy and single leaves, which are also dependent on the LAI and solar zenith angle as follows:

$$f_c = 1 - f_l = 1 - \exp\left(\frac{-0.5LAI}{\cos Z}\right) \tag{6.14}$$

α_{cS} is the combination of the direct and diffuse components of radiation. The direct component is expressed as follows:

$$\alpha_{cS1} = \frac{0.5\omega}{\left[\left(1-\omega\right)^{0.5} + \dfrac{0.5}{\cos Z}\right]\left[1-\left(1-\omega\right)^{0.5}\right]\cos Z} \tag{6.15}$$

where $\omega = \alpha_l + \tau_l$ is the scattering coefficient with τ_l as single leaf transmittance.

The diffuse component is obtained when the sun zenith angle (Z) equals 60°. It is expressed as follows:

$$\alpha_{cS2} = \frac{\omega}{\left[1+\left(1-\omega\right)^{0.5}\right]^2} \tag{6.16}$$

The underlying soil albedo is a function of soil wetness and sun zenith angle. It is expressed as follows:

$$\alpha_u = \alpha_{uw} + 0.001\left[\exp\left(0.00358Z^{1.5}\right)-1\right] \tag{6.17}$$

where α_{uw} expresses the effect of soil wetness. A functional relationship describes the variation of albedo with soil moisture and is reported by McCumber (1980) following Idso et al. (1975).

The crop LAI was estimated by Jensen et al. (1990) and Allen et al. (1994) as follows:

$$LAI = 5.5 + 1.5\ln(h_c) \tag{6.18}$$

where h_c is crop average height.

Eq. (6.18) was calibrated for short and high grass and was not directly applicable to tall crops as sorghum. Therefore, crop height was divided by 10 to make it comparable to grass height. The adjusted equation was tested with the LAI measured by Oguntunde

(2004) on maize at different phenological stage. The measured *LAI* was similar to estimated values but with an overall overestimation.

The set of equations (Eq. 6.12 to Eq. 6.18) was used to estimate crop and soil surface albedo. During the dry season, when there are no crops, Eq. (6.11) was reduced to the soil surface albedo (α_u), and its contribution to the total surface albedo was proportional to the rate of the soil surface, which was not covered by a sheanut canopy (80%). During the rainy season, with the presence of crops, the total contribution of crop albedo and the underlying soil albedo was 80 %, because the contribution of soil surface albedo was already taken into account in Eq. (6.11).

6.4   Results and discussions

In this section, the seasonal dynamics of surface albedo and its effect on actual evaporation are presented followed by the diurnal course, its relation with sun zenith angle and actual evaporation and finally the evaluation of the adopted models.

6.4.1   Seasonal trend of albedo

Figure 6.2 shows that the measured sheanut tree albedo is higher than the soil surface albedo, and the relative difference is about 12 % on average. The values are higher during the dry season and lower during the rainy season with a global decreasing trend. The relative decrease is about 28 % and 19 % for soil surface and sheanut albedo, respectively. The coefficient of variance (*CV*) is 10 % and 6 % for soil and sheanut, respectively. Figure 6.2 clearly shows that surface albedo varies with the season. This can be explained by the fact that during the dry season, the study area has a large portion of bare soil with little available moisture. The grasses are also completely dry as with a color tending to white. Therefore, a bigger portion of incoming radiation was reflected, thus increasing the surface albedo. This result agrees with Oguntunde (2004), who showed a clear increase in the bare soil surface albedo with decreasing soil wetness and surface roughness. Idso et al. (1975) and Cresswell et al. (1993) also made similar observations. Likewise, sheanut leaves become senescent, and most of them are dusty during the dry season, which reduces their capacity to absorb radiation and increases their albedo.
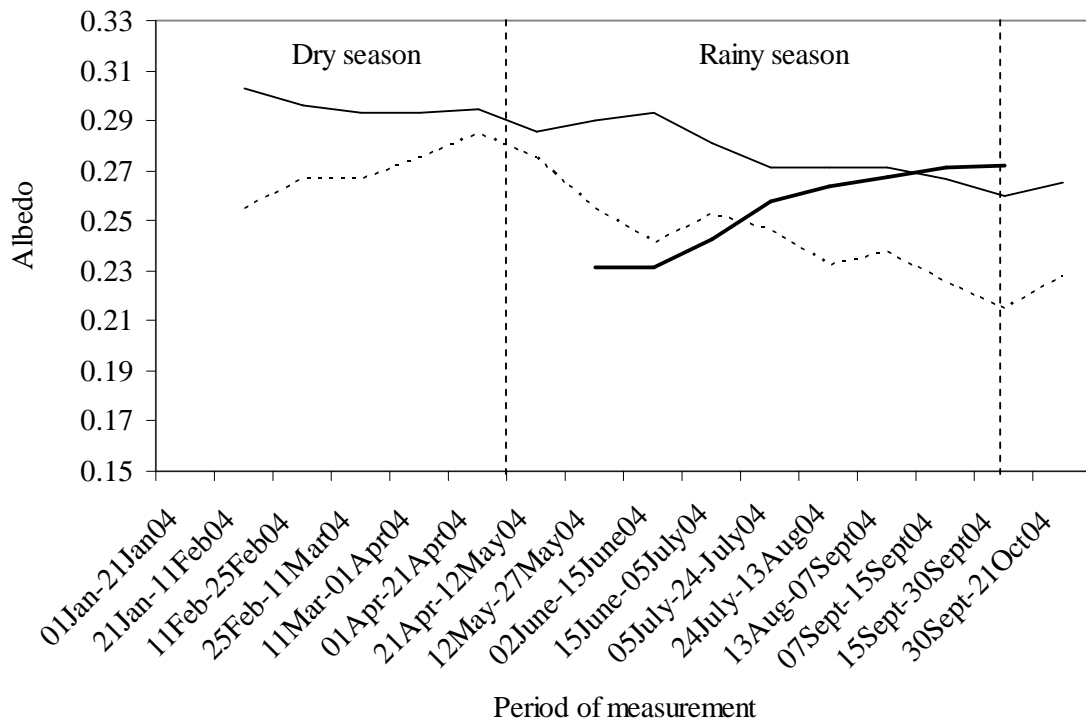
Figure 6.2:   Seasonal pattern of sheanut tree albedo (light stick line), soil surface albedo (dashed line) and sorghum albedo (bold stick line)

In contrast to the dry season, during the rainy season the surface tends to be dark due to soil wetness and the green grasses. In that period, the soil surface absorbs more radiation and reflects less, hence the albedo reduction. For sheanut, the leaves are renewed and cleaned by the frequent rain, which change their transmissivity effect by reducing the reflection. The overall effect is a decrease in the albedo.

The sorghum albedo was monitored during the growing season (from May to September), where a gradual increase in surface albedo from seeding to maturity with a $CV = 7$ % was observed. The relative total increase was about 10 % from seeding to maturity. These results are similar to the observations of Oguntunde (2004) for maize.

6.4.2   Effect of seasonal dynamics on actual evaporation

The effect of the measured of the seasonal dynamics of evaporation was measured by plotting the evaporative fraction (EF) versus the weighted value of albedo. The evaporative fraction is the amount of the available energy that goes into the evaporation and varies between 0 and 1, and expresses the change in biosphere-atmosphere

interaction (Oguntunde, 2004). When the evaporative demand equals 0, all available energy goes into heating the ambient air. This situation can occur in the Sahara, where the moisture is very low and the actual evaporation rate tends to zero. When this ratio equals 1, moisture is abundant in such a way that all the available energy is consumed by the evaporation of available moisture. The plot (Figure 6.3) shows a linear decrease with increasing albedo, with a significant determination coefficient ($r^2 = 0.83$). The equation is expressed as follows:

$$EF = -11.36\alpha + 3.37 \qquad (6.18)$$
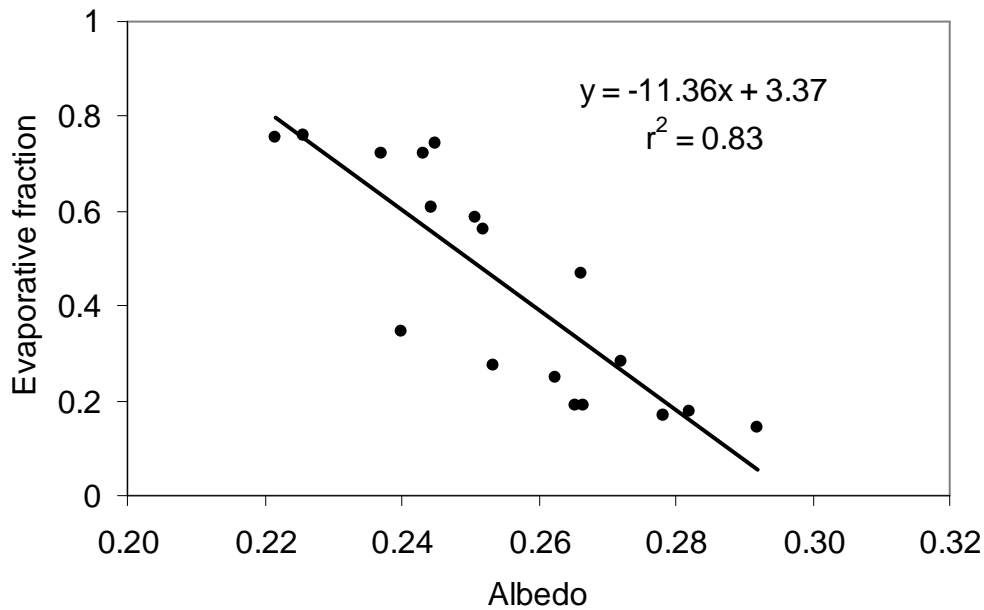
Figure 6.3: Plot of the seasonal evaporative fraction (EF) versus the seasonal surface albedo (from January to November 2004)

The statistic on this regression reveals that the model constant ($SD = 0.35$) and the coefficient ($SD = 1.35$) was significant at $p < 0.0001$. α accounts for 83 % of the variability of EF. As net radiation is closely related to surface albedo, a seasonal decrease in surface albedo will have a similar effect on net radiation. Therefore, the 83 % of the variability of EF due to α will be related to the net radiation. Figure 6.3 shows the very high evaporative fraction during the rainy season when the albedo is relatively low (wet surface), but it decreases progressively when the environment becomes dryer. Therefore, increasing surface albedo will impact negatively on the

evaporation and might result in local and regional climate change through the modification of the boundary layer as mentioned by Margolis and Ryan (1997). Therefore, the effect of albedo on actual evaporation is resulted to the interaction between the atmosphere and the local environmental climate. High albedo corresponds to low actual evaporation rate and dryer atmosphere and warm ambient air. Low surface albedo corresponds to high evaporative fraction and lower boundary layer and relatively cool environment.

6.4.3   Diurnal trend of albedo

The diurnal trend of surface albedo is in contrast to that of the incoming radiation. It decreases from morning to noon, where it reaches its minimum value and increases again until sunset (Figure 6.4-a, b and c). Minnis et al. (1997) suggested that dew and wind speed are the main reason for this variation of surface albedo with sun zenith angle. In fact, in the early morning (until 9:00), leaves are covered by a fine layer of dew, which increases the reflectance. This increase leads to an increase in surface albedo. This effect is even more pronounced when the wind is light (fewer disturbances in canopy inclination), which is the case in the early morning. Physically speaking, Pinter (1996) shows that at 15° (sun zenith angle) and within the visible red waveband (0.65-0.69 μm), reflectance increased significantly when dew covered the reflecting surface. This observation gives better a explanation of the high surface albedo in the early morning. As the zenith angle increases, wind speed also increases due to the increase in surface temperature and boundary layer turbulence, and dew disappears progressively, while the vegetation absorbs more and more radiation. Higher absorption of radiation results in the reduction of surface albedo. A contrasting phenomenon
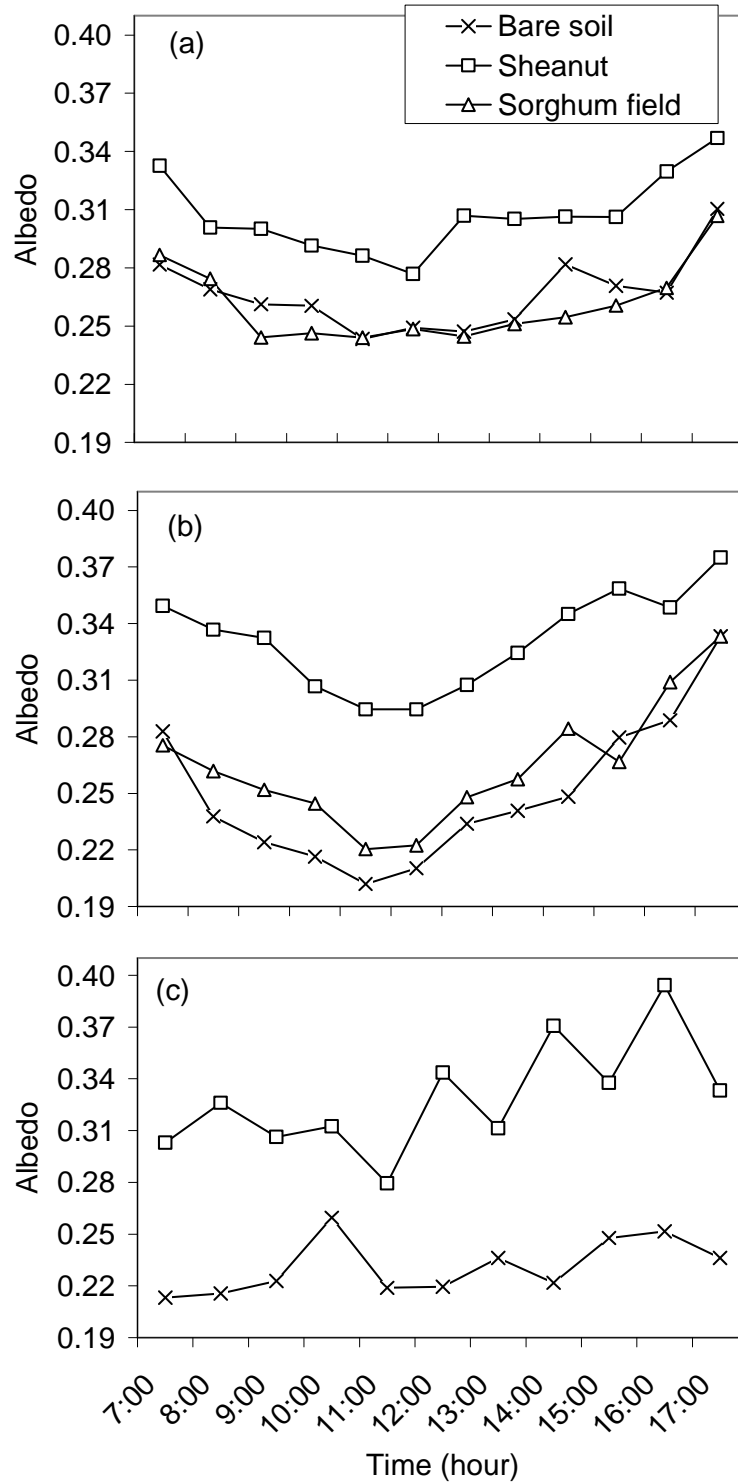
Figure 6.4: Diurnal pattern of surface albedo for bare soil, sheanut tree and sorghum. (a) corresponds to DOY189 and was under clear sky. (b) corresponds to a DOY 190 and was under clear sky until 13:00 and clouded sky for the rest of the day. (c) corresponds to the DOY273 and was under clouded sky

From early morning to noon can be observed when the zenith angle starts decreasing again in the afternoon.

This trend (exponential decrease in surface albedo with sun zenith angle) was disturbed for DOY273 due to the diffuse light because of the cloud cover. The incoming and reflected radiation is almost constant throughout the day, which results in a relative constant albedo.

In all cases, sheanut tree surface albedo was higher than bare soil and sorghum field surface albedo. For DOY189 and DOY190, the variation of bare soil albedo and sorghum field albedo was quite similar and did not differ appreciably. In fact, in July, sorghum field albedo was mostly determined by the soil surface because it was low. There was also an asymmetric trend of the value of albedo according to the morning and the afternoon. The value in the afternoon was higher than that in the morning for approximately the same zenith angle. For DOY189, the relative increase was about 10 %, 6 % and 7 % for bare soil, sheanut and sorghum field, respectively. Likewise for DOY190, the increase was even more pronounced with 15 %, 8 % and 15 % for the bare soil, sheanut and sorghum field, respectively. For DOY273, a similar phenomenon was observed, where the increase was 12 % and 9 % for bare soil and sheanut tree, respectively. This is assumed to be caused by the wind speed and direction as mentioned by Minnis et al. (1997), Song (1998) and Oguntunde (2004).

a. Effect of sun angle and cloud on diurnal trend of albedo

The effect of sun zenith angle and cloud are clearly shown in the Figure 6.5. Anderson (1954) proposed the empirical equation (power function), which describes the evolution of surface albedo with the sun zenith angle and as expressed as follows:

$$\alpha = aZ^b \tag{6.19}$$

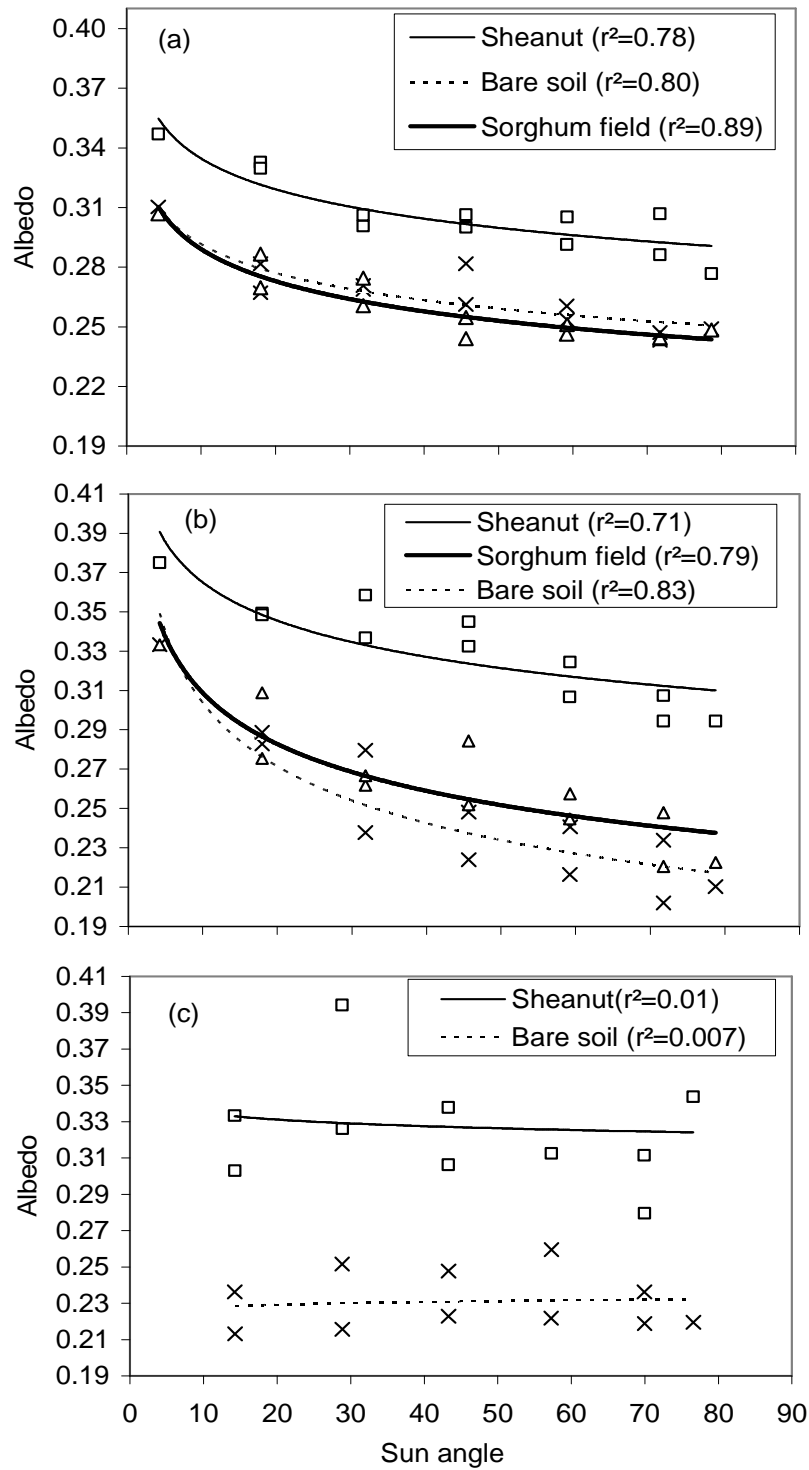where a and b are the regression coefficients and Z the sun zenith angle.

Figure 6.5: Correlation between surface albedo and sun angle for different cloud cover conditions: (a) DOY 189 under clear sky condition; (b) DOY 190 under clear sky condition until 13:00 and clouded for the rest of the day; (c) DOY 273 under clouded condition

A similar power function was fitted between the measured diurnal surface albedo and the sun zenith angle. For DOY189 and DOY190, where the sky was clear and half clouded, respectively, the regression shows a higher correlation between both variables and varies between 0.70 and 0.90. For the DOY273, where the sky was completely covered by the cloud, no correlation could be found. As mentioned by Brutsaert (1982), during days with sunshine, the albedo of most surfaces depends on the sun zenith angle, but this dependence decreases with increasing cloudiness which dampens the zenith angle control on albedo. This situation can be seen in Figure 6.5, where there is a weak decrease in the correlation between surface albedo and sun angle from DOY189 and DOY190 due to the cloud condition during the afternoon of DOY190. For the very cloudy day (DOY190), no correlation could be found because of the diffuse light.

b. Effect of diurnal variation of surface albedo on actual evaporation

Figure 6.6 shows the plot of the albedo of bare soil, sheanut tree and sorghum field versus the evaporative fraction for DOY189 and DOY190. No relevant relationship between surface albedo and evaporative fraction can be found. Therefore, the diurnal evaporation seems to be more determined by other environmental factors (net radiation and vapor pressure deficit) than by the reflective properties of the evaporating surface. This situation can be explained by the fact that the evaporative fraction does not vary appreciably during the day despite some falls and rises during the early morning and late afternoon. The diurnal variation of the evaporative fraction is more stable and does not follow the variation of the surface albedo, which is related to sun zenith angle, cloud cover, and wind speed and direction. Therefore, the diurnal dynamics of surface albedo is not relevant in the seasonal dynamics of actual evaporation. However, it has been mentioned in model to account for the time and the location of measurement through the solar zenith angle.
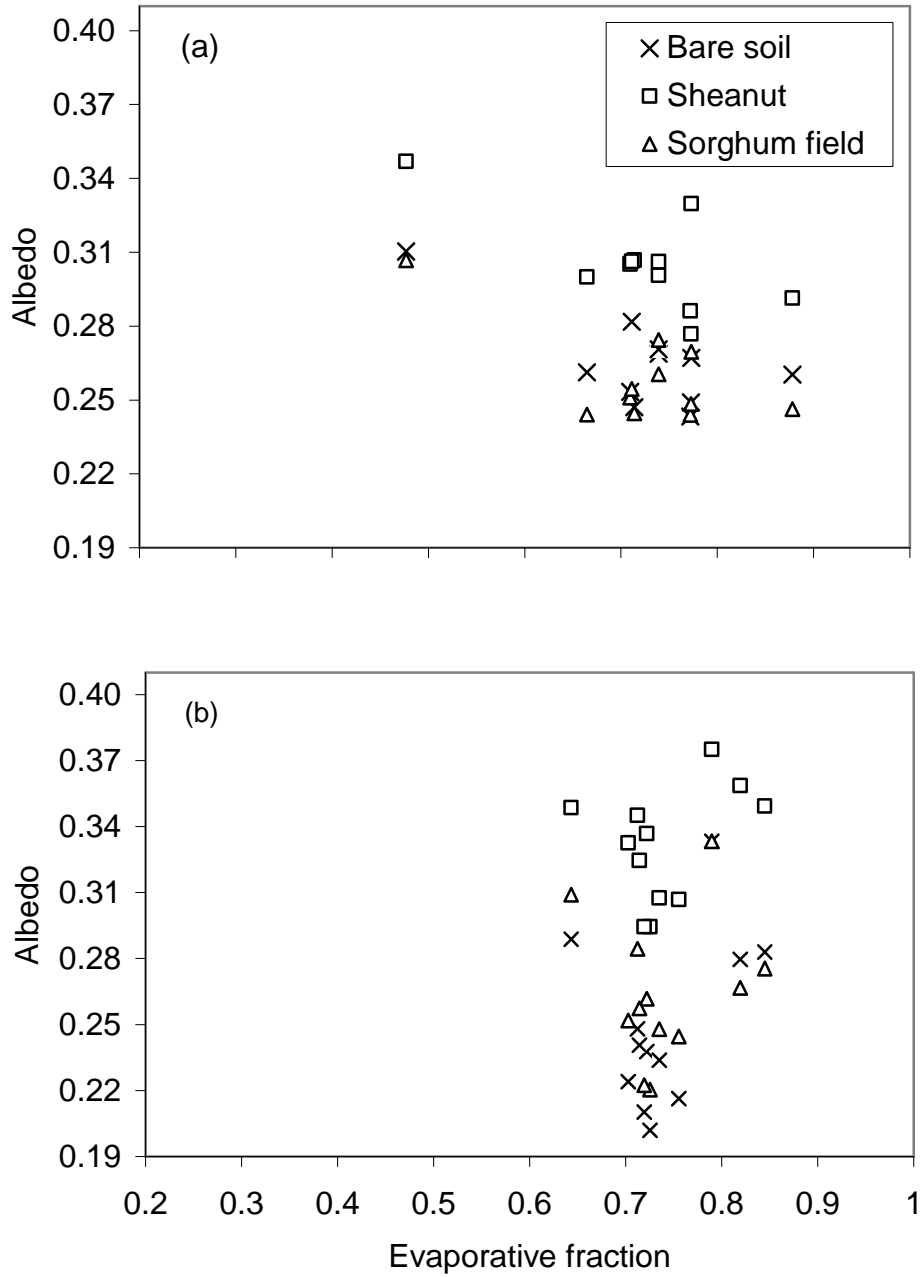
Figure 6.6: Plot of surface albedo of bare soil, sheanut and sorghum field versus evaporative fraction: (a) DOY189 and (b) DOY190

6.5 Model evaluation

6.5.1 Sheanut tree albedo

Equations 3 to 11 were used to simulate sheanut albedo. Figure 6.7 shows the plot of the measured albedo versus the predicted one. The values agree quite well with the simulated albedo, which accounts for about 76% of the measured albedo. The MBE and RMSE are -0.004 and 0.00009, respectively. The negative values of the MBE shows

that the model leads to an overall underestimation. Similar situation was observed by Yin (1998), who tested on several types of vegetation canopies and in different parts of the world. In each case, a good agreement was found, but some of the factors were statistically significant according to the type of the forest. For instance, for deciduous forest, the seasonal stress multiplier is not relevant, because most trees are leafless for most the year in and around the stressful season. Therefore, without leaves, there is no spectral property to speak of, and hence the seasonal stress multiplier has no relevance. In this study, some of the best-fit coefficients found by Yin (1998) did not match with sheanut tree canopy. Therefore, there is a need to set these coefficients in each situation to improve the accuracy of the simulated albedo of this model.

The model can also be used to predict the albedo for surfaces covered by grass. In this case, Yin (1998) noted that the results are improved when an adjustment of the leaf size is taken into consideration. In this case, an effective leaf size (S_e) have to be used in the case of canopy with long and narrow leaves, especially for tall grasses as found in West Africa. This effective leaf size is expressed as follows:

$$S_e = S_l \exp\left[-k_L \times \max\left(0, L_l - 30\right)\right] \tag{6.19}$$

where S_l is leaf size as previously defined, L_l is leaf length [cm]; k_L is a calibration, where the coefficient must be set for each type of grass.
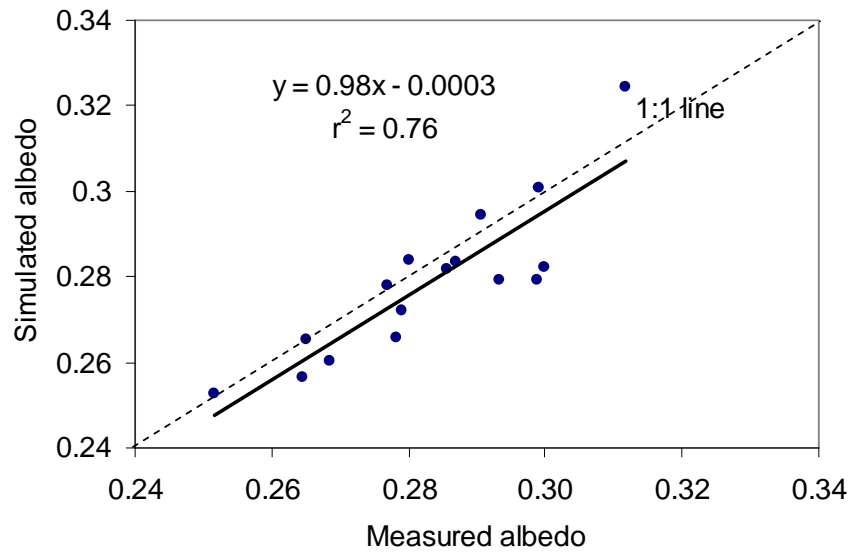
Figure 6.7:   Graph 1:1 line comparing simulated and measured albedo of the sheanut trees

6.5.2   Sorghum albedo

The model proposed by Oguntunde (2004) for maize also performed in sorghum field. Figure 6.8 shows the plot of the predicted against the measured albedo. The prediction accounts for more than 90% of the observed albedo with MBE and RMSE of 0.0015 and 0.0001, respectively. The model results in an overall overestimation of sorghum albedo. However, the overestimation might come from the estimation of the LAI from Eq. (18), which was found to overestimate the LAI .
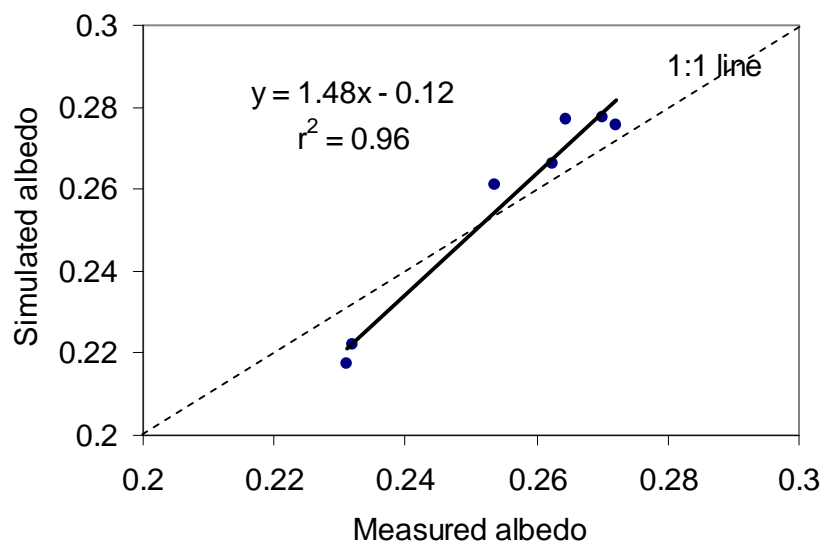

Figure 6.8:   Graph 1:1 line comparing simulated and measured albedo of sorghum

6.6   Conclusion

The results of this study showed that the seasonal dynamics of surface albedo had a negative impact on actual evaporation. This impact was implicitly related to the seasonal dynamics of vegetation and the climatic condition, which determine soil moisture availability. This impact was found to be insignificant on a diurnal basis, but there is a necessity to represent these diurnal dynamics in seasonal models because of the close relationship between surface albedo and sun zenith angle under clear sky conditions. These diurnal dynamics were insignificant during days with clouded sky condition. Therefore, the inclusion of a clearness index in the models can be useful, because it will discard the sun angle during days with clouds. The models were sensitive to the LAI. A small change in the LAI leads to a large change in the simulated surface albedo. Therefore, there is a need of the use of the true LAI according to the crop growth stage.

The tested models can be a valuable addition to the SVAT and General Circulation Model (GCM) for the savanna zone of West Africa so as to remedy the practice of using a fixed average albedo value, because they can be used to depict the true value of albedo at a spatial and temporal scale. As suggested by Oguntunde (2004), for a more detailed interaction between land-use/cover change and actual evaporation, integration of seasonal albedo into the numerical study are necessary. Therefore, the tested models could be relevant in such in-depth interaction studies.

7 IMPACT OF LAND-USE INTENSITY ON SURFACE RUNOFF: MEASURED SCALE EFFECT ON THREE SMALL WATERSHEDS

7.1 Introduction

Surface runoff is one of the major components of the hydrological processes in the inland valleys in West Africa. Inland valleys are small watersheds defined as the upper reaches of the river systems. They are an integrant characteristic of the West African landscape (van de Giesen et al., 2000). These areas are often very fertile and conserve humidity for a long time even in the case of a prolonged absence of rainfall. Because of increasing peasant farming and the loss of soil fertility in the upland, a shift of agricultural activities has been widely observed in these environments and has resulted in a threat to the natural resources. The consequence of this widespread environmental problem is an appreciable change in the land cover and the herby induced hydrological effects such as a change in surface runoff coefficient, infiltration rate, evaporation and rainfall at a large scale. During field work, farmers regularly asked about the storage time of water in the streams of inland valleys. To them, this storage time is today reduced to only few days where there was permanently water. The threat to the natural resource has resulted in reducing the scale effect, thus to the availability of the water resources, because of the increase of surface runoff in detriment of the infiltration to the deeper groundwater. In fact, the scale effect is a clear reduction of surface runoff with increasing slope length, and the understanding of this process has gained interest in the past two decades. Many authors have shown evidence of this effect in many parts of the world: Australia (Ben-Hur, 1991), Nigeria (Lal, 1993, 1997a, 1997b), Burundi (El-hassanin et al., 1993), Israel (Yair and Lavee, 1985; Agassi et al., 1985), Cote d'Ivoire (van de Giesen et al., 2000; Masiyandima et al., 2003), and Ghana (Ajayi, 2004). The spatial variability of the physical soil properties (Yair and Lavee, 1985; Bonell and Williams, 1986; Sivapalan and Wood, 1986; Julien and Moglen, 1990) and the temporal dynamics of the rainfall intensity (van de Giesen et al., 2000) are the main causes for this scale effect. Furthermore, vegetation cover and agricultural land-use can also play an important role. Therefore, the main objectives of this study were: 1) to provide the evidence of the scale effect in a region with a monomodal rainfall pattern, 2) to show that the scale effect decreases with increasing agricultural activities, and 3) to show that the scale effect is important in water resource availability. The results should contribute to the first specific objective of the VinVal project.

7.2   Trial sites

According to the selection criteria required to meet the overall objective of the VinVal project, three small watersheds were selected in the province of Kompienga (10°55&11°55 N – 01°25&01°23 E). The watersheds were all in the same agro-ecosystem and showed a gradient of agricultural land-use intensity: high, medium and low land-use intensity. The selected watersheds were Tanyele (high land-use intensity), Bounou (medium land-use intensity) and Sambouali (without agricultural land-use) (Figure 7.1). All watersheds have an area of about 10 km² (Kabore et al., 2003).

These two major land-use types were practiced in these watersheds: Agriculture activities were carried out by the local communities (Gourmantche and Mossi) during the rainy season, especially in Tanyele and Bounou, and in all watersheds transhumance was practiced by shepherds (Fulani). The crops were rain-fed crops such as sorghum, millet, maize, sesame and cotton.

According to the phytogeographical classification of White (1983), the south-east region of Burkina Faso belongs to the Sudan climate zone. The annual precipitation for the study area lies between 900 and 1000 mm (Kabore et al., 2003). A rainfall peak was observed between May and October with another pronounced peak in August or September. Temperatures are very high with a peak of about 40 °C in March-April. Lower temperatures were observed in August and between December and January (22 °C on average). The region is characterized by the endemic tree species *Vitellaria paradoxa,* which dominates the vegetation cover. Other important trees are *Parkiia biglobosa*, *Andansonia digitata*, and *Anea microcarpa*. Fallow vegetation are dominated is *Combretum micrantum* and the herbaceous stratum by *Androogon gayanus*, and *Penninsetum pedicelatum.*

In all the watersheds, the up-land and the low-land are characterized by breastplate mounds and some emergent granite rock formations, which mark their crests. The terrains are very flat (slope ≤ 3 ‰) and the main type of soil is Lexisoil (more than 60 %) as in the major part of West Africa (Ademola, 2004). With respect to the soil texture, in Tanyele, the soil consists of sandy loam (71 % sand, 24 % silt and 5 % clay), in Bounou of loam (34 % sand, 48 % silt and 16 % clay) and in Sambouali of clay loam (25 % sand, 47 % silt and 28 % clay).
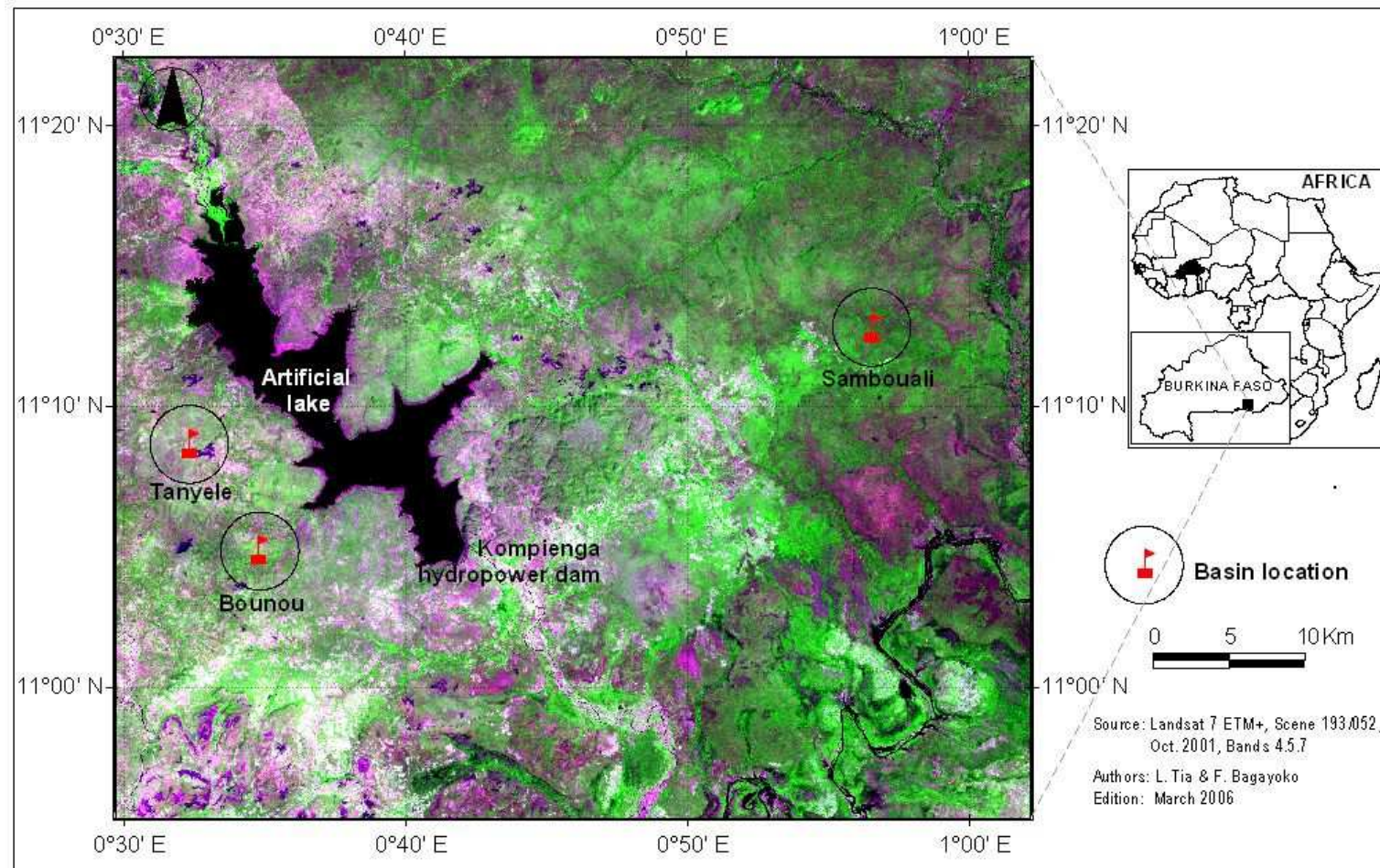
Figure 7.1:   Location of the experimental sites: Tanyele (high land-use intensity); Bounou (medium land-use intensity); Sambouali (without agricultural land-use and covered with natural vegetation)

7.3 Methods and materials

Investigations were made on a plot and watershed scale.

7.3.1 Monitoring of the rainfall

Rainfall (depth and intensity) was measured at each site with a HOBO rain gauge (tipping-bucket) provided with time-stamp data logger, which was calibrated indoor and in situ. The data were downloaded every two weeks. Furthermore, three totaling rain gauges were installed across each watershed to capture the rainfall spatial variability. The totaling rain gauges were controlled daily at 8:00.

7.3.2 Measurement on a plot scale

During the rainy season of 2004, a set of runoff plots was installed in each watershed. Each set consisted of a 0.80 m x 1.25 m and a 2 m x 5 m plot. The short plot was connected to a buried oil drum with a pipe of a diameter of 100 mm, while the long plot was connected to two buried oil drums. The plots were oriented downhill and had a slope of 2 %. A graduated bucket was introduced carefully into each drum in such a way that the water running off the plots flowed into them through the pipes. The drums were closed with a lid to protect from rainfall. External surface runoff was prevented from running into the plots by a thick metal sheet of 20 cm height. After each runoff-generating rainfall, the volume of the collected water was read. The bucket was emptied and replaced in the oil drum. When the capacity of the bucket is surpassed, the remaining volume of water in the oil drum was also measured and the total runoff collected for that rainfall event was a cumulative of all measurements. In the case of the long plot with two oil drums, the volume of the collected runoff was the sum of the volume in each bucket.

In order to measure the scale effect, the runoff coefficient of the long slope (C_{10}) was divided by the runoff coefficient of the short slope (C_1), and the result was compared with the ratio of the area of the short plot (S_1) and long plot (S_{10}). In case C_{10}/C_1 equals 1, there is no scale effect because the same amount of runoff is collected from the short, and the long plot. If $S_1/S_{10} < C_{10}/C_1 < 1$, scale effect is important, and will mainly depend to the temporal dynamics of the rainfall intensity. When

$S_1 / S_{10} < C_{10} / C_1$, scale effect is also important and will depend to the spatial variability of the physical properties of soil surface. Finally, if equals $S_1 / S_{10} = C_{10} / C_1$, the same absolute amount of runoff is collected from both the short and long plots. In fact, S_1 / S_{10} is the theoretical minimum that one would expected C_{10} / C_1 to be greater or equal. The indices 10 and 1 correspond to the area of the long plot and the short plot, respectively.

7.3.3   Measurement on a watershed scale

In addition to surface runoff from the plot, each rainfall that generated the runoff at the outlet of the watersheds was detected by a pressure transducer (diver), since the outlets were not equipped with an adequate discharge measurement structure.

Scale effect on a watershed scale was estimated by extrapolating the observations on a plot scale with the model proposed by van de Giesen et al. (2000). The required input variables are the rainfall intensity (P) [mm h^{-1}], saturated hydraulic conductivity (K_{sat}) [mm h^{-1}], soil roughness (K_m), sorptivity (S) [mm s$^{-0.5}$] and hill slope length [m] (L_s). Total runoff on a watershed scale was estimated by multiplying the sum of the individual runoff from the hill slope by the drain density and the area of the watershed. Values of the input variables are given in Table 7.1.

Table 7.1:   Input variable for the estimation of the surface runoff

	Tanyele	Bounou	Sambouali
Area (ha)	1313	1472	669
Slope length (m)	205	230	238
Drain density (m ha^{-1})	13.6	9.4	24.7
Measured K_{sat} (mm h^{-1})	227	195	55
Selected K_{sat} (mm h^{-1})	25.9	13.2	6.8
Selected K_m (rainy season)	33	25	25
Selected K_m (other periods)	20	13	5

Sorptivity (S) is a measure of the capillary uptake or removal of water in porous media (Philip, 1957). S was calibrated with the model of van de Giesen et al. (2000). For this, the calibration begun with the values of K_{sat} and K_m mentioned in

Table 7.1 and the optimum value of S was found by trial and error estimating the observed runoff from the short and long plots for each rainfall event. If sorptivity that simulates accurately the observed runoffs from the short and long plots was not found, all K_{sat}, K_m and S were varied simultaneously to obtain their optimum. As the short plot did not work properly in Tanyele, only the measured runoff from the long plot was used for the calibration. The accuracy of the estimations of the total runoff on a watershed scale was check with the discharge measurements at the outlet of the watersheds. which were estimated with the Manning Equation as follows:

$$Q = K_m S_c R_{hy}^{2/3} I^{1/2} \qquad (7.1)$$

where Q is discharge at the outlet [m^3 s^{-1}], S_c is wetted section of the stream channel [m^2], R_{hy} is hydraulic radius [m], and I is slope of the stream channel [-]. Stream channels of each watershed were assumed to have trapezium shape. The characteristics of each stream channel are given in Table 7.2.

Table 7.2:   characteristics of the stream channel of the watersheds

Characteristic	Tanyele	Bounou	Sambouali
Width of the stream channel	7	7	10
Width at the bottom	2	1.7	3
Slope of the stream	0.003	0.0005	0.002

Pressure transducer data on the flow at the outlet were available for the whole rainy season in Tanyele and Bounou, and for short period in Sambouali. Therefore, measurements in Bounou were used for the validation of the estimations, where all necessary data were available.

A decrease in the scale effect with increasing land-use intensity was shown by comparing the observation in each watershed. The results were compared to the observation in other regions with a bimodal rainfall pattern (Cote d'Ivoire and Ghana)

7.4   Results and discussions

First, the reduction of the runoff coefficient from the short and the long plots with decreasing land-use intensity is discussed. Second, the measured scale effect, its

reduction with increasing land-use intensity and trend during the whole rainy season is commented. Finally, the calibration of the sorptivity and the estimation of the total runoff from the different watersheds are discussed.

7.4.1 Reduction of runoff coefficient

In all sites, a clear reduction in the runoff coefficient from the short and long plots was observed (Table 7.3). The reduction was about 82 % and 90 % in Bounou and Sambouali, respectively. From one site to another (decreasing land-use intensity), there was a significant reduction in the runoff coefficient. The total rainfall of 825 mm over the whole rainy season produced 35 % and 14 % of the runoff from the short plots in Bounou and Sambouali, respectively. With respect to the long plots, only 8 %, 5 % and 2 % of the runoff was observed in Tanyele, Bounou and Sambouali, respectively. The results are consistent and are similar to the observations in Cote d'Ivoire (van de Giesen et al., 2000) and in Ghana (Ajayi, 2004), all regions with a bimodal rainfall pattern. According to Ajayi (2004), rainfall intensity, ponding time and plot size are the main reason for the large runoff coefficient observed from the short plot. In fact, high rainfall intensity during a short time may clog and seal the soil surface and therefore reduce the infiltration rate and increase runoff. High rainfall intensity also stimulated the ponding of the short plot in a short time and subsequent raindrops after ponding directly contributed to the runoff. Similarly, the plot being short, the water running did not have much opportunity to infiltrate before reaching the bottom. All these facts combined may explain why short plots produce more runoff than long plots. However, the absence of an abundant vegetation cover can play an important role in the rapid surface clogging and sealing, because similar rainfalls in Tanyele and Sambouali resulted in a different runoff coefficient, which cannot be explained without taking into account the vegetation cover and the difference in soil physical properties. The high rainfall depth might result from a long rainfall duration giving the water more opportunity to infiltrate in both the short and the long plots. In fact, the short plots became saturated more quickly than the long plots. Given that all raindrops contribute to surface runoff after saturation, high rainfall depth can also explain difference between the runoff coefficient of the short and the long plots.

Table 7.3: Measured runoff coefficient, ratio (C_{10}/C_1) and relative reduction of runoff coefficient.

Date of rainfall events	Rainfall (mm)			Ru. coeff. from short plots (%)			Ru. coeff. from long plots (%)			Ratio (C_{10}/C_1)			Reduction of ru. coeff. (%)		
	Tanyele	Bounou	Sambouali	Tanyele	Bounou	Sambouali	Tanyele	Bounou	Sambouali	Tanyele	Bounou	Sambouali	Tanyele	Bounou	Sambouali
12-Jun-04	16.00						7.14								
15-Jun-04	18.60						7.38								
16-Jun-04															
17-Jun-04	6.80	25.2	13.8		20.25	3.81	0.22	3.58		0.18	0.00			82.31	100.00
20-Jun-04		35.2			21.80			2.35		0.11				89.21	
22-Jun-04			25			11.58			0.87			0.07			92.50
30-Jun-04		25.8	10.8		5.77	18.27		2.95		0.51	0.00			48.95	100.00
3-Jul-04	9.20						4.81								
7-Jul-04		32.4	25		22.72	7.37		2.86		0.13	0.00			87.43	100.00
10-Jul-04		49.6			46.38			6.99		0.15				84.94	
11-Jul-04	41.40						31.49								
13-Jul-04			14.6			4.51						0.00			100.00
17-Jul-04	29.80	61	30.2		27.95	26.14	19.51	5.81	2.08	0.21	0.08			79.21	92.05
19-Jul-04	32.60	4			39.47		23.59	1.15		0.03				97.08	
22-Jul-04		27.8			43.67			5.65		0.13				87.07	
24-Jul-04	41.20	70.6			67.60		17.27	16.09		0.24				76.20	
27-Jul-04	15.30						0.24								
30-Jul-04	39.40	15.8			85.40		2.39	7.62		0.09				91.07	
31-Jul-04	7.30	14.2	18.2		12.11	2.89	0.40	6.74	0.60	0.56	0.21			44.37	79.32
11-Aug-04	7.00	17.9	44		28.51	12.46	8.06	3.96	9.26	0.14	0.74			86.10	25.70
14-Aug-04	13.60						10.52								
16-Aug-04	24.00						4.48								
22-Aug-04	4.20						3.13								
23-Aug-04	18.60	33.9	28		57.37	13.63	11.74	6.26	1.82	0.11	0.13			89.10	86.63
24-Aug-04		10.5			52.47			6.50		0.12				87.62	
25-Aug-04			22			13.16			1.83			0.14			86.11
26-Aug-04	14.60	20.3			31.80		1.64	4.29		0.14				86.50	
4-Sep-04	0.80		12.2			16.18	21.50					0.00			100.00
8-Sep-04	19.80	37.2	14.2		47.91	18.53	3.47	5.37	0.26	0.11	0.01			88.79	98.61
9-Sep-04	23.20	18.1			24.45		1.73	3.57		0.15				85.41	
14-Sep-04			8			29.61			0.46			0.02			98.45
15-Sep-04	3.60						4.49								
17-Sep-04		10.8	10.4		47.25	15.18		6.69	1.00	0.14	0.07			85.85	93.39
20-Sep-04	24.20	15.1			24.83		1.49	2.60		0.10				89.52	
21-Sep-04		10.1			10.33			3.71		0.36				64.06	
25-Sep-04			20			9.21			0.52			0.06			94.34
26-Sep-04		13.5			19.76			3.78		0.19				80.87	89.81
30-Sep-04	4.60						5.80								
1-Oct-04		13.9			34.76			5.10		0.15				85.33	
5-Oct-04	20.00						0.66							81.68	
Mean value of runoff coefficient (%)				35	14		8	5	2						

a. Measured scale effect

For most of the rainfall events, C_{10}/C_1 was less than S_1/S_{10} in Sambouali, where only 4 rainfall events produced a ratio above 0.1. In Bounou, up to 20 rainfall events produced a ratio above 0.1 (Figure 7.2). Following this trend, more ratios above 0.1 could be expected in Tanyele. van de Giesen et al. (2000) designed theoretical runoff scenarios over time to show when the spatial variability of soil physical properties and the temporal dynamics of rainfall intensity create a scale effect. The first scenario stipulates that the surface runoff occurs for only a brief time with a discharge increasing until the rain stops and the discharge drops back to zero. In this case, only a part of the plots (short and long) contributes to the collected runoff and the ratio C_{10}/C_1 is smaller than the theoretical minimum of 0.1. In the second scenario, the rain lasts long enough for the rain dropping at the top of the short plot to reach the bottom after which all infiltration excesses contribute to surface runoff until the rains stops (equilibrium state). Here, the long plot does not reach this state and the discharge just increases until the rain stops after which it decreases again. In the third scenario, the rain lasts long enough and the runoff continues for such a long time that the short and the long plots reach the equilibrium. According to Julien and Moglen (1990), in the first scenario the spatial variability is the major cause of the scale effect. Therefore, it is also probably one of the reasons of the scale effect in Bounou and Sambouali, because 9 % and 72 % of the ratios were less than 0.1 in Bounou and Sambouali, respectively. This is also probably the case in Tanyele. The low annual rainfall observed in the rainy season of 2004 and the irregularity of the rains might have enhanced the role of spatial variability in creating the scale effect in Sambouali because of the importance of antecedent soil moisture in the generation of surface runoff. The soil was sometime completely dry between two successive rainfalls events. However, the high importance of spatial variability in creating a scale effect in Sambouali is also more likely related to vegetation cover and density. In fact, one of the focuses of this study was to show the importance of vegetation cover in the reduction of surface runoff and enhancing the scale effect. The reduction of surface runoff from one site to another through the vegetation cover is quite easy to prove and has been reported by authors (Kincaid and Williams, 1966; Lane et al., 1988, Albergel et al., 1988), and in theses studies, it was concluded that the runoff was negatively related with vegetation density. In contrast, the

role of the vegetation cover in creating a scale effect can be a source of discussions, because creation of scale effect may greatly depend on the ability of the vegetation to intercept the raindrops and on the frictional resistance affecting the runoff. Interception and frictional resistance will be more pronounced in an area with more vegetation and will create the scale effect. Such a situation was observed in this study, especially in Sambouali. In fact, in addition to the reduction in runoff coefficient mentioned in section 7.4.1, the mean value of the ratio C_{10}/C_1 decreased as much as 72 % when comparing the observations in Bounou and Sambouali, respectively. This reduction corresponds to the same percentage of the increase in scale effect from the first to the second site, which cannot only be the effect of the variability of soil physical properties. Consequently, the stream flow peak was more pronounced in Tanyele and Bounou than in Sambouali. This confirms the observation on both fields at the watershed outlet where, the occurrences of stream flow were detected by the pressure transducers. Only a few rainfall events produced a flow at the outlet in Sambouali in contrast to Tanyele and Bounou.
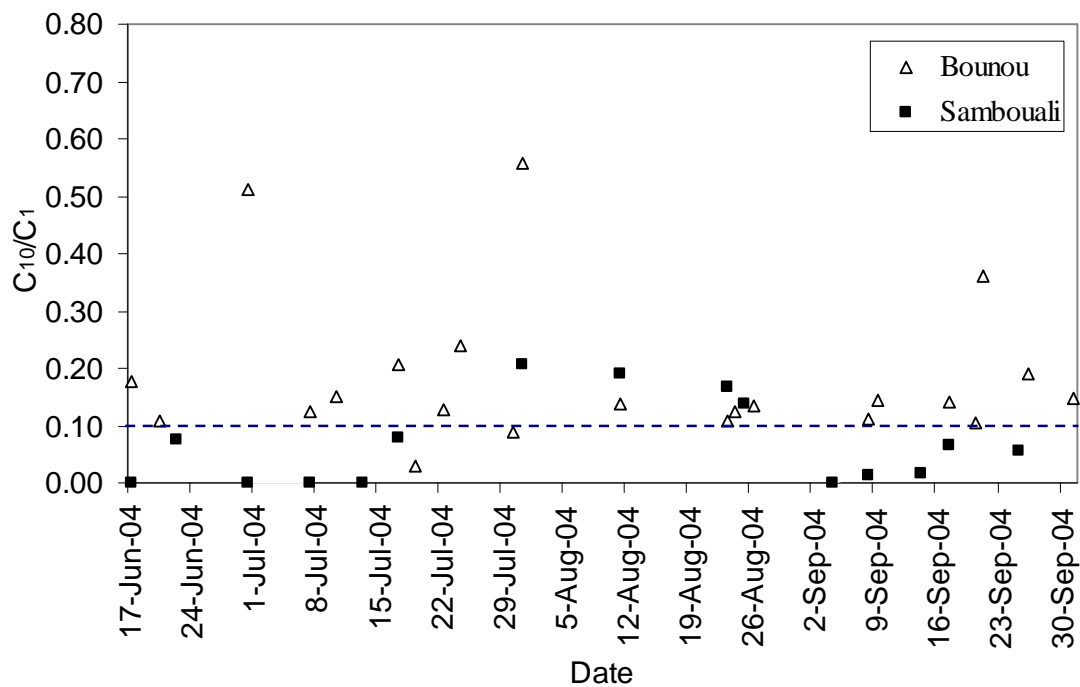
Figure 7.2:   Ratio C_{10}/C_1 compared to S_1/S_{10} (dashed line) for Bounou and Sambouali

b. Comparison of results with observations in Cote d'Ivoire and Ghana

The results obtained here were compared to the observations in Côte d'Ivoire and in Ghana. As previously mentioned, the significant reduction in the runoff coefficient from the short to the long plots was the common denominator. The reduction is less pronounced in Cote d'Ivoire than in Ghana and in Burkina Faso, but quite similar in the later two countries. The difference between the reductions might be explained by the difference in soil surface features, vegetation cover, rainfall pattern and operating method. Interesting to point out is the clear impact of the vegetation cover on the runoff coefficient in all studies. In Cote d'Ivoire, the runoff coefficient for the plots installed on bare soil produces a quite similar runoff coefficient and the scale effect is almost the same. However, the large difference in the scale effect between bare soil and soil covered with weedy fallow and rice (38%) and from similar plots is one of the most striking features of this study. A similar phenomenon was observed in Ghana and confirms the importance of a vegetation cover in enhancing the scale effect (Table 7.4-6).

Table 7.4: Average runoff coefficient observed in Côte d'Ivoire (van de Giesen et al., 2000)

	Short plot		Long plot		C_{10}/C_1	Runoff coeff. reduction(%)
	Tototal runoff (litres)	Runoff coeff. (C_1)	Total runoff (liters)	Runoff coeff. (C_{10})		
A1	397	0.37	2156	0.21	0.57	43
A2	495	0.46	2801	0.27	0.59	41
A3	316	0.29	597	0.06	0.21	79

A1: plot installed on bare soil with some fallow vegetation and rainfed rice
A2: plot installed on bare soil with some fallow vegetation and rainfed rice
A3: plot installed on soil with weedy fallow and rainfed rice

Table 7.5: Average runoff coefficient observed in Ghana (Ajayi, 2004)

	Short plot		Medium plot		Long plot		Runoff Coeff. Reduction(%)
	Total runoff (liters)	Runoff coeff.	Total runoff (liters)	Runoff coeff	Total runoff (liters)	Runoff coeff.	
A2	473	0.327	186	0.129	77	0.053	84
B2	306	0.212	225	0.156	77	0.055	74

A2: plot installed in rainfed maize field
B2: plot installed on soil covered with natural vegetation

Table 7.6: Average runoff coefficient observed in Burkina Faso

	Short plot		Long plot		C10/C1	Runoff coeff. Reduction(%)
	Total runoff (liters)	Runoff coeff. (C_1)	Total runoff (liters)	Runoff coeff. (C_{10})		
A3	N.A	N.A	454	0.08		
B3	216	0.35	373	0.05	0.14	86
C3	37	0.14	64	0.02	0.14	86

A3: site with high land-use intensity
B3: site with medium land-use intensity
C3: site without agricultural activities and covered with natural vegetation

7.4.2   Estimation of annual total runoff on watersheds scale

The estimation started by the calibration of the necessary variables in the three watersheds.

a. Calibration of the input variables

From the result obtained in the section 7.4.1, and if the values of K_{sat} and K_m found in literature are assumed correct, the main physical parameter explaining the significant decrease in surface runoff comparing Tanyele to Sambouali is sorptivity. However, the calibrated K_{sat}, K_m and S show that all parameters play a role according to their variation over time (Figure 7.3, 7.5 and 7.7).

K_{sat} and S follows similar pattern, while K_m increased gradually from the onset to the end of the rainy season. The average K_{sat} was about 28.3, 42.8 and 43.3 mm h^{-1} in Tanyele, Bounou and Sambouali, respectively. The large difference in K_{sat} between Tanyele and the others sites can be related to the minor biological activities and crust effect in this site, as natural vegetation was not dense than in Bounou and Sambouali. In contrast to K_{sat}, the average values of K_m were higher in Tanyele (34.8) and Bounou (32.9) than in Sambouali (24), where the bare soil was dominant at the onset of the rainy season. In fact, in Sambouali all vegetation was burnt during the previous dry season. With respect to the sorptivity, the average values were 2.50 mm s$^{-0.5}$, 0.142 mm s$^{-0.5}$ and 0.145 mm s$^{-0.5}$ for Tanyele, Bounou and Sambouali, respectively. These values of sorptivity are in the range of the results of Talsma (1969) and Smith (1999).

The accuracy of the calibrations is shown by the comparison between the observed and the estimated runoff from the short and long plots. For Tanyele, as the calibration was based on the measurements from the long plot, the bias errors (MBE) are lower (Figure 7.4), where MBE was 0.07 liters on average. Here, the calibrated K_{sat}, K_m and S seem to be very accurate, but should not reflect the real situation in the field, as the upscaling from the short to long plots could not be done.
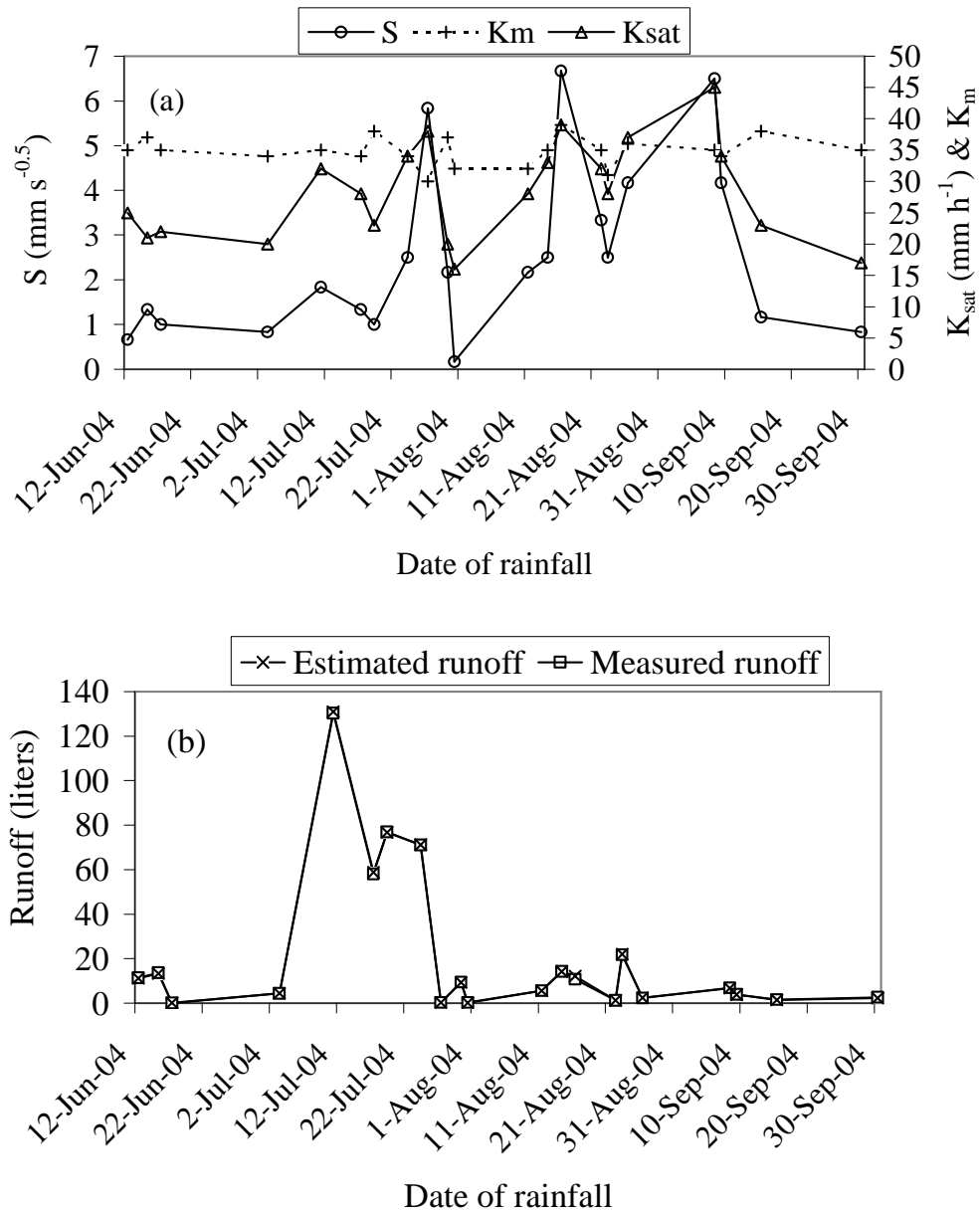
Figure 7.3:   (a) Calibrated saturated hydraulic conductivity (K_{sat}), soil roughness (K_m) and sorptivity (S); (b) comparing between observed and the simulated runoff on a plot scale in Tanyele
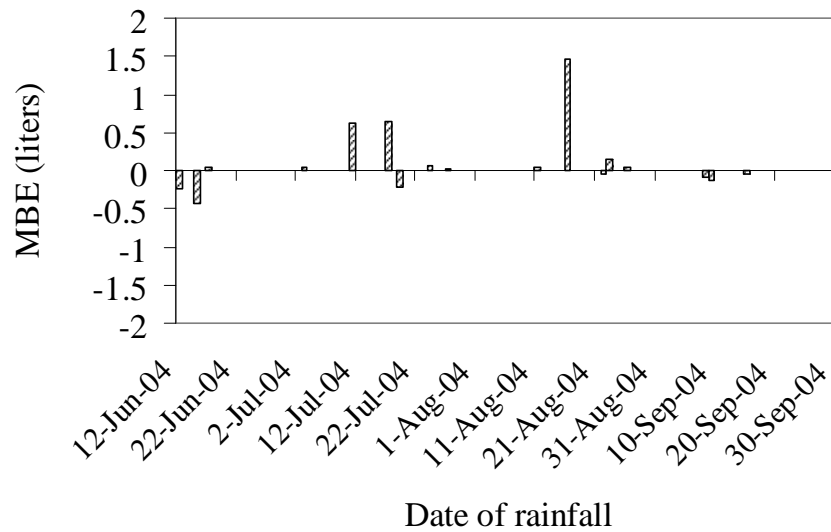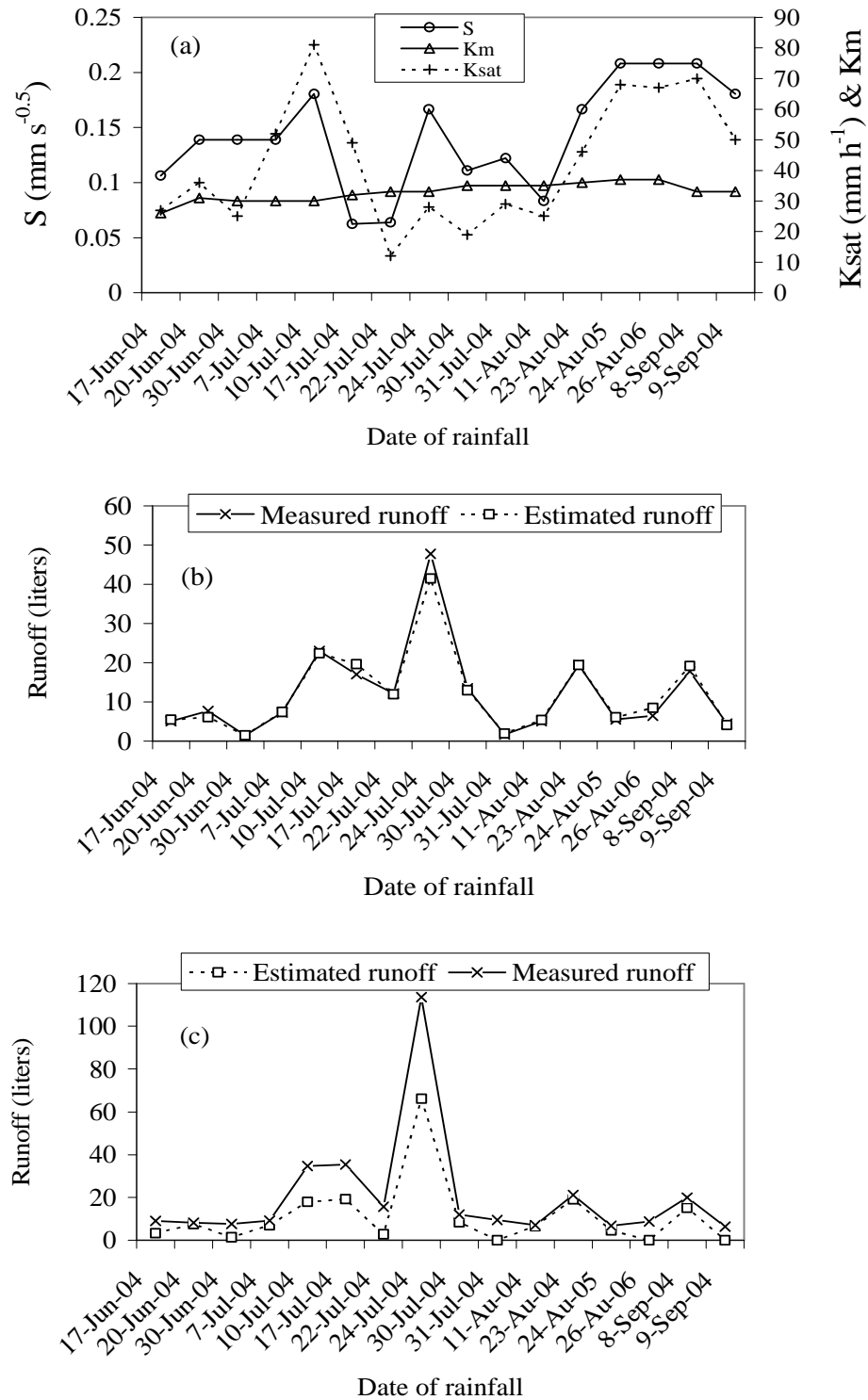
Figure 7.4:   Variation of the mean bias error in the estimation of the surface runoff in Tanyele (long plot)

For Bounou, the calibrated variables reflect more the real situation on the field. As it can be seen on Figure 7.5 (a and b), the calibrated K_{sat}, K_m and S simulate more accurately the runoff in the short plot (MBE= -0.12 liters) than the runoff in the long plot (MBE= -9.13 liters). The average MBE was -0.12 and -9.13 liters for the short and long plots, respectively (Figure 7.6). Because of the size of the short plot, the spatial variability can be considered as minor, which cannot be the case for the long plot. It was also observed that the calibration was more problematic when the scale effect on surface runoff is less pronounced. For instance, the rainfall of 24 July 2004 (70.6 mm) generated a runoff of about 48 and 114 liters in the short and long plot, respectively. For this particular rainfall, a MBE of -6 and -47 liters was observed in the short and long plot, respectively. The double effect of the temporal dynamics of rainfall intensity and plots size may explain this observation. In fact, regards to the high rainfall depth, the equilibrium state was reached in both short and long plots before which all rainfalls contribute to surface runoff. Therefore, as the plots were with different widths (0.85 and 2 m for the short and long plots, respectively), the total runoff in the long plot will tend to double the runoff in the short plot in term of proportion. In this case, the optimum K_{sat} and S for the short plot will underestimate the measurements from the long plot.

Figure 7.5:   (a) Calibrated saturated hydraulic conductivity (K_{sat}), soil roughness (K_m) and sorptivity (S); (b) comparing between observed and the simulated runoff on a plot scale in Bounou
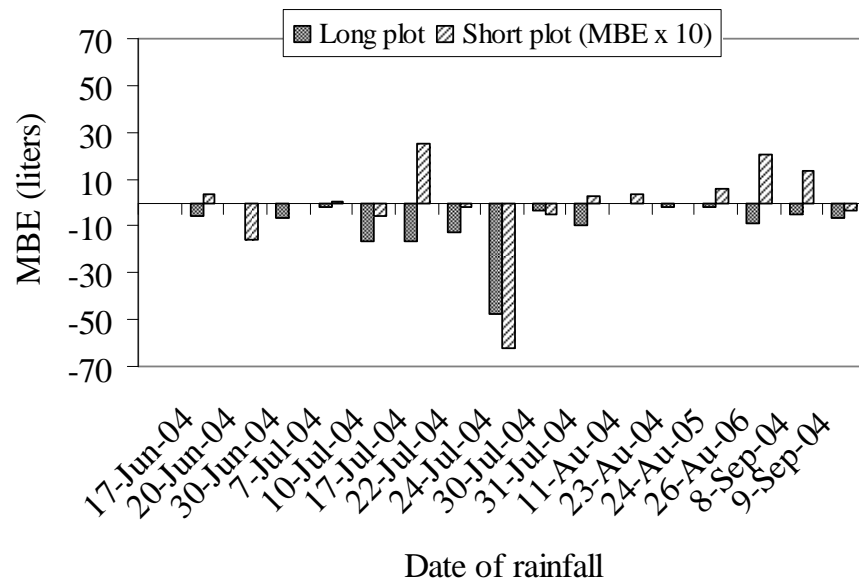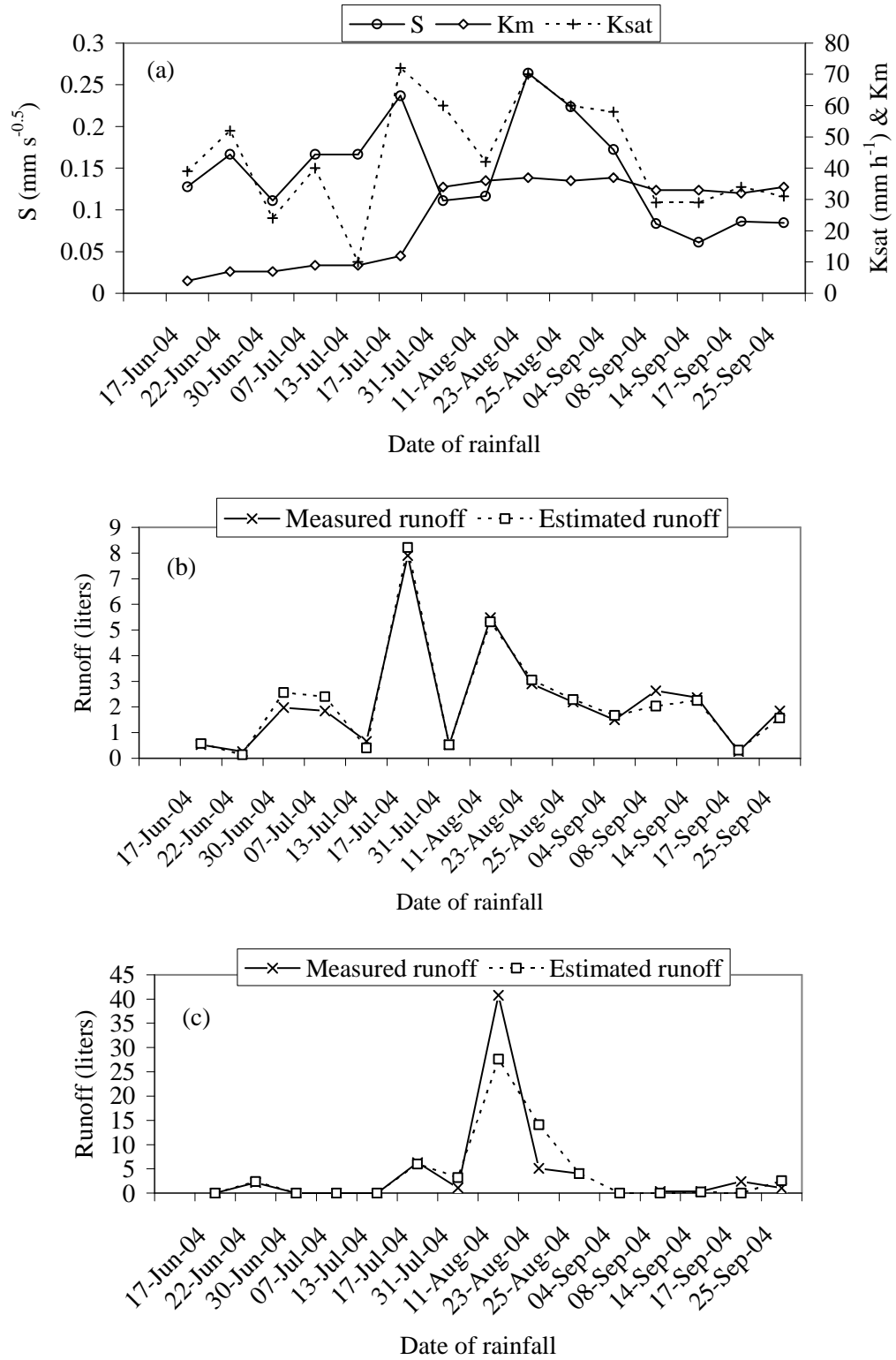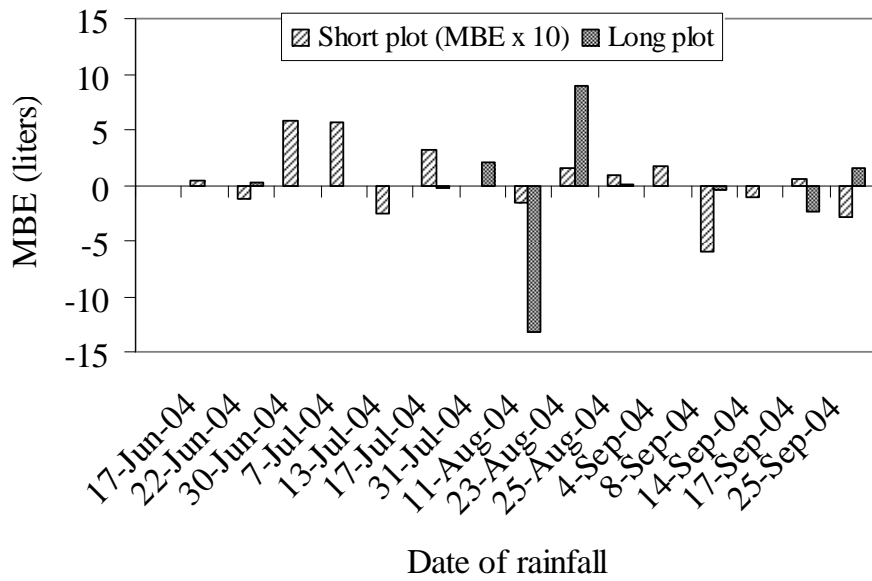
Figure 7.6:   Variation of the mean bias error in the estimation of the surface runoff in Bounou

For Sambouali, similar observation in Bounou was found. The average MBE was 0.03 and -0.23 for the short and long plots, respectively (Figure 7.8). Also, the scale effect was less pronounced for the rainfall of 11 August 2004 (44 mm), which showed similar high error with regards to the estimation of the runoff in the long plot as in Bounou for the rainfall of 24 July 2004.

Figure 7.7: (a) Calibrated saturated hydraulic conductivity (K_{sat}), soil roughness (K_m) and sorptivity (S); (b) comparing between observed and the simulated runoff on a plot scale in Sambouali

Figure 7.8: Variation of the mean bias error in the estimation of the runoff in sambouali

The results confirm the trend of the decrease of surface runoff according to increasing vegetation cover and decreasing land-use intensity. The trend of the calibrated K_{sat} and S somehow follows the calendar of the agricultural activities in Tanyele and Bounou. The values are relatively lower before tilling, because the soil was more compact and less able to absorb or infiltrate water. After tilling and seeding, K_{sat} and S were improved and increased before the soil in both sites became sealed and clogged, which again reduced the sorptivity. This process was more pronounced in Bounou, where S was 0. 06 mm s$^{-0.5}$, than Tanyele, where the minimum S was 0.17 mm s$^{-0.5}$, but K_{sat} was similar in both site (about 16 mm h^{-1} in Tanyele and 12 mm h^{-1} in Bounou). This was in mid and late July and early August, where the rainfall is more regular. Hoeing is reflected in the graph by a peak, and the following rainfall sealed and again clogged the soil, which resulted in lower sorptivity. For Samouali, K_{sat} and S were relatively constant from June until mid July. As this site was without agricultural activities the sorptivity remained constant until the soil was completely saturated, which was observed in mid of August. After this decrease, the next rainfall producing a runoff was observed 12 days later. Therefore, within this relatively long period, the soil dried out and its ability to absorb water was restored, which is shown an increase in K_{sat} and S. The following rainfall led to a relative decrease.

b. Estimation of total runoff

After the calibration of all variables, the total runoff from each watershed and for each rainfall event was estimated by multiplying the simulated runoff from the hill slope with the drain density and the area of the watershed. For the whole rainy season, the values were 18021 m³, 1913 m³ and 753 m³ in Tanyele, Bounou and Sambouali, respectively. Similarly, the measured discharges (Q) were 8112 m^3 and 2129 m^3 for Tanyele and Bounou, respectively.

As mentioned in section 7.3.3, the measurements in Bounou were used to check the accuracy of the estimated total runoff on watersheds scale. Figure 7.9 shows a relatively good agreement between the estimated and measured discharge, showing that when calculations are based on appropriate data, the model of van de Giesen et al. (2000) can be used to estimate the total runoff on a watershed scale. Comparing the estimated total runoff and total discharge in Bounou, it can be seen that both are similar. The estimated total runoff was less than the measured discharge by 216 m^3 (about 10%).
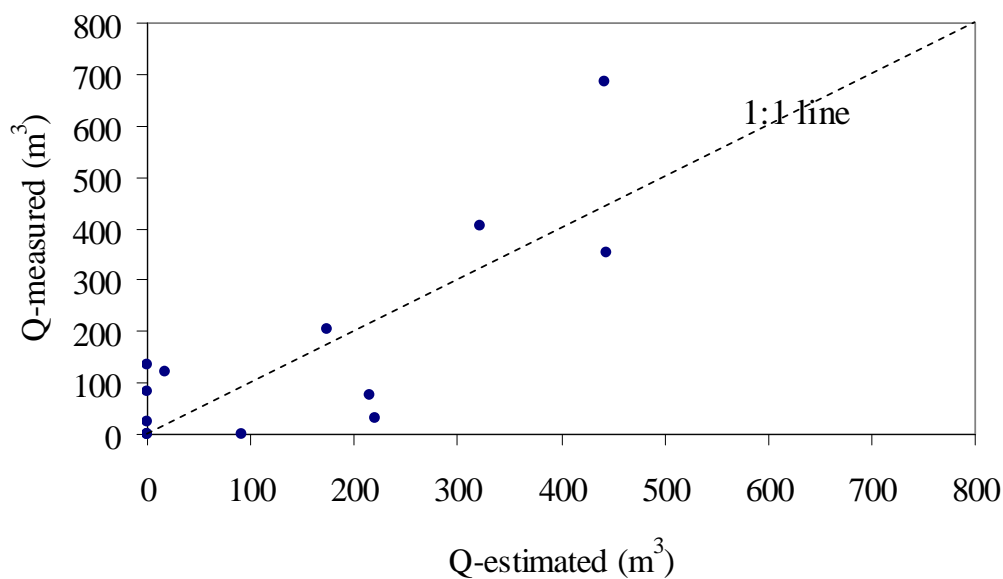
Figure 7.9:   Comparison between the estimated and measured total runoff on a watershed scale in Bounou

In Tanyele, the estimated and measured total runoffs differ significantly. In this site, as point measurements of surface runoff were not available, calibration and estimations were based on the measurements from the long plot (10 m^2), which is not appropriate. Therefore, the measured total discharge was kept as the model of van

Giesen et al. (2000) led to an overestimation. In Sambouali, calibrations and estimations were based on both the short and long plots measurements of the surface runoff. Therefore, estimations in this site can considered as accurate on the light of the relatively good agreement obtained in Bounou.

Comparing the total runoff at the outlet of the watersheds and the observation from the short plots, it becomes clear that 5 % of the runoff observed in the short plot reached the outlet in Bounou and only 0.1 % was observed at the outlet in Sambouali. With respect to the observation in the long plots, 2.1 % of the observed runoff reached the outlet in Tanyele and this percentage was 0.79 and 0.68 in Bounou and Sambouali, respectively. On a watershed scale, the total runoff in Tanyele was 4 times larger than in Bounou, 11 times than in Sambouali, whereas the magnitude was 3 times between Bounou and Sambouali. The results show that areas with high land-use intensity and lower vegetation cover produced more surface runoff than the areas with medium land-use intensity or without agricultural land-use.

7.5 Conclusion

The principal finding of the study is the clear evidence of the scale effect on runoff in the savanna area with its monomodal rainfall pattern. The results show that the scale effect was important in all trial sites but more pronounced in the sites with less agricultural activities and covered with natural vegetation. Similarly, a significant reduction of the total discharge at the outlet of the watersheds with decreasing land-use intensity was observed as well. The results and observations show that vegetation cover is important in the process of reduction of surface runoff. Consequently, with the same amount of rainfall and similar agro-ecosystem, the water resource availability (groundwater, storage time in watersheds) will be more critical with higher land-use intensity if no measures are taken to ensure the permanence of water resources.

8   SUMMARY AND RECOMMENDATIONS

This chapter presents the summary, conclusion and recommendations of the whole research. The effect of land cover change and seasonal farming activities on actual evaporation is investigated from Chapter 3 to 6, while Chapter 7 deals with the scale effect on surface runoff.

8.1   Summary

8.1.1   Energy balance closure and footprint analysis

The quality and the representativeness of the first long-term Eddy Covariance (EC) measurements ever recorded over the West African savanna were investigated via the energy balance closure and the footprint analysis. The analysis covered four contrasting periods the complete dry season (January to March 2004), the dry to wet transition period (April to May 2004), the rainy season (June to September 2004) and the wet to dry transition period (October to November 2004).

The results show that the overall energy balance closure was satisfactory over the whole dataset for an eddy covariance study with regards to the results of other investigation on this issue. The regression fit between $(R_n - G)$ and $(H + \lambda E)$ was significant with a coefficient of determination (r^2) of 0.80 and a slope of 0.88, while the intercept was 25 W m^{-2}. The energy balance closure was affected by rain during the rainy season, where $r^2 = 0.69$ and by sampling problems during the transition periods, where r^2 were 0.80 and 0.86, respectively. During the rainy season, the measurements of most of the days with rain were excluded from the analysis because they did not satisfy the energy balance closure requirement, which may hinder a real evaluation of the dynamics of surface fluxes during that period. The study also indicated an asymmetric effect on the energy balance closure on a diurnal basis. This seems to reduce the measurement accuracy during the morning. Attention should be given to this issue in future, because the reality of this asymmetry could not be substantiated since net radiation and ground heat flux were estimated. The footprint analysis shows that the fetch ranged between 20 m (daytime) and 800 m (nighttime). This range showed that the fetch was adequate and fluxes sampled were representative, especially during the rainy season when the vegetal cover was dominated by crops and grasses with scale

length of a few meters. During the dry season when the surface is free of crops and grasses, the measurements were also representative, as about 60 % of the trees around the station were contributing to the measured fluxes. However, during the transition periods, sampling problems arose, and less than 30 % of the trees were contributing to the measured fluxes. The study reveals that the location of the station with regard to the dominant wind direction is important and can have a significant effect on the representativeness of the measurements. Therefore, this aspect should be added to the traditional criteria of selection of the best location when installing the eddy covariance system, especially in the savanna vegetation where trees are scattered.

8.1.2 Inter-annual energy partitioning

Seasonal variability of the energy partitioning was analyzed with a combination of eddy flux and weather data over intensely farmed land in the Tanyele watershed. The analysis covered one relatively wet year (2004) and one relatively dry year (2003).

The study shows that there is a clear pattern in the partitioning of available energy between the sensible heat and latent heat flux on a seasonal basis. The latent heat flux was the main consumer of the available energy during the rainy season (71 %), while the sensible heat flux was dominant during the dry season (77 %). The relatively wet rainy season of 2003 had higher peak of latent heat flux (194 W m^{-2} on average) than the relatively dry rainy season of 2004 (176 W m^{-2} on average). Similarly, the sensible heat flux was lower in 2003 (66 W m^{-2} on average) and higher in 2004 (81 W m^{-2} average) for the same period. Surface conductance peaked in 2003 and 2004 during the rainy season at 39 mm s^{-1} and 38 mm s^{-1}, respectively. During the dry season, surface conductance was strongly coupled to atmospheric demand but was much reduced due to low soil moisture availability and high vapor pressure deficit ($VPD > 4$ kPa). During the rainy season, the latent heat flux was decoupled from atmosphere demand. The study also shows multiple correlations between variables making it difficult to determine the exact individual contribution. However, the main driving factor is moisture availability, and all or parts of the other contributing variables in the process depend on this main factor. During the dry season, the main driving factors reducing the latent heat flux were vapor pressure deficit, net radiation was non-limiting. The vapor pressure deficit also has significant effects on the surface conductance and

137

vice-versa. During the dry season, the major part of the available energy goes into heating the atmosphere, thus increasing the sensible flux. During the transition periods and the rainy season, the phenomenon is reversed and the latent heat flux becomes the main consumer of the available energy, and soil moisture is no longer limiting. During these wetter parts of the year, vapor pressure deficit play minor roles while net radiation becomes the main driving factor. All processes also depend on the abundance and the distribution of rainfall over the rainy season.

Another important finding of this study is the clear and pronounced seasonal dynamics of roughness length for momentum. Usually, fixed values of roughness length for momentum are used in land surface models, since studies have shown that it has only minor effects on surface fluxes. The use of a fixed value of the roughness length for momentum is less accurate in the case of savanna vegetation, where there is a drastic change in vegetation cover according to the seasons. Moreover, agricultural activities amplify this change. Similarly, seasonal bush fires, which completely change the morphology of the vegetation cover, could also significantly affect the roughness length for momentum.

The pattern of coupling and decoupling was followed for formulation of actual the evaporation and surface conductance. The improved equations were based on the assumptions given by Smith and Jarvis (1998) and seemed to be consistent. These simpler equations developed can be an alternative to many of the sophisticated models available in the literature for the case of the savanna zone of West Africa. Inclusion of these equations in some of the well-known land surface transfer models should be considered for weather and climate models for the West African savanna.

8.1.3   Seasonal dynamics of vegetation cover and land surface models

The sensitivity of the NOAH LSM was evaluated with respect to the seasonal dynamics of the vegetation cover in the savanna area under intensive agriculture in eastern Burkina Faso, West Africa. The choice of the NOAH LSM was motivated by the fact that it has been already tested in different environments in West Africa, especially in Ghana.

Model sensitivity was tested by comparing the simulated surfaces fluxes using fixed values of the roughness length for momentum as the standard in the model and the

roughness length for momentum having the true seasonal value. The results show that the NOAH LSM was not sensitive to the change of the roughness length for momentum on a seasonal basis nor on a daily basis, which contradicts earlier results. The formulation of the coefficient (B_c) coupling the canopy transpiration to atmosphere was found to be the main cause of this. An improved formulation for this coefficient was given to remediate to this insensitivity and to improve the performance of the model. The model led to an overall underestimation of the latent heat flux throughout the monitoring period. The use of constant value for moisture conditions in soil layer appeared to be the reason for this underestimation, because long-term measurements of soil moisture were not available. The model gave a better estimation of the sensible heat flux. Recommendations are also given to enhance the performance of the model in the West African savanna environment.

8.1.4 Seasonal dynamics of surface albedo

Surface albedo is an important parameter in many models such as crop growth models, eco-hydrological models, and General Circulation Models (GCM). The present research was conducted over the savanna zone of eastern part of Burkina Faso, West Africa. The first objective was to investigate the effect of the seasonal and diurnal dynamics of surface albedo on actual evaporation. Also, the diurnal course of the albedo was measured and its relation with solar angle, cloudiness and potential effect on actual evaporation was established. The measured surface albedo was simulated with selected empirical models available in the literature.

The results show that there are a clear seasonal dynamics of surface albedo, which had a negative impact on actual evaporation. This impact was implicitly related to the seasonal dynamics of vegetation and climatic conditions, which determine soil moisture availability. On a diurnal basis, the impact was found to be insignificant, but there is a necessity to represent these diurnal dynamics in seasonal models because of the close relationship between surface albedo and sun zenith angle under clear sky conditions. The diurnal dynamics were insignificant during days with clouds. Therefore, the inclusion of a clearnex index in the models could be useful, because it would discard the sun angle during days with clouds. The models employed to simulate the seasonal dynamics of the sheanut and sorghum surface albedo gave better estimations, but were

very sensitive to the *LAI* . A small change in the *LAI* resulted to a large change in the simulated surface albedo. Therefore, the true *LAI* according to the crop growth stage should be used. The calibrated models can be useful to estimate sheanut tree and sorghum albedo at a spatial and temporal scale for the savanna zone of West Africa. They can be a valuable addition to the SVAT and General Circulation Model (GCM) so as to remedy the practice of using fixed average albedo values, because they can be used to depict the true value of albedo at a spatial and temporal scale. As suggested by Oguntunde (2004), for a more detailed interaction between land-use/cover change and actual evaporation, integration of seasonal albedo into the numerical study are necessary. Therefore, the tested models can be relevant in such in-depth interaction study.

8.1.5   Land-use and surface runoff

Surface runoff was measured with a set of runoff plots in three small watersheds (Tanyele, Bounou and Sambouali) with different agricultural land-use intensity in eastern Burkina Faso, West Africa. Land-use intensity in Tanyele was high, but Bounou intensity was medium, while Sambouali was not under agriculture but covered with natural vegetation. Each set consisted of one short plot of 0.80 m x 1.25 m (1 m²) and one long plot of 2 m x 5 m (10 m²) runoff plot. The objective of the research was to investigate the surface runoff scale effect in the savanna area with monomodal rainfall pattern, and to show that this effect was more pronounced in the area without agricultural activities and covered with natural vegetation. The surface runoff scale effect was measured by dividing the runoff coefficient from the long plot (C_{10}) by the runoff coefficient from the short plot (C_1) and then compared to the ratio of the surfaces (S_1 / S_{10}). The results show a clear reduction of surface runoff with increasing slope length and with decreasing land-use intensity. The plot of 1 m² did not give confident data in Tanyele. In fact, the precipitation of 825 mm observed in 2004 generated a 35 % and 14 % surface runoff from the short plot in Bounou and Sambouali, respectively. With regards to the long plot, 8 %, 5 % and 2 % was observed in Tanyele, Bounou and Sambouali, respectively. The scale effect in Sambouali was more pronounced than in Bounou with a magnitude of 72 %. On a watershed scale, the total runoff in Tanyele

was 4 time larger than in Bounou, 11 times than in Sambouali, whereas the magnitude was 3 times between Bounou and Sambouali. A difference in the interception and the frictional resistance of the vegetation was found to be important in the process of the scale effect and decrease of the surface runoff with decreasing land-use intensity

8.2   Conclusion and recommendations

The research shows that land-use and seasonal farming activities have a clear effect on the dynamics of surface fluxes, especially on actual evaporation, in the savanna zone of West Africa. This is illustrated by the pronounced seasonal dynamics of the roughness length for momentum and surface albedo, even if their effect is not the principal cause of the seasonal dynamics of surface fluxes. Moisture availability is the primary cause and its abundance enhances and stimulates the effect of the roughness length for momentum and surface albedo. Similarly, land-use intensity has a clear effect on surface runoff as shown by the clear decrease in runoff and increasing surface runoff scale effect with decreasing land-use intensity. Pertinent to the analyses in the different chapters, some useful and necessary recommendations are given as follows:

1. In order to improve the quality and the representativeness of long-term eddy covariance measurement on farm land in the savanna zone, the eddy covariance station must be well orientated with regard to the dominant wind direction. The location must also be adequate, so that a higher number of trees are covered by the sensor fetch. This criterion should be added to the traditional criteria of selection of the best location of installation of the eddy covariance station in the savanna zone of West Africa.

2. The insensitivity of land surface models with respect to the roughness length for momentum is less accurate in the savanna environment. Therefore, clear representation of seasonal values of the roughness length for momentum on eddy covariance measurement must be taken into account in their formulation. A similar consideration with respect to surface albedo is also needed. These data can be useful for better understanding of the complex feedback mechanisms in the biosphere-atmosphere interaction in the savanna zone of West Africa. However, the used of a fixed value of roughness length for momentum should be sufficient for the dry season, where all variables, except surface albedo, appear relatively constant.

3. The proposed formulation of actual evaporation and surface conductance can be relevant and should be taken into account for better understanding of the feedback mechanisms in the biosphere-atmosphere interaction in the savanna zone of West Africa. The proposed formulations do not need complex representation of root distribution in different soil layers. Moisture availability is implicitly taken into account by moisture indicators like Bowen ratio and evaporative fraction. However, independent data sets are needed to test them. Therefore, this should be the next step for their validation, and the flux network of the GLOWA-Volta and VinVal projects can be useful for that. The developed models can be an alternative to many of the sophisticated models available in the literature.

4. With respect to surface runoff models for the savanna zone of West Africa, the surface runoff scale effect must be clearly represented for better prediction of surface runoff at a watershed scale. Land-use intensity must also be taken into account and could be done through the surface roughness. Usually, surface roughness is expressed through the Manning coefficient in surface runoff models. This coefficient can be expressed as a function of canopy interception and vegetation frictional resistance.

9 REFERENCES

Agassi M, Shainberg I and Morin J. 1985. Infiltration and runoff in wheat fields in the semiarid regions of Israel. Geoderma 36: 263-276.

Ajayi A.E. 2004. Surface runoff and infiltration processes in the Volta Basin, West Africa: Observation and Modeling. ZEF Bonn, Bonn, Germany, 151p.

Albergel J. 1988. Genèses et prédétermination des crues au Burkina Faso. Etudes et Thèses, ORSTOM, Paris.

Allen R.G., Pereira L.S. Raes D. and Smith M. 1999. Crop evapotranspiration. Guidelines for computing crop water requirement. FAO Irrigation and drainage Paper 56, FAO, Rome.

Allen R.G., Smith M., Perrier A. and Pereira L.S. 1994. An update for the definition of reference evapotranspiration. ICID Bull. 43: 1-34.

Allen S.J., Wallace J.S., Gash J.H.C. and Sivakumar M.V.K. 1994. Measurement of Albedo Variation over Natural Vegetation in the Sahel. Int. J. Clim. 14: 625-636.

Alves I. and Pereira L.S. 1999. Modelling surface resistance from climatic variables? Agric. For. Meteorol. 42: 371-385.

Andreini M., van de Giesen N.C., van Edig A., Fosu M. and Andah W. 2000. Volta Basin water balance. ZEF Discussion papers Nr. 21, Bonn, Germany.

Anlauf R., Kersebaum K.Ch., Ping L.Y., Nuske-Schüler A., Richter J., Springob G., Syring K.M. and Utermann J. 1987. Models for processes in the soil: Programs and Exercises. CATENA paperback, Cremlingen-Destedt, Germany. 227p.

Aubinet M., Grelle A., Ibrom A., Rannik Ü., Moncrieff J., Foken T., Kowalski A.S., Martin P.H., Berbigier P., Bernhofer C.H., Clement R., Elbers J., Granier A., Günwald T., Morgenstern K., Pilegaard K., Rebmann C., Snijders W. and Vesala T. 2000. Estimation of the annual net carbon and water exchange of forest: the EUROFLUX meteorology. Adv. Ecol. Res. 30: 113-175.

Baldocchi D.D. and Vogel C.A. 1997. Seasonal variation of energy and water vapor exchange rates aboves and below a boreal jack pine forest canopy. J. Geophys. Res. 102: 28939-28951.

Baldocchi D.D., Hicks B.B. and Meyers T.P. 1998. Measuring biosphere atmosphere exchanges of biologically related gases with micrometeorological methods. Ecology 69: 1331-1340.

Ben-Hur M. 1991. The effects of dispersants, stabilizer and slope length on runoff and water-harvesting farming. Aust. J. Soil Res. 29: 553-563.

Bonell M. and Williams J. 1986. The generation and redistribution of overland flow on a massive oxic soil in an eucalypt woodland within the semi-arid tropics of North Australia. Hydrol. Process. 1: 31-46.

Bounoua L., Defries R., Gollatz G.J., Sellers P. and Khan H. 2002. Effect of land cover conversion on surface climate. Climatic Change 52: 29-64.

Bozier K. 2002. Aerodynamic roughness length and zero plane displacement height. http://www.ties.salford.ac.uk/people/keb/rskborg2.html, last updated March 2004.

Braimoh A.K. 2004. Modeling land-use change in the Volta Basin of Ghana. ZEF Bonn, University of Bonn, Germany.

Brotzge J.A. and Crawford K.C. 2003. Examination of the surface energy budget: a comparison of eddy correlation and Bowen ration measurement systems. J. Hydrometeorol. 4: 160-178.

Brutsaert W. 1982. Evaporation into the atmosphere: Theory, History, and Application. Kluwer, Boston, pp 299.

Burman R.D., Nixon P. R., Wright J.L. and Pruitt W.O. 1980. Water Requirements. In: M. E. Jensen (ed.) Design and Operation of Farm Irrigation Systems. ASAE Monograph No. 3. American Society of Agricultural Engineers. St. Joseph, MI. pp. 189-234.

Campbell G.S. 1977. An Introduction to Environmental Biophysics. Springer Verlag, New York. 159p.

Clark G.A., Smajstrla A.G. and Zazuela F.S. 1989. Amospheric Parameters Which affect Evapotranspiration. University of Florida, USA.

Carslaw H.S. and Jaeger J.C. 1986. Conduction of Heat in Solids. Clarendon Press, Oxford.

Chabot A.D. and Hicks D.J. 1982. The ecology of the leaf life spans. Ann. Rev. Ecol. Syst. 13: 229-259.

Chang S., Hahn D., Yang C.H., Norquist D. and Ek M. 1999. Validation Study of the CAPS Model Land Surface Scheme Using the 1987 Cabauw/PILPS Dataset. J. Appl. Meteor. 38: 31-39.

Chen F., Janjic D., Yang Z. and Mitchell K. 1997. Impact of atmospheric surface layer parametrization in the new Land Surface Scheme of NCEP mesoscale ETa model. J. Appl. Meteorol. 38: 405-422.

Charney J. G., Stone P. H. and Quirk W. J. 1975. Drought in the Sahara: A Biogeophysical Feedback Mechanism. Science 187: 434-435.

Courel M., Kandel R., and Rasool S. 1984. Surface Albedo and the Sahel Drought. Nature 307: 528-538.

Cresswell H.P., Painter D.J. and Cameron K.C. 1993. Tillage and water content effect on soil hydraulic properties and shortwave albedo. Soil Sci. Soc. Am. J. 57: 816-824.

Culf A.D., Foken T. and Gash J.H.C. 2004. The energy balance closure problem. In: Kabat et al. (eds.) Vegetation, Water, Humans and the Climate. Vol.1. Springer, Berlin, pp. 159-166.

Dale, H.V. 1997. The relationship between land-use change and climate change. Ecol. Appl. 7: 753-769.

De Bruin H.A.R. 1987. From Penman to Makkink. In: J.C. Hopghart (ed.) Evaporation and weather (technical Meeting of the Committee for hydrological Research, February, 1981), Comm. Hydrol. Res. TNO, Den Haag, Proc. And Inform 39: 5-30.

de Sherbinin A. 2002. Land-use and Land-Cover Change. In A CIESIN Thematic Guide. Palisades, N.Y: Center for International Earth Science Information Network of Columbia University.

Diallo B., Coulibaly P.L., Barry S., Kaboré O., Dipama J.M., Zerbo L. and Millogo M.C. 2002. Diagnostic exploratoire par la méthode accélérée de la recherche participative (MARP) dans les villages sites du projet VinVal, Burkina Faso. Rapport de Synthèse, INERA, Ouagadougou, Burkina Faso.

Dickinson R.E., Henderson-Sellers A. and Kennedy P.J. 1993. Biosphere-Atmosphere Transfer Scheme (BATS) Version 1e as coupled to the NCAR community Climate Model. National Center for atmospheric Research (NCAR) Techinical Note NCAR/TN-387-STR.72p.

Doorenbos J. and Pruitt W. 1975. Crop water requirement. Irrigation and Drainage Paper N°24, FAO, Rome, Italy.

Dong A., Grattan S.R., Carroll J.J. and Prashar C.R.K. 1992. Estimation of daytime net radiation over well-watered grass. J. Irrig. Drainage Eng. 118: 466-479.

Duadze S.E.K. 2004. Land-use and land-cover study of the Savannah ecosystem in the Upper West region (Ghana) using remote sensing. ZEF Bonn, University of Bonn, Germany.

Dugas W.A. 1991. Bowen ratio, eddy correlation, and portable chamber measurement of sensible and latent flux over irrigated spring wheat. Agric. For. Meteorol. 56: 1-20.

Dunne T. 1978. Field studies of hillslope flow processes. In: Kirkby M.J. (ed.) Hillslope hydrology. John Wiley & Sons, New York, NY: pp. 227-293.

Dunne T. and Black R.D. 1970. An experimental investigation of runoff production impermeable soils. Water Resources Res. 6: 478-490.

Dyer AJ. 1974. A review of flux profile relationships. Boundary-Layer Meteorol. 7: 63-372.

Ek M. and Holtslag A.A.M. 2004. Influence of Soil Moisture on Boundary Cloud Development. J. Hydrometeorol. 5: 86-99.

Ek M. and Mahrt L. 1991. A formulation for boundary-layer cloud cover. Ann. Geophysicae 9: 716-724.

Elagina L.G., Zubkovskii S.L., Kaprov B.M. and Sokolov D.Y. 1973. Experimental investigations of the energy balance near the surface. Trudy Glavny Geofiziceskij Observatorii 296: 38-45

Elagina L.G., Kaprov B.M. and Timanovskii D.F. 1978. A characteristic of the surface air layer above snow. Izvestia AN SSSR Fizika Atmosfery I Oceana 14: 926-931

Elbers J.A. 2002. Eddy Correlation system Altera; User manuel, Wageningen, Altera.

Eleston J. and Monteith J.L. 1975. Micrometeorology and Ecology. In: J.L. Monteith (ed.) Vegetation and the Atmosphere. Vol.1. Academic Press, London, UK.

El-Hassanin A.S., Labib T.M., Gaber E.I. 1993. Effect of vegetation cover and land slope on runoff and soil losses from the watersheds of Burundi. Agric. Ecosyst. Environ. 43: 301-308.

Esteves M. and Lapetite J.M. 2003. A multi-scale approach of runoff generation in a Sahelian gully catchment: a case study in Niger. Catena 50: 255-271

FAO 1993. Guidelines: land evaluation for rainfed agriculture. Soil Resources Management and Conservation Services. Land and Water Development Divison. Food and Agriculture Organization (FAO) of the United Nation.

Fiedler F.R., Gary P.E., Ramirez J.A. and Ahuja L.R. 2002. Hydrologic response of grasslands: effect of grazing, interactive infiltration and scale.

Finch J.W. and Harding R.J. 1998. A comparison between reference transpiration and measurements of evaporation for a riparian grass-land site. Hydrol. Earth Syst. Sc. 2: 129-136.

FAO 1993. Forest Resources Assessment 1990: Tropical Countries, FAO Forestry Paper 112, Rome.

Foken T. and Wichura B. 1996. Tools for quality assessment of the surface-based flux measurements. Agric. For. Meteorol. 78: 83-105.

Gash J.H.C. 1986. A note on estimating the effect of a limited fetch on micrometeorological evapotranspiration measurement. Boundary-Layer Meteorol. 35: 409-413.

Giambelluca T.W, Fox J., Yarnasarn S., Onibutr P. and Nullet M.A. 1999. Dry season radiation balance of land covers replacing forest in northern Thailand. Agric. For. Meteorol. 95: 53-63.

Gornitz V. 1985. A Survey of Anthropogenic Vegetation Changes in West Africa during the Last Century-Climatic Implications. Clim. Change 7: 285-325.

Goulden M.L., Wofsy S.C., Harden J.W., Trumbore S.E., Grill P.W., Fries T., Daube B.C., Fan S.M., Sutton D.J., Bazzaz A. and Munger J.W. 1998. Sensitivity of boreal forest carbon balance to soil thaw. Science 279: 214-217.

Goutorbe J.P., Dolman A.J. and Gash J.H.C. 1997. HAPEX-Sahel: a large scale study of land atmosphere interactions in the semiarid tropics. Ann. Geophysicae 12: 53-64.

Granier A. 1985. Une Nouvelle Méthode pour la mesure du flux de sève brute dans le Tronc des Arbres. Ann. Sci. For. 42: 193-200.

Granier A. 1987. Evaluation of transpiration in a Douglas fir stand by means of sap flow measurements. Tree Physiol. 3: 309-320.

Granier A., Biron P. and Lemoine D. 2000. Water balance transpiration and canopy conductance in two beech stands. Agric. For. Meteorol. 100: 219-308.

Helmer E.H., Brown S. and Cohen W.B. 2000. Mapping mountain tropical forest succesional stage and land-use with multi-date LANDSAT imagery. Int. remote sensing 21: 2163-2183.

Horton R.E. 1933. The role of infiltration in the hydrologic cycle. Trans. Am. Geophys. Union 14: 446-460.

Humphreys E.R., Black T.A., Ethier G.J., Drewitt G.B., Spittlehouse D.L., Jork E.M., Nesic Z. and Livingston N.J. 2003. Annual and seasonal variability of sensible and latent heat fluxes above a costal Douglas-fir forest, British Columbia, Canada. Agric. For. Meteorol. 115: 109-125.

Huntingford S.J., Allen R.J. and Harding R.J. 1994. An intercomparison of single and dual-source vegetation-atmosphere transfer models applied to transpiration from Sahelian Savannah. Boundary-layer Meteorol. 74: 397-418

Idso S.B., Aase J.K. and Jackson R.D. 1975. Net radiation-soil heat flux relations as influences by soil water variations. Boundary-Layer Meteorol. 9: 113-112.

Iziomon M.G. and Mayer H. 2002. On the variability and modeling of surface albedo and long-wave radiation components. Agric. For. Meteorol. 111: 141-152.

Idso S.B. and Jackson R.D. 1967. Thermal radiation from the atmosphere. J. Geophys. Res. 74: 5397-5403.

Intsiful J.D. 2004. Upscaling of land surface parameters through inverse SVAT modeling. PhD thesis. Cüvillier, Göttingen.

Jacquemin B. and Noilhan J. 1990. Sensitivity study and validation of land-surface parameterization using the HAPEX-MOBHILY data set. Bound-Lay Meteorol. 52: 93-134

Jarvis P. 1976. The interpretation of the variations in leafwater potentials and stomatal conductance found in canopies in the field. Philos. Trans. R. Soc. London, Ser. B 273: 593-610.

Jarvis P.G. and McNaughton K.G. 1986. Stomatal control of transpiration: scaling up from leaf to region. Adv. Ecol. Res. 15: 1-49.

Jarvis P.G., Massheder J.M., Hale S.E., Moncrieff J.B., Rayment M. and Scott S.L. 1997. Seasonal variation of carbon dioxide, water vapor and energy exchange of a boreal black pruce forest. J. Geosphy. Res. 102: 28953-28966.

Jarvis P.G., James G.B. and Landsberg J.J. 1976. Coniferous fores. In: Monteith, J.L. (Ed.), Vegetation and the atmosphere, Vol. 2. Academic,San Diego, CA, pp. 171-240.

Jensen M.E., Burman R.D. and Allen R.G. 1990. Evapotranspiration and irrigation water requirements. ASCE Man. Rep. Engin. Pract. 70, American Society of Civil Engineers, New York, NY.

Joel A., Messing I., Seguel O. and Casanova M. 2002. Measurement of surface Runoff from plots of two different sizes. Hydrol. Processes 16: 1467-1478.

Julien Y.P., Moglen G.E. 1990. Similarity and length scale for spatial varied overland flow. Water Resources Research. 26: 1819-1832.

Kabat P., Dolman A.J. and Elbers J.A. 1997. Evaporation, sensible heat and canopy conductance of fallow savannah and patterned woodland in the Sahel. J. Hydrol. 188-189: 494-515.

Kaboré O., Zerbo L., Dipama J.M. and Sandwidi J.P. 2003. Caractérisation biophysique des sites de VinVal au Burkina Faso. Rapport technique provisoire (projet VinVal), Ouagadougou, Burkina Faso.

Kasten F. and Czeplak G. 1980. Solar and terrestrial radiation dependence on the amount and type of cloud. Solar Energy 24: 177-189.

Kelliher F.M., Leuning R., Raupach M.R. and Schulze E.-D. 1995. Maximum conductances for evaporation from global vegetation types. Agric. For. Meteorol. 73: 1-16.

Kincaid D.R. and Williams G. 1966. Rainfall effect on soil surface characteristics following range improvement treatments. J. Range Manag. 19: 346-351.

Knisel, W. G. 1980. A field-scale model for Chemicals, Runoff, and Erosion from Agricultural Management Systems. U. S. Department of Agriculture, Science and Education Administration, Conservation Research Report No. 26, 643p.

Kumagai T., Taku M.S., Yoshinobu S., Toshiyuki M., Odair J.M., Koichiro K. and Masakazu S. 2003. Transpiration, canopy conductance and decoupling coefficient of a lowland mixed dipterocarp forest in Sarawak, Borneo. J. Hydrol. 287: 237-251.

Lal R. 1997. Soil degradative effects of slope length and tillage methods on alfisols in Western Nigeria, I, Runoff, erosion and crop response. Land Degradation Dev. 8: 201-219.

Lane L., Hernandez M. and Nichols M. 1997. Processes controlling sediment yield fromwatersheds as functions of spatial scale. Envir.l Model. And Software 12: 355-369.

Law B.E., Goldstein A.H., Anthoni P.M., Unsworth M.H., Panek J.A., Bauer M.R., Fracheboud J.M. and Hultman N. 2001. CO2 and water vapor exchange by young and old ponderosa pine ecosystems during a drought year. Tree Physiol. 21: 299-308.

Lebel T., Taupin J.D. and LeBarbe L. 1997. Space-time fluctuation of rainfall during HAPEX-Sahel. J. Hydrol., this issue.

Lettau H. and Davidson B. 1957. Exploring the atmosphere's first Mile, Vol. 1-2, Pergamon Press N.Y.

Leuning R.L. and Moncrieff J.B. 1990. Eddy Covariance CO2 flux measurements using open- and closed-path CO_2 analyzers: corrections for analyzer water vapor sensitivity and damping of fluctuations in the air sampling tubes. Boundary-Layers Meteorol. 53: 63-76.

Linda A.W., Lawrence B.F. and Peter J.C. 2002. Seasonal and interannual variation in evapotranspiration, energy balance and surface conductance in northern temperate grassland. Agric. For. Meteorol. 112: 31-49.

Littleboy M., Cogle A.L., Smith G.D., Rao K.P.C. and Yule D.F. 1996. Soil management and productio of Alfisols in the semi-arid tropics .4. Simulation of decline in productivity caused by soil erosion. Australian J. Soil Res. 34: 127-138.

Llasat M.C. and Snyder R.L. 1998. Data error effects on net radiation and evapotranspiration estimation. Agric. and For. Meteorol. 91: 209-221.

Lloyd C.R. 1993. The effect of heterogeneous terrain on micrometeorological flux measurements: a case study from HAPEX-Sahel. Agric. For. Meteorol. 73: 209-216.

Makkink G.F. 1957. Testing the Penman formula by means of lysimeters. Int. J. Water Eng. 11: 277-288.

Mahe G., Paturel J.E., Servat E., Conway D. and Dezetter A. 2005. The impact of land-use change on soil water holding capacity and river flow modeling in the Nakambe River, Burkina Faso. J. Hydol. 300: 33-43.

Mahrt L. and Ek M. 1984. The influence of the atmospheric stability on the potential evaporation. J. Clim. Appl. Meteorol. 23: 222-234.

Margolis H.A. and Ryan M.G. 1997. A physiological basis for biosphere atmosphere interactions in the boreal forest an overview. Tree Physiol. 17: 491-499.

Martano P. 1999. Estimation of surface roughness length and displacement height from single-level sonic anemometer data. J. Appl. meteorol. 39: 708-715.

Masiyandima M.C., van de Giesen N.C., Diatta S., Windmeijer P.N. and Steenhuis, T.S. 2003. The hydrology of inland valleys in the sub-humid zone of West Africa: rainfall-runoff processes in the M'be experimental watershed. Hydrol. Processes 17: 1213-1225.

Mauser W. and Schädlich S. 1998. Modeling the spatial distribution of the evapotranspiration on different scales using the remote sensing data. J. Hydrol. 212-213: 250-267.

McCumber M. 1980. A numerical simulation of the influence of heat and moisture fluxes upon mesoscale circulations. Ph.D. dissertation, University of Virginia, 255p.

McNaughton K.G. and Jarvis P.G. 1983. Predicting effect of vegetation changes on transpiration and evaporation. In: Kozlowski, T.T. (ed.) Water Deficit and Plant Growth, Vol. II Academic Press. London, pp. 2-47.

Meijninger W., Moene A., Hartogenis O., de Bruin H. and Heusinkvel B. 2000. The Large Aperture Scintillometer; User manual and technical information, Meteorology and air quality group, Wageningen.

Minnis P., Mayor S., Smith W.L. and Young D.F. 1997. Asymmetry in the diurnal variation of surface albedo. IEEE Trans. Geosci. Remote Sensing 35: 879-891.

Moore C.J. 1976. Eddy flux measurement above pine forest. Quart. J. Roy. Meteorol. Soc. 102: 913-918.

Monteith J.L. 1965. Evaporation and the environment. Symp. Soc. Expl. Biol. 19: 205-234.

Pereira L.S., Perrier A., Allen R.G. and Alves I. 1999. Evapotranspiration: concepts and futures trends. Journal of Irr. and Drain. Engineering 122: 45-51

Návar J. and Synnott J.T. 2000. Surface runoff, soil erosion, and land-use in Northeastern Mexico Terra Volumen 18 (3).

Nicholson S. E., Tucker C. J. and Ba, M. B. 1998. Desertification, Drought, and Surface Vegetation: An Example from the West African Sahel, Bull. Amer. Meteorol. Soc. 79: 815-829.

Niyogi D. S., Xue Y., Raman S. and Alapaty K. 1999. Uncertainty in the Specification of Surface Characteristics, Part ii: Hierarchy of Interaction-Explicit Statistical Analyis. Boundary Layer Meteor. 91: 341-366.

Noilhan J. and Planton S. 1989. A simple parametrization of the land surface processes for meteorological models. Mon. Wea. Res. 117: 536-549.

Oguntunde P.G. 2004. Evapotranspiration and complementarity relations in the water balance of the Volta Basin: Field measurements and GIS-based regional estimates, PhD thesis. Cuviliier, Göttingen.

Oguntunde P.G. and van de Giesen N.C. 2004. Crop growth and development effects on surface albedo for maize and cowpea fields in Ghana, West Africa. Int. J. Biometeorol. 49: 106-112

Oke T.R. 1987. Boundary-Layer Climate. Methuen, New York, 434 p.

Orlenko L.R. and Legotina S.I. 1973. The energy balance over the underlying surface during KENEX-71. Trudy Glavny Geofiziceskij Observatorii 296: 46-56.

Pan H.L. and Mahrt L. 1986. Interaction between soil hydrology and boundary-layer development. Bound-Lay. Meteorol. 38: 185-202.

Paw U.K.T., Baldocchi D.D., Meyers T.P. and Wilson K.B. 2000. Correction of eddy covariance measurements incorporating both advective effect and density fluxes. Boundary-Layer Meteorol. 97: 487-511.

Penman H.L. 1948. Natural evaporation from open water, bare soil and grass. Proc. Roy. Soc. Serie A 193: 120-146

Philip J.R. 1957. The theory of infiltration: Sorptivity and algebraic infiltration equations. Soil Sci. 84: 257-264.

Puech C. and Chabi-Gonni D. 1984. Méthode de calcul des débits de crus décennale. CIEH, Ouagadougou.

Reich P.B., Koike T., Gower S.T. and Schoette A.W. 1992. Causes and consequences of variation in conifer leaf life-span. In: Smith, W.K. and Hinckley, T.M., (eds.) Ecophysiology in North America., 2nd ed., MacMillan, New York, 995p.

Reich P. B., Uhl C.,Walters M. B. and Ellsworth D. S. 1992. Leaf life-span in relation to leaf, plant, and stand characteristics among diverse ecosystems. Ecol. Monogr. 62: 365-392.

Reifsyder W.E. 1988. Evaporation and Environment. In: Reynolds, R.C., Thompson, F.B. (eds.) Forests, Climate and Hydrology. The United Nations University, Tokyo, pp. 117-127.

Reynolds O. 1894. On the dynamical theory of incompressible viscous fluids and the determination of the criterion. Phyl. Trans. Roy. Soc. London, A186, Part I 123-161.

Rochette P., Pattey E., Desjardin R.L., Dwyer L.W., Stewart D.W. and Dubé P.A. 1991. Estimation of maize (Zea mays L.) canopy transpiration by scaling up leaf stomatal conductance. Agric. For. Meteorol. 54: 241-261.

Rodier J.A. 1976. Evaluation de l'écoulement annuel dans les régions tropicales sèches d'Afrique Occidentale. Cashier ORSTOM, Sér. Hydrol., XIII (4) 269-306.

Rodier J. and Auvray C. 1965. Estimation of discharge of 10 year floods for catchments inférieur à 200 square miles in West Africa. CIEH/ORSTOM, Ouagadougou, Burkina Faso.

Sayer J., Harcourt C. S. and Collins N. M. 1992. Conservation Atlas of Tropical Forests, Africa. MacMillan, London.

Schüttemeyer D. 2005. The surface energy balance over drying semi-arid terrain in West Africa., University of Wageningen, the Netherlands, 154p.

Schuepp P.H., Leclerc M.Y., Macpherson J.I. and Desjardins R.L. 1990. Footprint prediction of scalar fluxes from analytical solutions of the diffusion equation. Boundary-Layer Meteorol. 50: 355-373.

Schimid H.P. 2002. Footprint modeling for vegetation atmosphere exchange studies: a review and perspective. Agric. For. Meteorol. 113: 159-183.

Sellers P.J., Bounoua L., Collatz G.J., Randall D.A., Dazlich D.A., Los S., Berry J.A., Fung I.Y., Tucker C.J., Field C.B. and Jensen T.G 1996. A comparison of radiative and physiological effects of doubled CO2 on the global climate. Science 271:1402-1406.

Sellers P.J., Randall D.A., Collatz G.J., Berry J.A., Field C.B., Dazlich D.A., Zhang C., Callelo G.D. and Bounoua L. 1996. A revised land surface parameterization (SiB2) for atmospheric GCMs. PartI: Model formulation. J. Climate 9: 676-705.

Sharman K. Singh H. and Pareek O. 1983. Rain water infiltration into a bare loamy sand. Hydrol. Science J. 28: 417-424

Shaw R.H. and Pereira A.R. 1982. Aerodynamic roughness of a plant canopy: A numerical experiment. Agric. Meteorol. 26: 51-65.

Shuttleworth W.J., Gash J.H.C., Lloyd C.R., Roberts J.M., Marques A.O., Fisch G., de Silva P., Ribeiro M.N.G., Molion L.C.B., de Abreu Sa L.D., Nobre C.A., Cabral O.M.R., Patel S.R. and de Moraes J.C. 1984. Eddy Correlation measurements of energy partition for Amazonian forest. Q.J. Roy. Meteorol. Soc. 110: 1143-1162.

Sivapalan M. and Wood E. F. 1986. Spatial heterogeneity and scale in the infiltration response of catchments, in Gupta, V. K., Rodriguez-Iturbe, I. and Wood, E. F. (eds.) Scale Problems in Hydrology: Runoff Generation and Basin Response. D. Reidel Publishing, Dordrecht, pp. 81-106.

Smith R.E. 1999. A technical note: Rapid measurement of soil sorptivity. Soil Sci. Soc. Am. J. 63: 55-57.

Smith D. M. and Jarvis P. G. 1998. Physiology and environmental control of transpiration by trees in windbreaks. Agric. For. Meteorol. 105: 159-173.

Song J. 1998. Diurnal asymmetry in surface albedo. Agric. For. Meteor. 92: 181-189.

Stannard D.I. 1993. Comparison of Penman-Monteith Shuttelworth-Wallace, and modified Priestley-Taylor evapotranspiration models for wildland vegetation in semiarid rangeland. Water Resources Research 29: 1379-1392.

Stewart J.B. 1988. Modeling surface conductance of pine forest. Agric. For. Meteorol. 43: 19-35.

Swinbank W.C. 1963. Longwave radiation from clear skies. Q. J. R. Meteorol. Soc. 89: 339-348.

Talsma, T. 1969. In-situ measurement of sorptivity. Aust. J. Soil Res. 7: 269-276.

van de Giesen N.C., Stomph T.J. and de Ridder N. 2000. Scale effects of Hortonian overland flow and rainfall-runoff dynamics in a West African catena landscape. Hydrological Processes 14: 165-175.

Tsvang L.R., Aligusseynov A.K., Perepelkin V.G., Sulev M.A., Meolder M.E. and Zeleny J. 1987. Experiments on the heat-balance closure in the atmospheric surface-layer and on the earth surface. Izvestiya Akademil Nauk SSSR Fizika Atmosfery I Okeana 23: 3-13

Turner B.L. II, Goran H. and Kates R.W. 1993. Population Growth and Agricultural Change in Africa. Gainesville, University of Florida.

Twine T.E. 2000. Correcting eddy-covariance flux underestimates over a grassland. Agric. For. Meteorol. 103: 279-300.

Ungaro F., Quaglino E., Gallorini D. and Pestarini M. 2004. Physical and hydrological properties of the soils on the three inland valleys of Ghana (Kumassi region) and Burkina Faso (Kompienga region). Research report, Timesis, Italy.

van de Giesen N.C., Kunstman H., Jung G., Liebe J., Andreini M. and Vlek P. 2002. The GLOWA-Volta project: Integrated assessment of feedback mechanisms between climate, land-use, and hydrology. Advance in Global Change Research 10: 165-175.

van de Giesen N.C., Stomph T.J. and de Ridder N. 2000. Scale effects of hortonian overland flow and rainfall-runoff dynamics in West African catena landscape. Hydrol. Processes 14: 165-175.

van de Giesen N.C., Stomph T.J. and de Ridder N. 2005. Surface runoff scale effect in West African watersheds: Modeling and Management options. Agric. Water Manag. 78: 109-130.

VinVal 2001. Impact of changing land-cover on the production and ecological functions of vegetation in inland valleys in West Africa. Available at http://www.alterra-research.nl/pls/portal30/docs/FOLDER/VINVAL/ p_main.htm., Last update: July 2004.

Wilson K.B. and Baldocchi D.D. 2000. Seasonal and interannual variability of energy fluxes overs a broadleaved temperate deciduous forest in North America. Agric. For. Meteorol. 100: 1-18.

White F. 1983. The vegetation of Africa: A descriptive memoir to accompany the UNESCO-AETFAT-UNSO Vegetation map of Africa. UNESCO, PARIS, 356p World Resources Institute, 1988. World Resources 1988–89, Basic Books, New York.

Wyngaard J.C. 1988. Flow-distortion effects on scalar flux measurements in the surface layers: Implication for sensor design. Boundary-Layer Meteorol. 42: 19-26.

Yair A., Lavee H. 1985. Runoff generation in arid and semi-arid zones. In: Anderson M.G., Burt T.P. (Eds.), Hydrological Forecasting. John Wiley & Sons, New York, pp. 183-220.

Yin X. 1997. Optical Air Mass: Daily Integration and its Applications. Meteorol. Atmos. Phys. 63: 227-233.

Yin X. 1998. The Albedo of Vegetated Land Surfaces: Systems Analysis and Mathematical Modeling. Theor. Appl. Climatol. 60: 121-140.

Zeng X., Dai Y.J., Dickinson R.E. and Shaikh M. 1998. The role of root distribution for climate simulation over land. Geophy. Res. Lett. 25: 4533-4536.

Zilitinkevich S.S. 1995. Non-local turbulent transport: pollution dispersion aspects of the coherent structure of convective flow. In: H. Power, N. Moussiopoulos and C.A. Brebbia (eds.) Air Pollution III- Volume I. Air Pollution Theory and Simulation. Computational Mechanics Publication, Southampton Boston, pp 53-60.